A Bio-Optical Approach to Phytoplankton Community Structure, Physiology and Primary Production in the Weddell Gyre

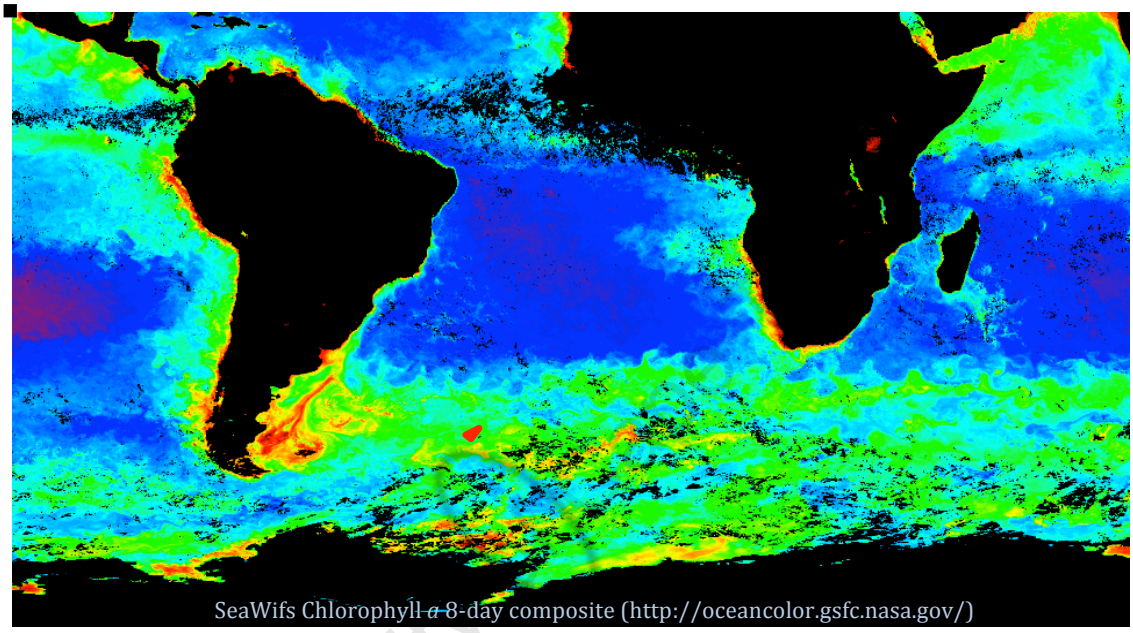

SeaWifs Chlorophyll *a* 8-day composite (http://oceancolor.gsfc.nasa.gov/)

By
Ceinwen Smith

Supervised by

Howard Waldron
Sandy Thomalla
Mike Lucas

Dissertation submitted in fulfillment of the requirements for the degree of

Master of Science

Department of Oceanography
University Cape Town
February 2014

Plagiarism declaration

I know the meaning of plagiarism and declare that all of the work in this dissertation, save for that which is properly acknowledged, is my own.

……..

Ceinwen Smith

"It is a reproach to every civilized country, that the people of this enlightened age posses so little accurate knowledge of the seas, islands and perhaps continents which exist in the polar regions of the southern hemisphere"

Benjamin Morell – *A Narrative of Four Voyages*, 1832

Abstract

The Southern Ocean is an important "sink" for anthropogenic CO_2, but it requires a detailed understanding of the sensitivity of the biological carbon pump to variability in physical forcing mechanisms in order to predict its continuing role. However, due to the remote and tempestuous nature of this region, *in situ* measurements of phytoplankton variability are scarce. Consequently, satellites, autonomous floats and gliders are increasingly being utilized as platforms for observing biogeochemical variability over broad spatial and temporal scales, through satellite ocean colour radiometry linked to inherent optical properties (IOPs) of the upper water column. In this study, the variability of *in situ* IOPs was investigated together with phytoplankton biomass, cell size, species composition and chlorophyll to carbon (Chl:C) ratios to isolate and understand the relationships between IOPs and biogeochemistry. These relationships were applied to a high resolution dataset from the Weddell Gyre, to produce detailed section plots of particulate organic carbon (POC), beam attenuation spectral slope between 470 nm and 650 nm ($c_{p(470:650)}$ as a proxy for size) and chlorophyll to beam attenuation (Chl:c_p) ratios (as a proxy for Chl:C ratios). Interpretation of these sections in the context of the different hydrographic and nutrient environments, provided insight into the causative factors driving the observed patterns of phytoplankton variability. In addition, estimates of carbon export from ^{15}N primary production experiments allowed the identification of regions of high and low carbon export potential in the Weddell Gyre. In summary, high biomass blooms observed in the Northern Limb of the Weddell Gyre (NLWG) and Antarctic Continental Shelf (ACS), were generally associated with the dominance of *Phaeocystis antarctica*, but differed in their Chl:c_p ratios, dominant cell sizes and potential for carbon export. It is suggested that these differences were predominantly driven by iron limitation. Iron relief at the ice shelf was likely responsible for the dominance of large colonies of *P. antarctica* and high Chl:c_p ratios, which in combination with strong sinking of surface waters and high f-ratios, resulted in the identification of the ACS as an important region for carbon export. Conversely, in the NLWG the dominance of solitary cells of *P. antarctica*, due to iron limitation, coupled with strong surface stratification and low f-ratios,

suggests that this region had less potential for carbon export, despite high biomass. The lower biomass blooms in the Central Weddell Gyre (CWG) region were associated with mixed communities of diatoms and dinoflagellates, variable stratification and moderate f-ratios. In the southern region of the CWG, however, high chlorophyll specific primary production rates, high Chl:c_p ratios and the dominance of large cells suggest high photosynthetic efficiency, due to iron relief and a higher potential for carbon export, compared to that inferred from f-ratios. The more northerly bloom, associated with small cells and lower Chl:c_p ratios, controlled by iron limitation and grazing, implies lower export potential. This study highlights the importance of undertaking comprehensive investigations, which combine bio-optical, biogeochemical and community structure data, to explore fine-scale phytoplankton variability over regional scales. While this preliminary assessment provides compelling evidence for the use of IOP-biogeochemistry relationships, with improved data collection techniques, the support of more ancillary data and a growing dataset of *in situ* ship-based and autonomous platform data, more robust empirical relationships may be established for this region. The application of these relationships to both high-resolution glider data and satellite ocean colour data will enable the observation of temporal changes in phytoplankton community structure and physiology that will ultimately improve our understanding of the sensitivity of the Southern Ocean biological carbon pump to predicted climate change.

Acknowledgements

I am forever grateful to my friends and family who have listened to my scientific ramblings, followed my numerous explorations and encouraged me throughout this thesis Your support was essential in maintaining my sanity throughout this arduous process. Thank you to my parents for providing me with the privilege of studying what I love, allowing me the opportunity to explore my scientific passion without any expectations and for listening with wide-eyed interest despite being totally out of their depth.

This project was made possible by the financial support of CSIR (Council for Scientific and Industrial Research, Stellenbosch) and GreenSeas (Norway), with travel and training support provided by UCT Postgraduate Funding Office.
This project would not have been possible without the help and support of the captains (Captain Hall and Captain Freddie) and crew of the SA *Agulhas*, the team at SANAP (South African National Antarctic Program) and the Department of Environmental Affairs for assisting the advancement of marine science in South Africa making the voyages to Antarctica possible.

Thank you to my three supervisors: Sandy Thomalla, from the CSIR for her endless patience, encouragement and invaluable feedback throughout the data collection, processing and write-up of this thesis; to Howard Waldron from UCT Oceanography Department for providing me with a work space, lab training in nutrient analysis and ^{15}N primary production techniques, feedback on my thesis structure and endless dry wit!; and to Mike Lucas from UCT Biological Science Department for his assistance with ^{15}N primary production analyses and feedback on several thesis drafts.

This project has provided me with an incredible opportunity to work alongside exceptional young scientists while exploring my own ability in a new field. To that end I am indebted to the SOCCO (Southern Ocean Carbon and Climate Observatory) and EarthObs groups at the CHPC (Centre for High Performance Computing) for their patience in sitting through my extended presentations,

giving feedback and encouragement when I felt confused and overwhelmed and providing a wonderfully supportive environment to learn.

Several individuals were involved in the collection and processing of the data, and whose help and hard work is much appreciated. Many thanks to Chief Scientific Officer Sebastiaan Swart and fellow oceanographic scientists on SANAE50 cruise, particularly the night-shift team for keeping me company through long hours in the wetlab. Thank you to Ffion Atkins for the processing of POC data, Craig Attwood for the nutrient analyses and Ian Newton for the analyses of particulate (POC) and isotopic (^{15}N-production) filter samples. I would never have managed to learn MatLab and process my data without the help, patience and script-writing skills of Luke Gregor and Sarah Nicholson. Thank you both, you guys were lifesavers!

I would also like to extend my thanks to the numerous scientists at the National Oceanographic Centre in Southampton, UK, for their help and patience in my laboratory training. In particular: Alex Poulton and Diane Purcell for sharing their expertise in phytoplankton taxonomy and enumeration and providing me with lab space during my microscopy training.

Thank you to the academic staff at Oceans and Coasts in Seapoint for sharing their wealth of knowledge, in particular Grant Pitcher and Lisa Mansfield for the use of their microscope lab and their invaluable input during the processing of microscopy data. I owe Trevor Probyn my gratitude for helping me make sense of my ^{15}N primary production data, putting up with my endless questions and confusion and helping me see the humour in a rather frustrating technique.

Finally to my friends, housemates and cabin-mates Terri Hutchings, Sarah Nicholson, Ffion Atkins and Tiara Walters for keeping me motivated to carry on when I wanted to give up, inspiring me to strive for excellence in my writing and helping me through the hardest times with dark chocolate and endless cups of tea!

Table of Contents

"…as the Earth system matures it keeps its climate always fit for life, and the invisible hand that regulates is feedback between its living and non-living parts".

James Lovelock – *Climate Change on Living Earth*, 2007

Chapter 1 General Introduction

1.1 The carbon cycle and climate change

Current changes in the concentration of atmospheric carbon dioxide (CO_2) are largely driven by anthropogenic activity, such as the burning of fossil fuels, cement production and agriculture (Sabine et al., 2004), which has increased atmospheric CO_2 concentrations by more than 35% in the last 200 years (Sabine and Feely, 2007). This increase in atmospheric CO_2 is regulated by the flux of CO_2 between three main reservoirs: the oceans, the terrestrial biosphere and the atmosphere (Figure 1.1). In the natural carbon cycle the concentration of atmospheric CO_2, driven by volcanic eruptions, respiration and natural fires (Figure 1.1), is a vital component in many of the Earth's systems (Watson and Orr, 2003). It provides a source of inorganic carbon required for photosynthesis, which produces oxygen to sustain life. Through the formation of carbonic acid, it is responsible for the weathering of rocks, which form the soils and nutrients to support life on land, in rivers and the sea. Finally it is an important greenhouse gas, which contributes to the balance of the Earth's climate. While the natural carbon cycle is roughly in balance, the same cannot be said for the anthropogenic carbon cycle.

Current anthropogenic CO_2 emissions are around 9 Gt C y^{-1} (1 Gt = 1 billion tons) and are increasing at a faster rate than the Earth's ability to absorb the excess, without considerable perturbation to global systems (IPCC, 2007). The anthropogenic carbon cycle is driven by the extraction and burning of fossil fuels and the production of cement, which produce around 7 Gt C y^{-1} with deforestation and land-use change responsible for roughly 1.5 Gt C y^{-1} (Sabine and Feely, 2007). Roughly 45% of these CO_2 emissions accumulate in the atmosphere as a greenhouse gas, which impacts the global climate system. The remainder is taken up by the other two reservoirs, with about 29% by the terrestrial biosphere and 26% by the oceans (Sabine et al., 2004; IPCC, 2007). In view of current energy consumption and a rapidly growing global population, this increase is expected to continue (Hoffert et al., 1998; Watson and Orr, 2003).

Given that previous perturbations in the earth's climate have been driven by relatively small changes in atmospheric CO_2 (Li et al., 1998), such large increases in anthropogenic emissions are expected to have a significant effect on the earth's climate, atmosphere, terrestrial and marine systems as well as biogeochemical cycles (IPCC, 2007).

The ocean is the largest reservoir of CO_2 (Yool et al., 2007) and is estimated to take up approximately ~2 Gt y^{-1} (Figure 1.1; Sabine et al., 2004) or ~26% of anthropogenic CO_2 (Takahashi et al., 2002; Raven et al., 2005; Mikaloff-Fletcher et al., 2006, Sabine and Feely, 2007). The oceanic uptake of CO_2 is driven by physico-chemical processes associated with Meridional Overturning and Thermohaline Circulation, which function over large spatial scales, as well as phytoplankton production, which occurs at smaller scales and is highly variable. Furthermore, seasonal and latitudinal variations in ocean circulation, climatology and biological activity results in high spatial and temporal variability in ocean CO_2 fluxes. This variability has led to the ocean being characterized as a patchwork of CO_2 'sources' and 'sinks' (Takahashi et al. 1997). Given the complex role of processes, pathways, sources and sinks of CO_2 in the marine environment (Figure 1.1, Sabine et al., 2007) it is vital to understand the biogeochemical processes driving variability in the marine carbon cycle. Figure 1.1 illustrates the important role of plants (grey arrows), both terrestrial (trees and grasses) and marine (phytoplankton), in fixing carbon during photosynthesis. It also highlights the significant anthropogenic source of carbon (red arrows) to the global carbon cycle, compared to the impact of weathering, rivers and volcanism (dashed arrows). Most carbon fixed by terrestrial plants is released back into the atmosphere through respiration and bacterial decomposition, but some is buried in soils. In the marine carbon cycle, <1% of carbon fixed by phytoplankton reaches the sea floor, while at least 90% is re-mineralized in the upper layers (~1000 m). The ocean's carbon reservoir, however, is 1-2 orders of magnitude greater than the terrestrial and atmospheric reservoirs, highlighting the importance of understanding how marine systems will respond to environmental and climatic changes.

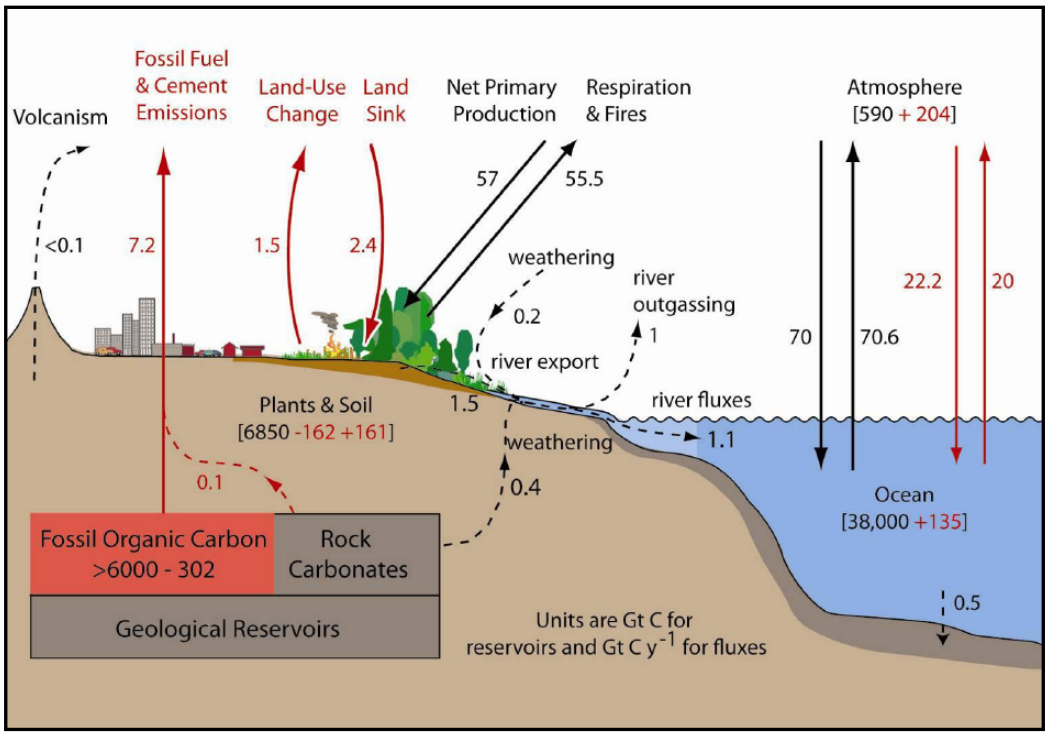

Figure 1.1 The natural (grey arrows) and anthropogenic (red arrows) pathways of the global carbon cycle estimated for 2000-2005 (Sabine et al., 2007). Arrows represent fluxes (Gt C y^{-1}) between ocean, atmosphere and terrestrial reservoirs (Gt C, circled values) highlighting the various 'sources' and 'sinks' in the carbon cycle. Figure reproduced from Sabine et al. (2007).

1.2 The biological and physical solubility pumps

The ocean's capacity to take up CO_2 is driven by the relative partial pressures of CO_2 in the atmosphere ($\rho CO_2.atm$) and the ocean surface ($\rho CO_2.H_2O$). Where $\rho CO_2.atm > \rho CO_2.H_2O$, the ocean will take up CO_2, but where $\rho CO_2.atm < \rho CO_2.H_2O$, the oceans will degas CO_2 to the atmosphere. This partial pressure gradient is driven by an inverse gradient in dissolved inorganic carbon (DIC) with depth, which is primarily regulated by the physical solubility pump and the biological pump (Volk and Hoffert, 1985; Falkowski and Raven, 1997), with additional contributions by the carbonate and microbial pumps.

The physical solubility pump is driven predominantly by temperature and salinity, where gases are more soluble in cold water than in warm water allowing more CO_2 to dissolve in colder waters. Temperature and salinity together control the density and sinking rate of surface water and thus the transport of CO_2 to great depths (Watson and Orr, 2003). As a result of increased gaseous solubility at low temperatures and surface water subduction, combined with the sinking flux of particulate organic carbon (POC), which is re-mineralized to DIC, cold, deep waters are enriched in dissolved carbon, relative to the atmosphere (Falkowski et al., 2000).

The biological carbon pump is driven by phytoplankton, the dominant primary producers of the ocean that fix 40-50 Pg C y^{-1} which equates to around half of global primary production (Field et al., 1998; Falkowski et al., 2000; 2008). By utilizing CO_2 during photosynthesis, phytoplankton remove approximately 26% of anthropogenic CO_2 (Le Quéré et al., 2009) from surface waters of the world's ocean. Biologically fixed carbon is sequestered into the deep ocean for hundreds to thousands of years when phytoplankton blooms collapse and sink below the seasonal thermocline. This process is referred to as the biological pump (Eppley and Peterson, 1979; Figure 1.2) and is regulated by the rate at which inorganic carbon is fixed into POC, as well as the flux of carbon to below the seasonal mixed layer (Eppley and Peterson, 1979). Consequently, carbon fluxes and the

efficiency of the biological carbon pump are modified by factors that drive phytoplankton growth (eg. light, temperature, degree of mixing, nutrients, iron), particle formation (eg. community structure, cell size and carbon content), sinking rates (eg. cell size, aggregation, ballasting and grazing) and particulate remineralization (e.g. bacterial activity and chemical dissolution) (Boyd and Trull, 2007; Finkel et al., 2010).

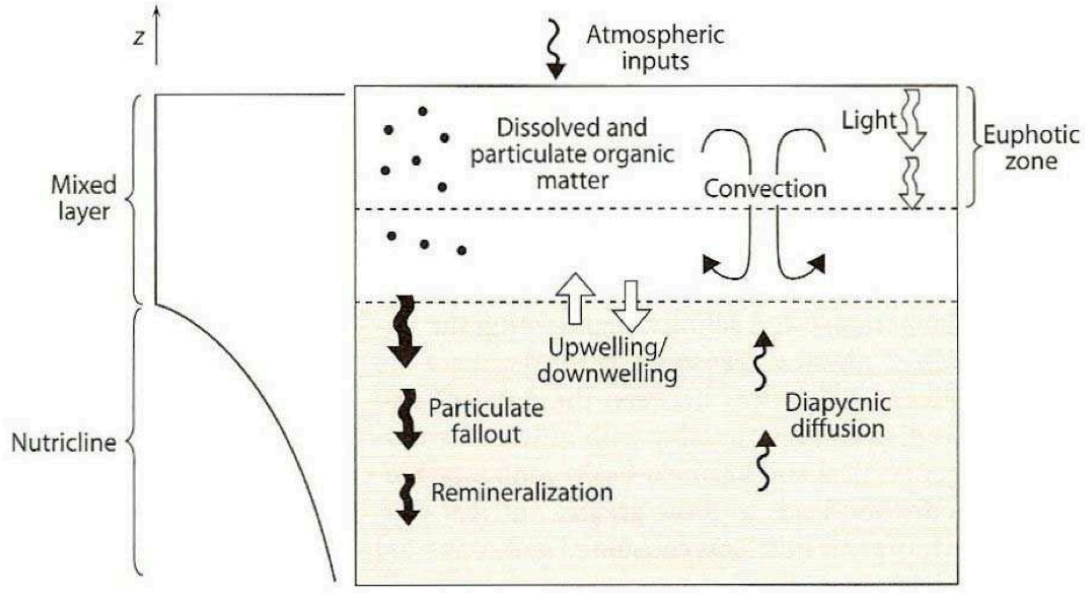

Figure 1.2 A schematic of the biological carbon pump, showing the processes involved in the movement of carbon through the water column. Figure reproduced from Williams and Follows (2003).

While the carbonate and microbial carbon pumps also contribute to the regulation of CO_2 partial pressure, they do so to a lesser extent and thus are only briefly described here. The carbonate pump is largely responsible for controlling the pH of seawater, through the balance between the three major inorganic forms of carbon (DIC): bicarbonate ion (HCO_3^-), carbonate ion (CO^{2-}_3) and aqueous carbon dioxide ($CO_{2(aq)}$), which includes carbonic acid (H_2CO_3). The effect of adding CO_2 to seawater increases the formation of H_2CO_3, HCO_3^- and H^+, which reduces the formation of and decreases the pH. This is important because decreases in pH in surface waters inhibits the ability of marine calcifying organisms, including planktonic species, to produce their calcium carbonate ($CaCO_3$), shells and skeletons (Fabry et al., 2008).

Conversely, the microbial carbon pump is associated with the recycling of dissolved and particulate organic carbon by bacteria, pico-plankton and

microzooplankton. While the microbial pump is responsible for recycling much of the organic carbon (as well as nitrogen and iron, which are discussed in sections 1.4.1 and 1.4.2 respectively) within the surface mixed layer the process generally increases in dominance below the euphotic zone, which contributes to the strong vertical gradient in carbon concentration between surface and deep waters.

The combined effect of the physical solubility and biological pumps, along with the carbonate and microbial pumps, regulates the rate of carbon export to the deep ocean, which is essential for the ocean's continued uptake of atmospheric CO_2 (Yool et al., 2007). For example, the sinking of surface water in the North Atlantic near Iceland and Greenland through thermohaline circulation is an important CO_2 sink driven by both the solubility and biological carbon pump associated with the spring phytoplankton bloom. The Southern Ocean, however, has been identified as the largest oceanic sink of natural and anthropogenic CO_2, driven by both the biological and solubility pumps (Caldeira and Duffy, 2000; Sigman and Boyle, 2000, Takahashi et al., 2002). The Southern Ocean is estimated to store around 50% of the global oceanic anthropogenic CO_2 inventory (Sabine et al., 2004), thus playing a disproportionately large role as a buffer for human driven increases in atmospheric CO_2 concentrations.

Although model predictions claim that oceanic CO_2 sinks are decreasing (Canadell et al., 2007), there is still much uncertainty surrounding the estimates of particle fluxes to the deep ocean (Gehlen et al., 2006), resulting in unbalanced carbon budget calculations (Burd, 2010). Long-term datasets and climate models indicate a trajectory of increasing global temperature as a result of rising atmospheric CO_2 concentrations, driving changes in the earth's climate (Watson and Orr, 2003). This in turn is expected to alter many environmental properties of the ocean (Feely et al., 2004; Sarmiento et al., 2004a; Doney, 2006) and strongly influence the effectiveness of many oceanic CO_2 sinks, including that of the Southern Ocean. Predicted changes in environmental properties as a result of global warming (Mitchell et al., 1995; Sarmiento et al., 2004a) are similarly

expected to drive shifts in species composition (Arrigo et al., 2010) with implications for the effectiveness of the marine CO_2 sink. For example, phytoplankton species show different adaptive capabilities to changing light intensity under different mixing regimes, thus increased surface stratification could result in the dominance of high light adapted species (Arrigo et al., 2010). These changes in species composition may in turn impact the efficiency of the biological carbon pump through changes in particle formation and sinking rates, while also affecting the transfer of energy across trophic levels and the efficiency of the food web.

1.3 The Southern Ocean

The Southern Ocean links the circulation of all the world's oceans (Rintoul, 1991) and plays an integral role in the regulation of CO_2 through the physical forcing of wind-driven mixing, surface heating and stratification (Sigman and Boyle, 2000) and the biological activity of plankton and bacteria (Takahashi et al., 2002). It is responsible for ~33% of the global organic carbon flux to the deep ocean (Schlitzer, 2002) and is considered one of the most important oceanic CO_2 sinks (Metzl et al., 1999; Caldeira and Duffy, 2000; Sigman and Boyle, 2000, Takahashi et al., 2002). In addition, the Southern Ocean physical and biological pumps, along with the global ocean thermohaline circulation (e.g. sub-Antarctic Mode Water and Antarctic Intermediate Water formation, see Talley et al., 2008), play an important role in regulating the supply of nutrients to thermocline waters of the entire Southern Hemisphere as well as the North Atlantic (Sarmiento et al., 2004b). The Southern Ocean in turn plays a large role driving low latitude productivity (Sigman and Boyle, 2000).

Even so, adequate knowledge of many Southern Ocean processes still eludes us and it is by far the most under studied of the world's oceans due to logistical difficulties involved in *in situ* data collection over large temporal and spatial scales. Thus the factors regulating the observed variability in CO_2 fluxes are poorly understood (Hiscock et al., 2007). This lack of field data has necessitated the use of satellite and model data to improve our understanding of this complex region. For example, long-term datasets and climate models suggest that increased surface warming and freshening in the Southern Ocean will result in stronger surface mixed layer stratification, which may reduce nutrient supply to the euphotic zone and hinder phytoplankton growth (e.g. Bopp et al., 2001). Alternatively, shallower mixed layer depths might improve the light environment consequently improving phytoplankton growth and associated carbon export, providing that nutrients are not limiting (Boyd et al., 2002; Taucher and Oschlies, 2011). Despite abundant macronutrients in much of the Southern Ocean, however, light and iron co-limitation of phytoplankton growth is common (Maldonado et al., 1999; Van Leeuwe and De Baar, 2000; Moore et al.,

2007a,b; Pollard et al., 2009). This in part accounts for the region's high nutrient low chlorophyll (HNLC) characteristics (Chisholm and Morel, 1991).

Due to the important role the Southern Ocean plays in the global carbon cycle, the difficulties involved in data collection and the high spatial and temporal variability of the region, recent advances in and increasing reliance on satellite data have expanded our observational capacity and improved our knowledge of the factors driving this variability. However, while satellite remote sensing provides broad-scale data for investigating patterns of phytoplankton variability, regular validation with *in situ* observations is vital, if we are to increase the accuracy of capturing the biogeochemical variability of the ocean through remotely sensed optical properties. Remotely sensed optical properties are essentially a measurement of the proportion of solar radiation entering the ocean that is reflected back out to space. This reflectance can be related to the *in situ* optical measurements of absorption, backscattering and beam attenuation (defined below in Section 1.6), which are defined by the optical properties of seawater and its constituents (i.e. dissolved, suspended and particulate). The increasing dependence on remote sensing and autonomous instruments (e.g. gliders and bio-optics floats) and the growing need for regional specific satellite algorithms highlights the relevance of this study, which investigates empirical relationships between *in situ* optical properties, phytoplankton ecology and marine biogeochemistry in the Weddell Gyre. This regional study uses optical measurements to explore some of the potential drivers of phytoplankton physiology and their role in the Southern Ocean biological carbon pump.

1.4 Factors controlling phytoplankton growth and community structure

Phytoplankton growth in the HNLC waters of the Southern Ocean is primarily controlled by two mechanisms: namely, the 'bottom-up' controls of light, iron and silicate availability (Moore and Abbott, 2002; Boyd et al., 2007; Moore et al., 2007b; Arrigo et al., 2008); and the 'top-down' control of grazing by micro- and macro-zooplankton (Smetacek et al., 2004; Behrenfeld, 2010). Both mechanisms regulate the seasonal fluctuations in phytoplankton biomass and productivity. These controlling factors combined determine the strength of the biological pump and the potential for carbon export.

There has been a wealth of work produced over the past few decades exploring the environmental (bottom-up) and biological (top-down) factors that influence the growth and distribution of phytoplankton (Sarthou et al., 2005; see review by Boyd et al., 2010). How these factors interlink is often uncertain (Van Leeuwe et al., 2007; Cullen and Boyd, 2008) thus each factor discussed below may have additional or variable influence on phytoplankton production in the presence of other limiting factors (Saito, et al., 2008; Boyd et al., 2010).

1.4.1 Macronutrients

The most important macronutrients utilized by phytoplankton are, nitrogen (N), silicate (SiO_4) and phosphate (PO_4). Despite high concentrations of these nutrients in the Southern Ocean, phytoplankton biomass is low (Bathmann et. al., 1997; Boyd et al., 2002; Arrigo et al., 2008).

Nitrogen is taken up by phytoplankton in three forms: nitrate (NO_3), ammonium (NH_4) and urea, with preferential uptake by all phytoplankton generally following the sequence: NH_4>urea>NO_3 (Glibert et al., 1982a; Probyn et al., 1985). This order of preference is established on the basis of the energetic requirements needed to assimilate each of the nitrogenous nutrients. As it requires more energy to assimilate NO_3 than the reduced forms of N (NH_4 and

urea), phytoplankton preferentially assimilate the latter. Where reduced N supply cannot meet N demands, phytoplankton take up NO_3, which in any case is typically available in much higher concentrations in the Southern Ocean (see review by Cochlan, 2008).

Phytoplankton production as measured by N uptake is described as either 'new' (export) or 'regenerated' (recycled) production (Dugdale and Goering, 1967; Eppley and Peterson, 1979; Glibert et al., 1982a,b) depending on the form of N utilized. New production in the upper ocean is based on N sources that are 'new' to the euphotic zone, that require replenishment from below the thermocline (NO_3) or via aerosol inputs (NO_3 and NH_4 deposition) or through N_2 fixation by diazotrophs (Luo et al., 2003; Zender et al., 2003; Cochlan, 2008). Regenerated production on the other hand is based on recycled N within the euphotic zone such as NH_4, urea and amino acids derived from phytoplankton detritus, zooplankton fecal pellets and through bacterioplankton and microzooplankton activity.

While the distinction between 'new' and 'regenerated' production may be compromised by nitrification in the euphotic zone (Lipschultz, 2001; Falkowski et al., 2003; Capone et al., 2005; Yool et al., 2007), this is not considered to be significant in the NO_3-rich polar oceans (Fernandez and Raimbault, 2007; Yool et al., 2007). In high latitude regions such as the Southern Ocean, where the flux of NO_3 to the surface is high and nitrification in surface waters is considered negligible, distinguishing between new and regenerated production is relatively uncomplicated.

Partitioning between new and regenerated N uptake can be summarised in the form of f-ratios. The f-ratio describes the proportion of new production based on NO_3 uptake (ϱNO_3) relative to the uptake (ϱ) of all forms of N (f-ratio = $[\varrho NO_3]/[\varrho NO_3 + \varrho NH_4 + \varrho Urea]$). As such, the f-ratio gives an indication of the proportion of production that is potentially available to higher trophic levels or exported to the deep ocean (Eppley and Peterson, 1979; Savoye et al., 2004; Lucas et al., 2007; Cochlan, 2008). The utility of the f-ratio assumes seasonal

steady-state, no storage of N in surface waters and that nitrification in euphotic waters is minimal (e.g. Lucas et al., 2007). Measurement of N uptake rates using stable ^{15}N-isotopes (Dugdale and Goering, 1967) provides estimates of phytoplankton production (in terms of N) and potential carbon export rates based on the f-ratio (Eppley and Peterson, 1979; Savoye et al., 2004), assuming a Redfield C:N ratio of 6:1. In short, where the f-ratio is high (e.g. f = 0.6), this indicates that 60% of phytoplankton N demands are met by new N, typically NO_3, and that 60% of the production is exported from the euphotic layer. Conversely, where f = 0.1, for example, this would imply that 90% of the production is based on regenerated N and that just 10% of the fixed N is exported below the seasonal mixed layer.

Phosphate (PO_4) is present at low concentrations, typically <1-2 μmol l^{-1}, but it rarely limits phytoplankton growth (Koeve, 2001), and is unlikely to play a dominant role in limiting primary production in the Southern Ocean. It is, however, known that N_2 fixation rates by diazotrophs are strongly controlled by PO_4 and iron availability (Hutchins and Fu, 2008; Moore et al., 2009), but this process does not occur in the HNLC Southern Ocean. A consideration of Redfield N:P stoichiometry by and within different phytoplankton taxa (e.g. *Phaeocystis* vs diatoms), however, reveals a complex discussion of how phytoplankton can manipulate ambient N:P ratios (Arrigo et al., 2002). In the context of the typical HNLC scenario of the open Southern Ocean, the discussion has more academic rather than practical implications and other nutrients are considered to exert far stronger influences.

Silicate concentrations in the Southern Ocean for example exhibit a very marked concentration gradient from north to south. North of the Antarctic Polar Front (APF) at ~50 °S, SiO_4 concentrations are low (<2-4 μmol l^{-1}) and may limit diatom growth, or certainly the proliferation of substantial diatom blooms. Surface waters south of the Polar Front, on the other hand, are characterized by SiO_4 concentrations that frequently exceed 5-20 μmol l^{-1}, which rises to >100 μmol l^{-1} close to the Antarctic continent. Thus phytoplankton are not generally limited by SiO_4 south of the APF, but can become so, for diatoms in summer and autumn, in

sub-Antarctic waters north of the APF (Nelson et al., 2001; Coale et al., 2004; Boyd et al., 2010).

This is because diatoms require biogenic SiO_4 for the formation of their opaline frustules; which being denser than water and other organic matter, promote sinking through aggregate formation, thus exporting much of the carbon associated with the diatom cells from the surface to the deep sea (Armstrong et al., 2002). SiO_4 limitation in the sub-Antarctic has been shown to lead to community shifts from diatom to non-diatom dominance, which have implications for food webs, export rates and CO_2 sequestration (Brzezinski et al., 2003; Sarmiento et al., 2004b). Furthermore, Si:N ratios appear to be controlled by iron availability, as shown by Moore et al., (2007b) in the Crozet natural iron bloom experiment. Both experimental and *in situ* observations exhibited a marked decrease in Si:N removal ratios under enhanced iron concentrations, which were further reduced under higher irradiance (Moore et al., 2007b).

1.4.2 Iron

The iron hypothesis was first proposed by Martin (1991) who hypothesized that increased iron supply to the Southern Ocean during the last glacial maxima resulted in increased phytoplankton growth rates, which lowered atmospheric CO_2 concentrations. The argument is however partly flawed, because changes in atmospheric CO_2 concentrations at that time were not solely due to phytoplankton growth rates, but caused indirectly by Milankovitch orbital forcing (Milankovitch, 1930; Imbrie et al., 1993).

Even so, the absence of a continental land mass makes the Southern Ocean one of the most iron impoverished of the world's oceans (De Baar et al, 2005; Boyd et al., 2007; Pollard et al., 2009), where surface iron concentrations are at pico-molar rather than nano-molar concentrations.

Iron is a particularly important micronutrient within photosystems I and II (Strzepek et al., 2012; Behrenfeld and Milligan, 2013), it is instrumental in the

biosynthesis of chlorophyll (chl-a) and is suggested to influence colony formation in *Phaeocystis* species (Hutchins et al., 2002). Iron is also a critical component of the enzymes nitrate and nitrite reductase, which allows the uptake of NO_3 by phytoplankton and the subsequent intra-cellular reduction to NH_4, the precursor for protein synthesis. It is the absence of dissolved iron in surface waters that is thought to contribute to the unused pool of NO_3 (~20-25 μmol l^{-1}) in surface waters of the HNLC Southern Ocean (e.g. Lucas et al., 2007; Cochlan, 2008)

In a recent global compilation of dissolved iron (dFe) measurements, Tagliabue et al. (2012) report high variability in surface dFe concentrations between regions (Antarctic versus sub-Antarctic) and across the different ocean basins of the Southern Ocean. They attribute this variability to the different processes that drive dFe in these regions. For example, in the Atlantic sector dFe in the upper 100 m was higher in the Antarctic region (0.47±0.69 nM) compared to the sub-Antarctic region (0.30±0.55 nM), while the Atlantic basin was characterized by higher dFe concentrations than both the Indian and Pacific basins. These regional and basin differences were associated with differences in biological activity and degree of Fe inputs (Tagliabue et al., 2012). Surface waters generally had lowest dFe concentrations (0.1-0.5 nM) due to biological activity, but increased with depth below the mixed layer (>0.4 nM) due to bacterial remineralization. Surface waters near the Antarctic continental shelf, however, were enriched (0.61±1.14 nM) relative to open ocean waters (0.31±0.45 nM), due to the influence of seasonal melting of sea-ice (Klunder et al., 2011).

While spatial variability in dFe supply to surface waters has a significant impact on the distribution of phytoplankton blooms, the initiation of a bloom is strongly driven by temporal (seasonal and episodic) variability of dFe inputs. For example, through aeolian inputs associated with rain events depositing particulate Fe originating from Patagonia (Klunder et al., 2011), as well as melting of sea-ice and icebergs in spring and summer releasing both dFe and particulate Fe (Grotti et al., 2005; Klunder et al., 2011). Continental shelf sediments provide additional Fe inputs to the surface through re-suspension during deep winter mixing or upwelling events (Boyd et al., 2012). In some areas, however, the extension of the Antarctic ice-sheet restricts the Fe supply from the

continental shelf to surface waters adjacent to the ice-sheet, thus concentrations tend to decrease from the open ocean to the shelf (Klunder et al., 2011). Fe in particulate form whether from melting sea-ice or the re-suspension of shelf sediments is not accessible to phytoplankton but may provide an additional source of dFe through photochemical breakdown during suspension in surface waters (Boyd et al., 2012).

Furthermore, higher production rates were associated with elevated dFe concentrations in the Antarctic compared to the sub-Antarctic may be explained by lower primary production rates due to ice cover and low light levels for half the year, while the higher concentrations in the Atlantic were associated with higher iron inputs through aeolian deposits, compared to those for the Indian and Pacific (Tagliabue et al., 2012).

Phytoplankton growth in the Southern Ocean is however, not limited by iron alone. Meso-scale iron enrichment experiments in the Southern Ocean (De Baar et al., 1990; Coale et al., 2004; Boyd et al, 2007; Pollard et al., 2007, 2009) show strong evidence that phytoplankton growth is controlled by iron-light co-limitation. For example, during the SOFeX experiment, iron addition increased primary production, but the potential for a large bloom was not realized due to deep mixed layers (>40 m) and self-shading which resulted in light limitation of phytoplankton growth (Coale et al., 2004). More recent work has examined an iron induced diatom bloom in an Antarctic Circumpolar Current (ACC) eddy and reported the successful export of at least half of the algal biomass below 1000 m (Smetacek et al., 2012), highlighting the important link between iron supply and carbon export under favorable light conditions. Larger cell sizes promoted by iron availability (Karsh et al., 2003) also result in greater sequestration of CO_2 (Watson et al., 2000; Pollard et al., 2009).

The distributions of macronutrients, iron and primary production are not uniform in the Southern Ocean but delimited by the fronts of the ACC into zones of similar physical, chemical and biological properties, with similar seasonal evolutions (e.g. Treguer and Jacques, 1992; Trull et al., 2001; Pollard et al., 2002;

Thomalla et al., 2011). North of the sea-ice zone in the ACC, low surface chl-a concentrations (~0.2-0.5 mg m^{-3}) are largely due to deep mixing and iron limitation (Boyd et al., 2000; Sokolov and Rintoul, 2007), while enhanced productivity is associated with increased iron supply at oceanic fronts (Moore and Abbott, 2000; Sokolov and Rintoul, 2007), sub-Antarctic islands (Pollard et al., 2007, 2009) and continental shelves (Fitch and Moore, 2007). The mechanism of iron supply is thought to be upwelling at oceanic fronts (Sokolov and Rintoul, 2007), deep mixing at the continental shelf (Johnson et al., 1999) and dust deposition (Cassar et al., 2007) and run-off from volcanic iron-rich sub-Antarctic islands (Pollard et al., 2009). Highest chl-a concentrations (~2-4 mg m^{-3}) are generally found in the high light and iron regions of the summer marginal ice zone (MIZ)(Arrigo and van Dijken, 2003). In the MIZ, melting sea ice in spring and early summer provides inputs of iron (Grotti et al., 2005) and increases stratification, causing subsequent increases in both iron and light availability (Smith and Nelson, 1986), and results in phytoplankton blooms.

1.4.3 Light and Mixed Layer Depth

Phytoplankton require sufficient solar radiation within a specific spectrum (400-700 nm) in order to photosynthesise, fix CO_2 and metabolize nutrients, but they may also be inhibited if light levels are too high (Strzepek et al., 2012; Behrenfeld and Milligan, 2013). Photosynthetically active radiation (PAR) is a measure of light that is available for phytoplankton production, which is restricted to the euphotic zone (Z_{euph}) defined as the depth at which PAR is >1% or >0.1% of surface irradiance (Falkowski and Raven, 1997). The depth of Z_{euph} varies significantly between water types (open ocean versus coastal ocean, oligotrophic versus eutrophic) and depends on the dissolved and suspended constituents of the water. The particulate portion, consisting of phytoplankton and detritus, has a significant impact on the absorption and scattering of light that penetrates the surface, which reduces the depth of Z_{euph}, and increases light limitation with depth.

The mixed layer depth (MLD) may be defined as a homogenous layer that forms

a boundary between the deep ocean and the atmosphere (Brainerd and Gregg, 1995). The dominance of turbulent mixing driven by surface heating, wind-stress and fresh water influx within this layer maintains virtually uniform temperature, salinity and density characteristics (Wang et al., 2010). Wind stress has a profound effect on the deepening or shoaling of the surface mixed layer and therefore controls the extent to which phytoplankton cells are mixed through the euphotic zone into the aphotic layer. This concept is central to the critical depth models of photosynthesis (Nelson and Smith, 1991, Sverdrup 1953), whereby the mixed layer needs to be shallower than a critical depth to allow net positive population growth.

The effect of deep mixing is especially relevant in the Southern Ocean, where rough weather and turbulent seas frequently mix the water column to depths of 50-100 m in summer (Nelson and Smith, 1991; Knox, 1994). Deep MLDs are especially prevalent during winter when strong surface winds and heat loss deepens the MLDs to 200-400 m (Thomalla et al., 2011). Particularly shallow MLDs (~20 m) are associated with fronts, eddies and the MIZ where summer ice-melt increases freshwater flux. The resultant increased stratification and shallow MLDs drive increased phytoplankton production (Allanson et al., 1981; Lutjerharms et al., 1985; Bidigare et al., 1986; Nelson and Smith, 1991; Dower and Lucas, 1993), which in the presence of sufficient iron may be dominated by new production, with higher potential for carbon export (Cochlan, 2008).

1.4.4 Temperature

Changes in temperature are thought to have an impact on phytoplankton metabolic rates such that low temperatures may at times limit phytoplankton growth (Raven and Geider, 1988, Sosik and Mitchell, 1994) and photosynthesis (e.g. review by Davidson, 1991). Yet, phytoplankton adaptations to variable temperatures are strong and polar species have had ~15 million years to adapt to low temperatures in the Southern Ocean. A strong temperature gradient occurs between the warmer sub-Antarctic waters (5-10 °C) to the north and the colder more variable Antarctic waters (between ~5 °C and -1.8 °C) to the south

of the Antarctic Polar Front. This rapid latitudinal change in temperature, reaching the freezing point of seawater (-1.8 °C) in places, has a direct impact on phytoplankton physiology. For example, phytoplankton maximal growth rate may be described as a function of temperature, which doubles with every 10 °C increase (Eppley, 1972). In contrast, phytoplankton grown at low temperatures are less efficient at utilizing available light (Tilzer et al., 1986) and their ability to repair damage to their photo-receptors when recovering from photo-inhibition, is reduced (Alderkamp et al., 2010). Thus, while temperature is not considered a strong driver of phytoplankton biomass and community structure in the Southern Ocean, it may act as an additional factor controlling the upper limit of phytoplankton growth and has been shown to be a strong driver of biogeographical zonation of some species (Boyd et al., 2010).

1.4.5 Grazing

In the iron-limited Southern Ocean, grazing by meso- and micro-zooplankton may control the biomass of slow-growing phytoplankton that are unable to escape grazing pressure (Smetacek et al., 2004; Behrenfeld, 2010). Grazers also play a strong role in driving community structure, particularly with regard to cell size (Schoemann et al., 2005).

Low iron concentrations favour the growth of small cells, which absorb nutrients more efficiently as a result of their high surface to volume ratio (Twining et al., 2004). Reduced cell size, on the other hand, encourages grazing by micro-zooplankton (who have similar growth rates to their phytoplankton prey) and are thus able to maintain the abundance of small cells at relatively low concentrations in much of the Southern Ocean (Froneman et al., 1996; Irigoien et al., 2005; Schoemann et al., 2005). Consequently, low chl-a concentrations in the sub-Antarctic and the adjoining permanent open ocean zone consist year-round of "grazer-controlled populations in an iron-limited ecosystem" (Price et al., 1994). Conversely, in regions of the Southern Ocean that are both iron and light replete, larger cells are expected to have their requirements for growth met. Under these nutrient replete conditions, large cells escape grazing pressure by

macro-zooplankton, due to relatively faster growth rates, resulting in large cell dominated blooms (Schoemann et al., 2005), which may be moderated by microbial uptake and recycling of iron.

The microbial food-web plays a key role in the rapid recycling of much of the iron that is required by plankton in the upper ocean (Strzepek et al., 2005), while microbes may also control diatom bloom dynamics through their more efficient iron uptake rates (Boyd et al., 2012). Heterotrophic bacteria and pico-phytoplankton (<1 um) have been reported to dominate carbon biomass and contribute between 70 and 83% to the Fe pool (Strzepek et al., 2005; Boyd et al. 2012). The proportion of this biogenic pool that is regenerated, however, depends on the selective grazing by microzooplankton. For example, Strzepek et al. (2005) show that in the sub-Antarctic, only 25% of biogenic iron from pico-phytoplankton was recycled (compared to 90% for bacteria) as a result of grazing. Furthermore, the fate of this recycled iron, appears to differ between herbivory and bacterivory pools. Such that a higher proportion (~3-fold) of dissolved iron released during herbivory was taken up by the community compared to that taken up from the bacterivory pool. This may indicate that iron released by herbivory is more bioavailable to phytoplankton, but also that bacterivory releases a higher proportion of iron than herbivory. When both iron supply and demand are assessed, estimates suggest that iron regeneration through grazing could supply 30 to >100% of biogenic iron demand in the sub-Antarctic (Strzepek et al., 2005).

While this microbial recycling of iron maintains a large portion of the initial iron pool in the surface mixed layer, much of it is likely to be unavailable to diatoms, due to it being bound to strong ligands and the fact that diatoms have a lower affinity for recycled iron relative to smaller cells (Boyd et al., 2012). Thus, the efficient recycling and subsequent efficient uptake of regenerated iron by small cells, may control diatom growth, particularly in the latter stages of a bloom, with significant implications for biogeochemical cycling and carbon sequestration (Finkel et al., 2010; Boyd et al., 2012).

1.5 Phytoplankton physiology, community structure and their role in the biological pump

Over millennia phytoplankton species have adapted to survive under certain conditions. When these conditions change, becoming less favourable for a particular species (e.g. light or nutrient limitation), another more resilient, well-adapted species may gain a competitive advantage. Shifts in species dominance modify the elemental composition of particulate material (Finkel et al., 2010), define the dominant cell size and alter the pathway of primary production through the food web. As such, community structure influences the proportion of phytoplankton biomass exported to deep waters (Finkel at al., 2010). For example, large cells are heavier, sink faster and are less prone to grazing and therefore play a greater role in removing carbon from the surface waters, in the form of POC. Conversely, smaller cells have slower sinking rates, are influenced by higher grazing rates and are more likely to be consumed or remineralized in the upper layers, so retaining carbon in the euphotic zone (Longhurst, 1991; Lal, 2008).

Phytoplankton communities in the Southern Ocean are largely dominated by pico- (<2 μm) and nano- (2-20 μm) phytoplankton, consisting of autotrophs, bacteria and heterotrophic protists, which form what is known as the microbial loop (Azam et al., 1983). New production and potential carbon export, however, is characterized by large micro-phytoplankton (20-200 μm) such as diatoms, which are less abundant than small pico- and nano-plankton, but still play an important role in the export of carbon due to their sheer size, affinity for forming aggregates and resultant higher sinking rates (Smetacek, 1985; De La Rocha and Passow, 2007; Richardson and Jackson, 2007). Phytoplankton adaptation and diversification in the Southern Ocean, in response to the widely varying physical-chemical regimes, has resulted in the highest percentage of endemism among diatom species of any oceanic region (Priddle and Fryxell, 1985). Diatoms are believed to be major contributors to carbon export in the Southern Ocean, but this does not always apply. In general, large, heavily silicified diatoms are thought to escape grazing pressure and effectively form aggregates due to chain

forming tendencies and the common presence of spines/setae. This results in a high proportion of living cells being removed from the surface oceans when they die.

It has been shown that shifts in phytoplankton species dominance in Ross Sea communities are driven by changes in MLD (Arrigo et al., 1999). Diatoms prefer the highly stratified, high light, shallow waters (5-20 m) near the ice shelf, while *Phaeocystis antarctica* dominates in areas of deeper mixing (25-50 m). The two different communities have important implications for rates of primary production, trophic webs and potential for CO_2 drawdown. Diatoms are slower growing than *P. antarctica*, resulting in lower production and carbon uptake rates (56% more C taken up per mole PO_4 by *P. antarctica*). Consequently, the authors predict a decline in CO_2 drawdown with climate driven increases in stratification, as a result of a shift to a more diatom-dominated community (Arrigo et al., 1999).

While species dominance can strongly influence phytoplankton cell size and distribution, changes in cell size may also result from physiological responses to environmental drivers (Finkel et al., 2010). There is a growing awareness for the importance of defining phytoplankton community size distribution not only in observational research but also in modeling (Doney, 1999), where size class partitioning has been applied to phytoplankton communities in several biogeochemical models (Armstrong, 1999; Doney, 2001; Denman, 2003). Increasing observational studies, experimental research and biogeochemical model development will lead to a sounder understanding of the response of phytoplankton community size structure to different physical-chemical regimes and predicted climate driven changes. This will enhance our knowledge of the biological pump and the ocean's proficiency as a continuing CO_2 sink (Kohfeld et al., 2005).

1.6 Bio-optics as a tool for investigating phytoplankton variability

The difficulties involved in collecting *in situ* observational data in the remote Southern Ocean has rendered satellites an essential tool on the quest for a better understanding of phytoplankton phenology and the drivers of variability (e.g. Behrenfeld and Boss, 2003; Dierssen et al., 2006; Behrenfeld et al., 2009). In order to exploit a wealth of remote sensing data (in the form of apparent optical properties - AOPs) from a phytoplankton physiology and community structure perspective, we need to first develop and be able to interpret relationships between inherent optical properties (IOPs) and *in situ* observations of the particle field, which ultimately drives the optical signal visible from space (IOCCG, 2006).

1.6.1 The underwater light field

Photosynthetically available radiation (PAR) is a measure of the irradiance (E) available to phytoplankton within the water column. Irradiance, and hence PAR, decreases exponentially with depth as a result of absorption and scattering by suspended particles (e.g. mineral, organic and detrital), dissolved constituents and the water itself (Morel, 1974). While the attenuation of light is rapid in the upper 5-10 m, it becomes more constant below 10 m, where the spectral distribution changes little with depth (Morel, 1974).

Roughly half the solar radiation in the infrared (>800 nm) is absorbed just below the surface, where it is responsible for surface layer heating (Morel, 1974), but becomes negligible below 1 m. The orange-red spectrum (600-700 nm) makes up around 1/3 of the remaining solar radiation, but is quickly absorbed and generally absent below 10 m. As a result, within the top 10 m, around 2/3 of total solar radiation penetrating the sea surface is absorbed, which along with wind-driven turbulence is responsible for the warm surface mixed layer – a vital pre-requisite for primary production (Falkowski and Woodhead, 1992; Morel and Antoine, 1994). Due to this strong absorption of light in the red wavelengths, the

remaining light penetrating the ocean, which is then backscattered, is blue. This backscattering of light is called upwelling irradiance (E_u), and causes the ocean to appear blue.

Phytoplankton utilize both upward (E_u) and downward (E_d) irradiance for photosynthesis and possess specialized carotenoid-protein complexes in order to absorb the green-blue wavelengths (400-550 nm) present below ~15 m in clear waters. In addition to absorbing light for photosynthesis, phytoplankton (being major contributors to the particle field of the open ocean) affect the direction, quantity and spectral shape of the irradiance within the water as well as the radiance transmitted back through the atmosphere where it is observed by satellite-based sensors as water-leaving radiance (L_w). Remote sensing reflectance (R_{rs}), the foundation of ocean colour radiometry (OCR), is equal to upward water-leaving radiance divided by down-welling irradiance ($R_{rs} = L_w/E_d$) (Figure 1.3), both of which depend on the wavelength, intensity and angular distribution of light. These properties of reflectance, radiance and irradiance along with the diffuse attenuation coefficient (how light changes with depth), are defined as apparent optical properties (AOPs). AOPs inform us about the colour and brightness of the ocean, how light changes with depth and describe the angular distribution of light in the sea (Bernard, 2009). By accounting for the effects of the atmosphere and ocean surface, and through the application of inverse reflectance algorithms and radiative transfer equations, AOPs can be linked to IOPs (Figure 1.3), which tell us about the constituents of the water (Preisendorfer, 1961; IOCCG, 2006). While measurements are relatively easy to acquire, the interpretation of AOPs in terms of constituents is difficult.

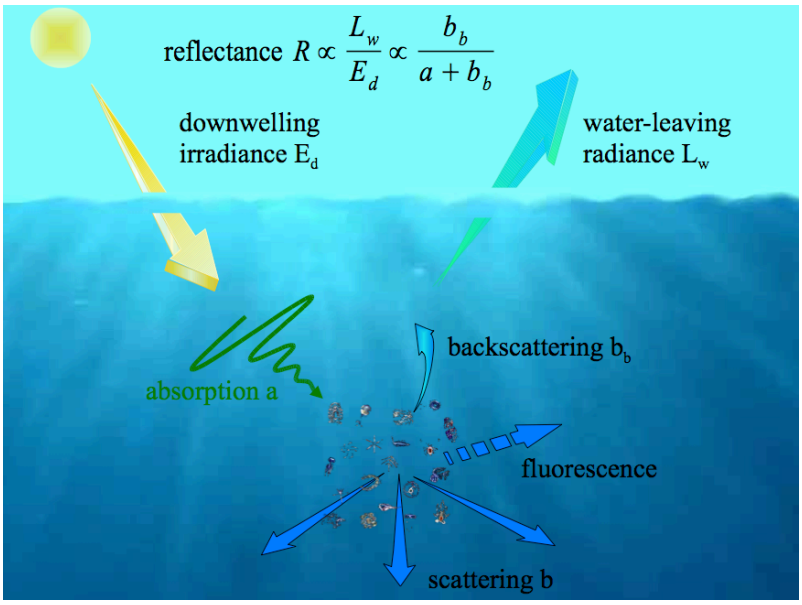

Figure 1.3 Diagram showing the interaction between light, the ocean and its constituents. The various AOPs (irradiance, radiance and reflectance) and IOPs (absorption, scattering and backscattering) are included. Figure reproduced from Bernard (2009).

1.6.2 Inherent Optical Properties

Inherent optical properties are those properties of a medium that depend on its composition (particulate, suspended and dissolved) but are independent of the incoming light, and cause changes in light intensity, spectral composition and angular distribution (Preisendorfer, 1961). There are two possible pathways of light within water; it is either absorbed or scattered. Absorption results in the loss of a photon, whereas scattering causes its re-direction. The two fundamental IOPs are thus, absorption (a) and the volume scattering function (β). The remaining IOPs; total scattering (b), backscattering (b_b) and beam attenuation (c = a + b), are commonly derived from these two. Detailed descriptions of all IOPs have been included below, however for this study only beam attenuation and backscattering were measured.

1.6.2.1 Absorption

The absorption of light by water and its constituents (i.e. phytoplankton, detritus and Gelbstoff) have differential effects on light across the visible spectrum (see

Figure 1.4), with phytoplankton biomass and associated chl-a concentrations influencing absorption to the first order (Prieur and Sathyendranath, 1981). Specific absorption coefficients for phytoplankton types have been distinguished from detritus and other components based on their distinct characteristics of spectral shape (Morrow et al., 1989; Roesler et al., 1989; Sathyendranath et al., 2004; Sathyendranath and Platt, 2007; see Figure 1.6 for example) and pigment spectral properties (Bidigare et al., 1986; Barlow et al., 1993). Strong absorption by particulate and dissolved constituents occurs in the blue wavelengths, while the red wavelengths are dominated by the absorption of water and the second smaller peak of chl-a at 670 nm (Figure 1.4). The strong absorption of pure water in the red and near infra-red has an absorption co-efficient measured at 0.015 m^{-1}; coloured dissolved organic matter (CDOM) or 'Gelbstoff' absorbs strongest around 440 nm, at 0.05 m^{-1}; Phytoplankton specific absorption peaks at around 440 nm and ranges from 0.025 m^{-1} mg Chl-a^{-1} in productive waters (1 mg Chl-a m^{-3}) to 0.005 m^{-1} for unproductive waters (0.2 mg Chl-a m^{-3}). Detritus (from the breakdown of phytoplankton), absorbs much like Gelbstoff but with some additional shoulders due to the breakdown of phaeopigments (see Falkowski and Woodhead, 1992).

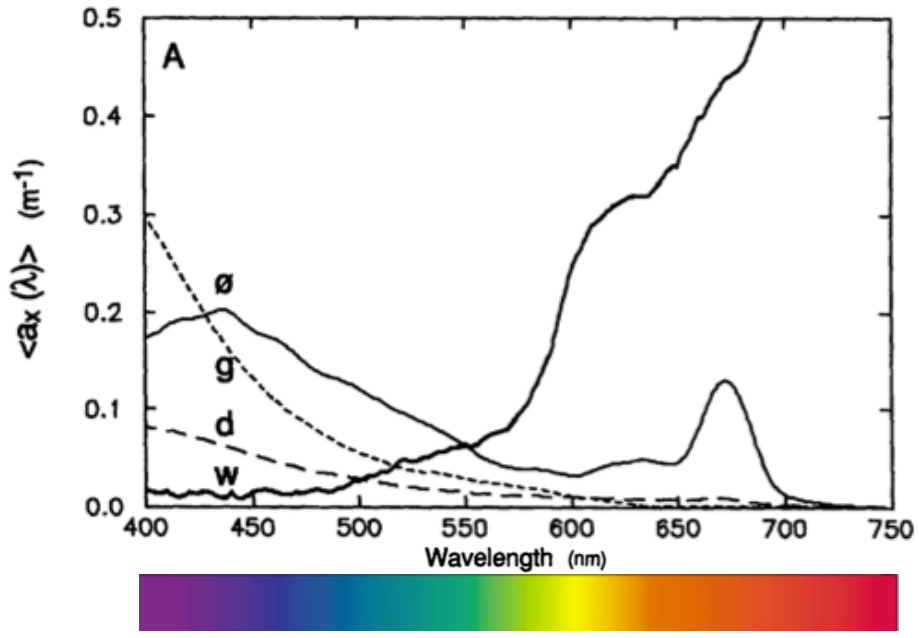

Figure 1.4. Mean spectral absorption by phytoplankton (Ø), Gelbstoff (g), detritus (d) and pure water (w) – in Smith and Baker (1981). Figure reproduced from Roesler et al. (1989).

1.6.2.2 Scattering & backscattering

Scattering by water occurs equally in all directions – unlike by particles where 0.1-2% of scattering occurs at > 90 ° (Morel, 1974) – but overall has a very small impact on the light field when compared to absorption. Backscattering, which is roughly equal to half of scattering, makes a significant contribution to the upwelling irradiance that is observed by ocean colour sensors (Falkowski and Woodhead, 1992).

The backscattering coefficient (b_b) is not affected by dissolved constituents and thus is equal to the sum of backscattering by particles (b_{bp}) and that of water (b_w) (IOCCG, 2011), expressed as:

$$b_b(\lambda) = b_{bw}(\lambda)+b_{bp}(\lambda)$$

where λ is the wavelength of irradiance measured (i.e. at 470 nm and 650 nm in this study). By accounting for b_{bw} an estimate of particle concentration, can be attained from b_{bp}.

Backscattering by pure water is strongest in the blue wavelengths, while particles backscatter stronger in the red (Morel, 1974). Such that, increased particle concentrations may be associated with higher backscattering in the red wavelengths, however, this is strongly dependent on particle size, shape and composition (e.g. organic vs mineral). For example, spectral b_{bp} may also provide a proxy for particle size, which has been shown using remote sensing reflectance data (Loisel et al., 2006; Kostadinov et al., 2009) and spectral b_{bp} from glider data (Niewiadomska et al., 2008).

1.6.2.3 Beam attenuation

Beam attenuation may be described as the loss of light energy, due to a combination of absorption and scattering, as it propagates through a medium. The beam attenuation coefficient, c (m^{-1}) measured using a transmissometer, is thus a measurement of the loss of photons as a beam passes through a known

path length of water (further discussed in Section 2.2.8.1). Once the effect of seawater has been removed, c gives an indication of the concentration of dissolved and suspended material in the water (IOCCG, 2011). For example, in highly productive or murky waters, measurements of c will be higher than in clear waters. In Case I waters, which are generally defined as open ocean waters where the concentration of phytoplankton is higher than that of other particles (Morel and Prieur, 1977), such as in the Southern Ocean, phytoplankton are considered the primary determinant of changes in the attenuation of light through the water column. (Bishop, 1999; Behrenfeld and Boss, 2003). Particulate beam attenuation or c_p can thus be used to determine the concentration of phytoplankton cells, and their associated detritus, within the water.

The spectral shape of beam attenuation varies with particle size, while differences in shape and roughness (Pak et al., 1970) increase the observed effective size of particles. Thus, a linear relationship between c_p and particle concentration will only result when the combined effects of size, shape and index of refraction are negligible (Baker and Lavelle, 1984).

1.6.3 *In situ* IOPs and the impacts of POC and phytoplankton cell size, species dominance and physiology

Linking IOPs to *in situ* measurements of particulate organic carbon (POC) and phytoplankton cell size, species dominance and physiology is important because a significant relationship between these parameters will enable the use of bio-optical data (*in situ*, autonomous platforms and remote sensing observations) to infer POC and phytoplankton community structure and physiology. As a consequence, the retrieval of high-resolution biogeochemical data from these bio-optical platforms will provide us with a better understanding of phytoplankton dynamics over broader spatial and temporal scales.

By quantifying phytoplankton community structure and their key physiological responses (e.g. cell size, functional type, elemental stoichiometry) to

environmental forcing, which in turn effect marine food-webs and the carbon-climate system (Finkel et al., 2010), we may better predict marine ecosystem responses to environmental and climate change. Developing the parameters that define these phytoplankton characteristics, through the application of IOPs as proxies, will improve our ability to observe not only the variability in phytoplankton biomass but may also provide detailed information on the cell size distribution, species composition and elemental stoichiometry of the phytoplankton community. These physiological traits may potentially constrain phytoplankton growth rates, food web structure and biogeochemical cycling of carbon (Finkel et al., 2010). Thus, understanding their response to climate change will improve our understanding of the biological pump and the oceans role as a long-term CO_2 sink (Kohfeld et al., 2005). Furthermore, the use of IOPs as proxies will enable us to explore the intricacies of phytoplankton dynamics across oceanic ecosystems, over decadal time scales (remote sensing) and at high frequency in both time and space (autonomous floats and gliders).

Previous studies have shown strong relationships between IOPs and the concentration and size distribution of particles (Baker and Lavelle, et al., 1984; Boss et al., 2001; Coitti et al., 2002). While yet others have used IOPs to infer physiological responses to nutrient and light limitation (e.g. Behrenfeld et al., 2009), derive information about phytoplankton functional types (e.g. Bricaud and Stramski, 1990, 1995) and estimate bulk measurements of particulate organic carbon (POC) (Gardner et al., 2001). The significance of this study lies in the application and interpretation of these existing IOP-phytoplankton relationships using a small dataset from the Weddell Gyre. Thus contributing to the development of regional specific empirical relationships, which will provide a high-resolution, broad-scale method for investigating the variability of phytoplankton biomass, community structure and physiology. Finally, the interpretation of these relationships, within the context of the distinct hydrographic and nutrient conditions for the current dataset, aims to provide insight into the drivers of the observed variability within the Weddell Gyre.

1.6.3.1 IOPs and Particulate Organic Carbon

It is assumed that, in the open ocean, phytoplankton and their related materials are the primary determinants of the particle field (i.e. the contribution by mineral particulates is negligible) (Morel, 1974; Eppley et al., 1992; Green and Sosik, 2004). While particle concentration influences IOPs to the first order (Bishop, 1999); the size and packaging (e.g. pigment content, degree of aggregation and fluid content), composition (e.g. soft mucilage structure versus carbonate or calcite frustules) and structural characteristics (e.g. shape and surface roughness) of the particles also contribute to variations in the optical signal (Stemman and Boss, 2012). Because particle concentration has the strongest impact on IOPs, in waters where phytoplankton are the dominant particulate constituent, POC concentration and the associated IOP measurements, co-vary across a wide range (Stemman & Boss, 2012).

In a study based on data from the Ross Sea and Antarctic Polar Frontal Zone (APFZ), Stramski et al. (1999) found that particulate backscattering (b_{bp}) was well correlated with POC, however the relationship differed between regions, which they suggest was due to differences in community structure. The relationship between beam attenuation (c_p) and particulate matter however, proves more robust (Bishop, 1999; Claustre et al., 1999) and has been applied to a wide range of data across many oceanic regions. The global review of c_p and POC data by Gardner et al. (2001) suggests that although variations occurred between regions, a strong relationship holds over a wide range of hydrographic regimes.

It must be noted here, however, that although measurements of POC from c_p are superior to those from b_b, the sensors for the latter are smaller, cheaper and more easily attached to autonomous floats and gliders, resulting in a far higher abundance of b_b data relative to c_p. For this reason, b_b-derived POC still provides an important contribution to global datasets.

Ultimately, these empirical relationships between IOPs and the particle field can be applied to satellite ocean colour data, thus enabling broad-scale, year-round

monitoring of phytoplankton POC dynamics (e.g. Stramski et al, 1999). While estimates of carbon export are not yet retrievable from satellite-based sensors, broad-scale measurements of depth-integrated POC have been obtained from remote sensing reflectance, linked to IOPs (Stramski et al., 1999). These measurements have been used to calculate not only regional and seasonal estimates for POC but more recently estimates for the global ocean (Stramski et al., 2008). This ability to observe broad-scale variability in the particle field and calculate global estimates of POC concentration provides a valuable technique for quantifying carbon fluxes, identifying potential CO_2 'source' and 'sink' regions and improving our understanding of the global ocean carbon cycle. To estimate potential carbon export from remote sensing data, however, requires a sound understanding of how phytoplankton community structure and physiology impact AOPs. This in turn relies on the continued development of robust empirical relationships between IOPs, community structure and physiology.

1.6.3.2 IOPs and Particle Size

While particle concentration influences IOPs to the first order, particle size and packaging (degree of aggregation & fluid content), composition (e.g. soft mucilage structure versus carbonate or calcite frustules) and structural characteristics amount to additional variations in the optical signal (Stemman and Boss, 2012). IOPs are predominantly influenced by particles within the ~0.2-20 μm size range (Morel, 1974; Stramski and Kiefer, 1991; Boss et al., 2001, Bricaud et al., 2004), which corresponds to the phytoplankton community from pico- to nano-phytoplankton. The strongest influence however, is exerted by cells in the smallest (0.2-2 μm) size class (DuRand and Olson, 1996; Dall'Olmo et al., 2009). Variations in particle size, and thus the volume to area ratio, influence the spectral slope between the absorption peaks in the blue (~450 nm) and red (~670 nm) wavelengths (Pak et al., 1970; Ciotti et al., 2002; Figure 1.5). In addition, surface roughness and complex cell shape increase the observed effective size of particles. Thus, the effects of size, shape and index of refraction are important to consider in the relationship between IOPs and particle concentration (Baker and Lavelle, 1984; Clavano et al., 2007).

The IOP-particle size relationship has been established using both absorption (Ciotti et al., 2002) and beam attenuation (Baker and Lavelle, 1984; Boss et al., 2001; Oubelkheir et al., 2005), which show a strong influence of cell size on spectral shape. Small particles tend to result in a steep slope (thin line) between ~450 nm and ~670 nm, which becomes flatter (thick line) as particle size increases (Coitti et al., 2002; Figure 1.5). While algal absorption is characterized by the two peaks at ~450 nm and ~670 nm, the effects of pigment composition and the "package effect" (Morel and Bricaud, 1981) are both reduced at 670 nm (Bricaud and Stramski, 1990). The impact of changes in cell size and intra-cellular pigment concentrations therefore increases the "package effect", causing changes in the spectral shape of absorption (as well as beam attenuation) especially at ~450 nm (Bricaud and Stramski, 1990), where larger peaks are associated with small cells and high pigment concentrations.

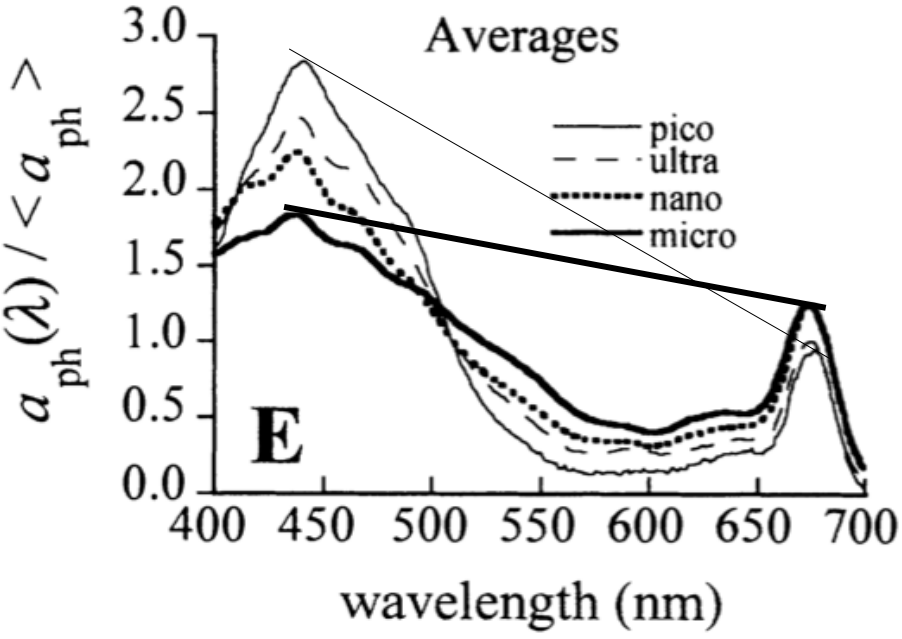

Figure 1.5 Averages of the spectral shape of phytoplankton absorption coefficients for different size ranges from smallest to biggest: picoplankton (0.2-2 μm), ultraplankton (2-5 μm), nanoplankton (5-20 μm) and microplankton (20-200 μm). Lines indicate the differences in spectral slope between the smallest (pico —) and largest (micro ━) phytoplankton cells. Figure reproduced from Ciotti et al. (2002).

The inversion method of estimating particle size distribution (PSD) from optical properties has been applied using various techniques (Boss et al., 2001; Jonasz and Fournier, 2007; Hirata et al., 2008; see Review by Stemman and Boss, 2012).

For example, Agrawal and Pottsmith, (2000) used measurements of near-forward scattering and applied them to a wide range of particle sizes to create PSDs for in situ and laboratory particle suspensions. Other studies, however, created PSDs using spectral characteristics of size distributions (Van de Hulst, 1981) based on in situ Coulter counter data (Boss et al., 2001).

In the Southern Ocean, which suffers from consistent under-sampling, satellite observations provide a valuable opportunity to develop broad-scale, ecosystem-appropriate products for investigating cell size variability (Coitti et al., 1999; Roesler and Boss, 2003; Ciotti and Bricaud, 2006; Loisel et al., 2006; Kostadinov et al., 2009; Briggs et al., 2011; Ferreira et al., 2013). In the study by Ferreira et al. (2013), for example, the authors examined a bloom with chl-a concentrations spanning two orders of magnitude and found that size structure, along with the co-variation of accessory pigments, played an important role in determining the variability in the IOP signal (Ferreira et al., 2013). These links between satellite AOPs, IOPs and in situ particle structure provide a tool to monitor phytoplankton regime shifts, which ultimately drive changes at higher trophic levels and the potential for carbon export (Finkel et al., 2010).

1.6.3.3 IOPs, Species Dominance and Physiology

The link between the *in situ* phytoplankton community and ocean colour has previously been used to investigate phytoplankton functional types (Ciotti et al., 1999; Sathyendranath et al., 2004; Dierssen et al 2006; Alvain et al., 2008; Kostadinov et al., 2009; Kowalczuk et al. 2010) and physiological responses to environmental conditions (Behrenfeld et al., 2009; Behrenfeld and Milligan, 2013) with compelling results. In one study, variations in fluorescence from satellite observations were linked to light and nutrient limitation, providing insight into the physiological responses of phytoplankton to light, iron and nutrient stress (Behrenfeld et al., 2009). The ability to observe broad-scale physiological changes and community shifts from space contributes to a better understanding of the factors driving these changes, and is vital for improving the predictive capacity of global ocean models (Stemman and Boss, 2012).

Variability in phytoplankton abundance, size distribution, community composition and associated pigment content are all important factors influencing IOPs. While increases in the "package effect" (Morel and Bricaud, 1981) may occur due to changes in size alone, variations in both size and pigment concentration and composition, occur as a result of changes in species structure (Bricaud and Stramski, 1990). Differences in absorption properties between phytoplankton species types, as a result of the proportional differences of intracellular chl-a and accessory pigments (Barlow et al., 1993; see Figure 1.6), have been used to identify phytoplankton species types (e.g. Barlow et al., 2002, Ferreira et al., 2013). These differences result in distinct absorption spectral shapes and peak heights at ~450 nm and ~670 nm spectra, which are clearly visible in mono-specific cultures (Roesler, 2013). The highest absorption peaks are associated with dinoflagellate and premnesiophyte species, which differed slightly in spectral shape and peak height, while cyanophyte species have equally high absorption at ~450 nm but significantly lower absorption at ~670 nm. In addition to species-specific spectral shapes, variations in peak heights within a single species may reflect changes in biomass as well as responses to changing conditions. For example, diatoms grown at high light intensities display higher absorption peaks in both the blue and red wavelengths, than those grown at low light (Figure 1.6).

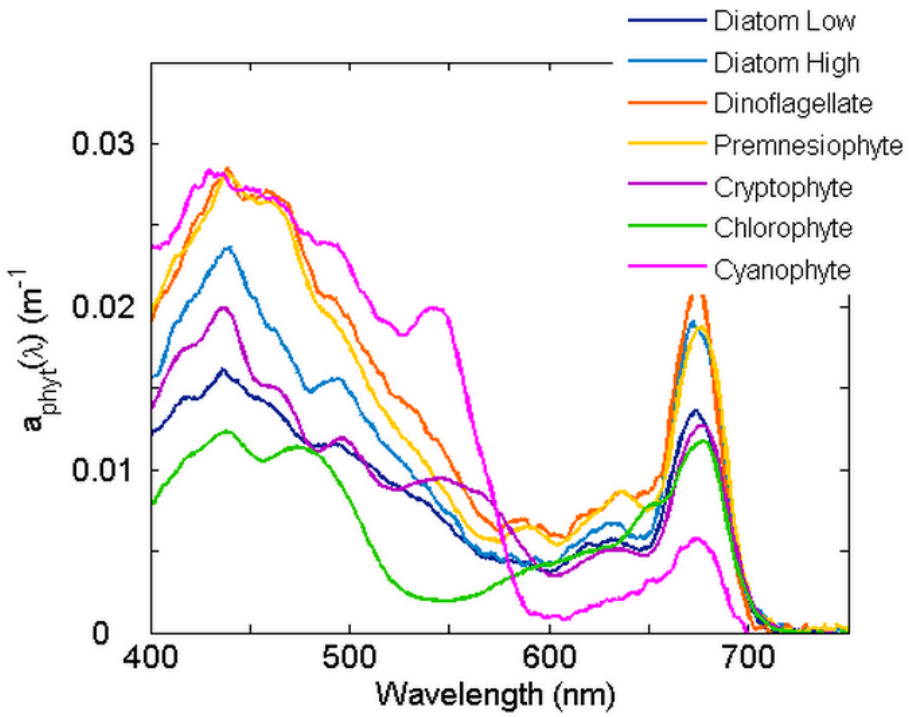

Figure 1.6 An example of absorption spectra for different monospecific phytoplankton cultures. Note the difference between diatoms grown at different light levels. Figure reproduced from Roesler (2013).
http://www.oceanopticsbook.info/view/absorption/absorption_by_oceanic_constituents

Phytoplankton cells respond to changes in nutrient concentrations, light intensity and temperature through physiological adaptations (Davidson, 1991; Behrenfeld et al., 2006; Moore et al., 2007a; Behrenfeld et al., 2009; Strzepek et al., 2012). These physiological responses result in a non-linear relationship between chl-a and carbon content in the euphotic zone (Geider et al., 1998; Behrenfeld and Boss, 2003; Armstrong, 2006). For example, changes in intracellular pigment concentration occur under varying light environments through the process of photo-adaptation (Bricaud and Stramski, 1990). This is observed through increases in pigment concentration, which improves a cell's ability to absorb light (Behrenfeld and Boss, 2003), in response to decreasing light availability with depth. Consequently, chl-a to carbon (Ch:C) ratios are observed to increase with depth.

Latitudinal variations in light intensity dictate that mean light availability decreases with increasing latitude. This in combination with the characteristically deep mixed layers of the Southern Ocean means that

phytoplankton in the high latitudes are often exposed to low light levels. Phytoplankton tend to acclimatize to their environments such that intermittent exposure to high light intensities causes photo-inhibition in these low-light adapted phytoplankton (Strzepek et al., 2012). Under these conditions cells quickly become light saturated and may respond by reducing their intracellular chl-a concentration and/or actively dispersing the excess light energy to avoid cellular damage (Behrenfeld et al., 2009). Furthermore, intracellular iron concentrations and iron:carbon ratios are known to increase in temperate diatom species in response to decreasing irradiance. In contrast, a study by Strzepek et al. (2012) found that Southern Ocean species maintain relatively low intracellular iron concentrations and iron:carbon ratios, which decreased or remained the same with decreasing light conditions. Thus, suggesting that Southern Ocean species have overcome the limitation of iron and light at high latitudes by employing an acclimation strategy that does not require an increase in cellular iron, i.e. increasing the size, instead of the number, of photosynthetic units under low light conditions (Strzepek et al., 2012).

In the HNLC waters of the Southern Ocean, the co-limitation of light and iron drive physiological responses in phytoplankton (Moore et al., 2007a). Such that, low chl-a concentrations (observed using *in situ* or satellite fluorescence) that are coincident with shallow MLDs suggest that phytoplankton are not primarily light limited, but rather iron limited (see review De Baar, 1994; Behrenfeld et al., 2009). Physiological responses to limiting iron concentrations have been linked to changes in photosystem stoichiometry and an over-expression of pigment-protein complexes (Behrenfeld et al., 2008), as well as a reduction in photosynthetic efficiency measured using fast repetition rate fluorometry (Behrenfeld et al., 2006; Moore et al., 2007a). As a consequence, Moore et al., (2007a) reported low Chl:C ratios under iron-limiting conditions ($\sim$0.010 g g^{-1}), while ratios more than doubled under iron replete conditions ($\sim$0.025 g g^{-1}). Similar physiological responses have been detected using satellite fluorescence data (Behrenfeld et al., 2009), which can provide a valuable instrument for observing physiological responses to iron stress across the global ocean.

By examining the variability in Chl:C ratios using the ratio between fluorescence-derived chl-a and c_p-derived POC, we may infer the physiological responses of phytoplankton to variations in light intensity and iron availability (Behrenfeld and Boss, 2003; Behrenfeld et al., 2009), while also exploring the effects of changes in community structure (Bricaud and Stramski, 1990).

Although the link between remote sensing and carbon export is still lacking, these phytoplankton-IOP-satellite links give us the ability to make broad-scale observations of phytoplankton physiology and community structure, while providing insight into the environmental factors driving variability in production, distribution and potential carbon export rates. The development of these connections however, is still in its infancy and validation using *in situ* physiological and optical observations is desperately needed.

1.6.4 Research Goals and Aims

A better understanding of the factors that determine phytoplankton abundance, community structure and physiology are essential to improving our ability to predict the continuing role of the Southern Ocean as an efficient CO_2 sink. Due to the remote, tempestuous nature of the region satellites and autonomous platforms are increasingly being utilized as platforms for observing biogeochemical variability through ocean colour radiometry algorithms linked to IOPs. This reliance on remote sensing data necessitates the validation of these relationships using *in situ* IOPs linked to discrete biogeochemical measurements, phytoplankton physiology indices and community size structure data.

This project contributes to research carried out by the Southern Ocean Carbon and Climate Observatory (SOCCO) and is based on data collected in the Weddell Gyre during the SANAE50 (50^{th} South African National Antarctic Expedition) cruise aboard the SA *Agulhas* in the Austral summer of 2010-2011. In this study, the relationships between IOPs and POC, phytoplankton biomass, cell size, species composition and physiology are investigated. These relationships are applied to produce high resolution sections of POC, cell size, and Chl:C ratios, to

explore the variability of phytoplankton biomass, community structure and physiology across the study region. Finally, these sections are interpreted within the context of the different hydrographic and nutrient environments, with the aim of investigating the causative factors driving the observed patterns of phytoplankton variability. Coupled with measurements of N uptake, these sections were ultimately used to infer regions of enhanced new production and increased potential carbon export.

The three main aims of this study are as follows:

Aim 1: To investigate how variability in IOPs can be explained by changes in POC and phytoplankton community structure (with regard to cell size, species dominance and physiology)

Aim 2: To apply the relationships developed in Aim 1 to explore variability in POC, phytoplankton cell size and physiology in the Weddell Gyre.

Aim 3: To interpret the observed variability of POC, phytoplankton, size structure, species dominance, physiology, primary production and carbon export in relation to their physical and chemical controls.

Addressing these three aims in the context of the Weddell Gyre, will act as a preliminary assessment of the first of many bio-optical surveys to be carried out by SOCCO, in this infrequently sampled region of the Southern Ocean. It is expected that the relationships developed here will provide the building blocks onto which further research, with a growing array of data (from more advanced instruments), may be built. This study will address these aims in the following chapter, which will begin with an introduction to the Weddell Gyre region, followed by a description of the material and methods used in this study and then a presentation of the results. The chapter will close with a discussion of each of the three aims, with Aim 3 discussed in the context of defined hydrographic regions, which are based on observations from this study, as well as supporting material from previous work.

Chapter 2 A bio-optical approach to phytoplankton community structure, physiology and primary production in the Weddell Gyre

2.1 Introduction

The region of this study focuses on the western region of the Weddell Gyre (see Figure 2.2.1), located in the South-West Atlantic sector of the Southern Ocean between the Southern Boundary of the ACC (~60 °S) and the sea ice zone (~70 °S). The wind-driven cyclonic circulation of the Weddell Gyre results in eastward transport of water along the northern limb, while westward transport along the Antarctic continental shelf forms the southern limb. The circulation of the gyre drives divergence in the center, and the resultant Ekman transport causes upwelling of sub-surface water across much of the Weddell Abyssal Plain (Bakker et al., 2008). These upwelling circumpolar deep waters are high in nutrients and dissolved inorganic carbon (Hoppema et al., 1997; Bakker et al., 2008), which has been shown to drive pronounced phytoplankton blooms (e.g. Moore and Abbott, 2000). Seasonal ice coverage, which strongly influences biogeochemical cycling and potentially the availability of iron (Smith and Nelson, 1986; Moore and Abbott, 2000), is an important feature of the Weddell Gyre region. The seasonal fluctuation of ice formation and retreat is most pronounced towards the east where the hydrography is highly dynamic, compared to the largely perennial ice cover found in the far west, along the Antarctic Peninsula (Bakker et al., 2008). The inter-annual variability of the ocean-atmosphere-ice system is highest at the northern (circumpolar) rim and strongly linked to global climate forcing (Martinson and Iannuzzi, 2003).

The response of phytoplankton dynamics to this spatial, seasonal and inter-annual variability has not been well documented due to the paucity of biogeochemical observations in this region (particularly in winter), highlighting the importance of local-scale repeat observations, particularly in areas of high variability. Recent work by Marinov et al. (2006) revealed that increasing nutrient uptake and carbon fixation by phytoplankton in spring and summer was

linked to high potential carbon export to the deep ocean. As such, this region provides an important area to investigate the relationships between phytoplankton community structure, primary production and carbon export in response to predicted increases in stratification and shoaling of the mixed layer (i.e. reduction in vertical nutrient transport) associated with climate change (Sarmiento et al., 2004a; Bopp et al., 2005).

This study, links inherent optical properties (IOPs) to particulate organic carbon (POC), phytoplankton community structure (size distribution and species dominance), physiology and primary production and in so doing aims to provide a broad-scale observation tool for investigating phytoplankton variability and carbon export in this important region of the Southern Ocean.

2.2 Study Site

This research focuses on a high-resolution CTD Transect across the Weddell Gyre, which commenced to the east of the South Sandwich Islands (58.5 °S; 25 °W) on 13th January 2011, continuing in a southeasterly direction, ending at the Antarctic Shelf (70.5 °S; 7.9 °W) on the 20th January 2011 (Figure 2.2.1). The high-resolution survey consisted of 42 CTD stations (20 nm apart), with an Underway CTD (UCTD) cast between each CTD, thus increasing the resolution of the physical data (Temperature and Salinity) to every 10 nm. The result was a detailed hydrographic, biogeochemical and bio-optical transect across the Weddell Gyre.

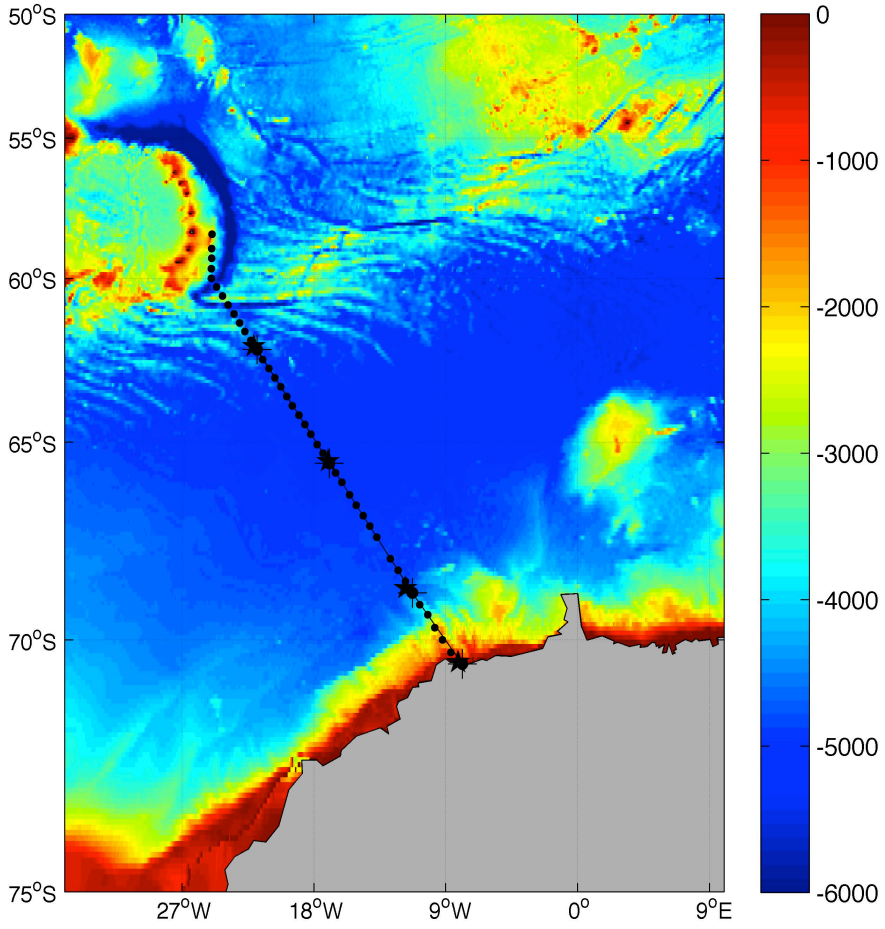

Figure 2.2.1 Bathymetry map of the study region showing all 42 stations along the CTD Transect. Primary productivity stations are marked with stars.

2.3 Methods

2.3.1 General Hydrography

A Sea-Bird SBE 9 CTD, mounted on a steel frame with a rosette of 24 Niskin bottles (12 L), was used to carry out high resolution hydrographic, bio-optical and biogeochemical measurements from the surface (5 m) to 500 m (250 m at the shelf). Data recovered included continuous measurements of temperature, salinity, density, oxygen, fluorescence, beam attenuation and backscattering. Continuous measurements were processed using the Seasave Win32 V 5.39c software package, which averaged the data for each cast into 1 m bins. Discrete water samples were collected from the up-cast of each profile to measure ambient concentrations of nutrients (nitrate, silicate, phosphate), chlorophyll *a* (chl-a) and particulate organic carbon (POC). In addition, water was collected for the measurement of ^{15}N primary production and size-fractionated chl-a at four stations (see Figure 2.2.1 and Table 2.3.1).

2.3.2 Water Masses, Mixed Layer Depth and Stratification

Water masses and front positions were defined using temperature, salinity and density characteristics together with prominent features in the hydrographic profiles, following the methods described in Orsi et al. (1995).

Mixed layer depth (MLD) was calculated using temperature measurements from combined CTD and UCTD profiles. A reference depth of 16 m (instead of 10 m as in De Boyer Monte'gut et al., 2004) was chosen to ensure instrument stability and assumed the MLD was always deeper than this reference depth. The MLD was defined as the depth where the temperature deviation from the reference was >0.2 °C.

The stability of the water-column, represented by the Brunt Väisälä frequency (N^2), was used to describe the degree of stratification in the upper ocean:

$$N^2 = - g/\rho^*(d\rho/dz) \qquad (1)$$

where g is observed gravity, varying with latitude between 9.818 (58 °S) and 9.826 (70 °S); ρ is density and $d\rho/dz$ is the change in density with depth.

2.3.3 Nutrients

Macronutrient samples were collected at varying depths down to 500 m (10-12 depths) at each CTD station. Nitrate (NO_3), Silicate (SiO_4) and Phosphate (PO_4) concentrations were measured on-board within 24 hours of collection. Due to limited chemical supplies however, SiO_4 samples were hand filtered through polycarbonate filters, frozen immediately and analyzed post-cruise at the University of Cape Town (UCT) Oceanography Laboratory. NO_3, SiO_4 and PO_4 were determined using a Lachat QuikChem 8500 Series 2 Flow Injection Analyzer using the following spectrophotometric methods:

NO_3 was determined based on the methods of Armstrong et al. (1967) and Grasshoff (1983), which involves the reduction of NO_3 to NO_2 by treating the sample with ammonium chloride and passing it through a cadmium column filled with copper-coated cadmium filings. The sample was then treated with sulphanilamide, which caused the NO_2 to form a diazo compound and subsequently with N-(l-naphthyl)-ethylenediamine, producing an intense pink dye. The concentration of NO_2 was determined colourimetrically at 543 nm (Riley and Chester, 1971), while the concentration of NO_3 was calculated by the difference between the initial and reduced NO_2 fractions.

SiO_4 was determined following the method of Grasshoff (1983), which involved the reduction of silicomolybdate to molybdenum blue by treating the sample with oxalic acid, followed by ascorbic acid. The concentration of SiO_4 was determined colourimetrically at 820 nm.

PO_4 was determined using the method described by Murphy and Riley (1962), which involved the reaction of orthophosphate, molybdate ion and antimony ion

and the subsequent reduction to blue phospho-molybdenum complex by adding ascorbic acid. The concentration of the complex was determined colourimetrically at 880 nm.

Ammonium (NH_4) and urea were determined manually on board according to the spectrophotometric methods described by Grasshoff et al. (1983) and Parsons et al. (1984), but scaled to 5 ml samples. Concentrations of NH_4 and urea were only measured for selected stations corresponding to primary production stations to estimate ^{15}N spike addition concentrations at ~10% of the ambient concentration. On board analysis of NH_4 using the indophenol-blue method (Grasshoff et al., 1983), however, produced inconsistent results, and thus spare water samples were filtered through Whatman 25 mm GF/F filters and frozen and re-run back at UCT using the OPA fluorometric method as described by Holmes et al. (1999).

The OPA method involved the use of a single stable working reagent consisting of solutions of sodium sulfite, borate buffer and OPA. The working reagent was added to 50 ml samples and left in the dark for 2-3 hours. Concentrations were determined fluorometrically using a Turner Trilogy Laboratory Fluorometer. The method also involves the quantification of background fluorescence (caused by substances in the sample that auto-fluoresce) and matrix effects (due to the reaction of the sample to OPA). This simplified technique provides more precise measurements over a wide range of concentrations (Holmes et al., 1999) and solves many of the analytical issues that are associated with the indophenol blue method (Grasshoff et al., 1983).

2.3.4 Chlorophyll *a*

Chl-a concentration was measured at 7 different depths down to a maximum of 250 m, of which five measurements were within the euphotic zone, as defined by the 1% light depth. These were chosen to capture the surface (surf), chl-a maximum (chl-max), thermocline (therm) and bottom of chl-a maximum (bot. chl-max), as well as the potential carbon export (export) depth at ~100-250 m.

All sampling depths were defined using the downcast fluorescence and temperature profiles. It ought to be noted, however, that although the chl-max sample was labeled as such, there was never a significant sub-surface fluorescence max to speak of. Thus the chl-max sample was simply retrieved from the middle of the observed high chl-a layer.

To recover chl-a pigment, samples of 250 ml were filtered onto Whatman 25 mm GF/F filters and extracted in 8 ml 90% acetone for 12-24 hours in the freezer. Chl-a absorbance was measured on a Turner Trilogy Laboratory Fluorometer and converted to concentration (µg Chl l^{-1} = mg Chl m^{-3}) using the calibration equation below:

$$\text{chl-a} = a_{chl} \times b \times (vol_e / vol_s) \qquad (2)$$

where a_{chl} is the measured absorbance, b is the calibration factor = 0.0941 (calculated from a dilution series of chlorophyll-a standard) and vol_e and vol_s are the volumes of acetone and sample respectively.

2.3.5 Fluorescence

Raw chl-a profile fluorescence was measured by a Wetlabs ECO-AFL/FL Fluorometer mounted on the CTD during all casts. All fluorescence values were dark corrected by subtracting an average dark value calculated from the fluorescence >400 m. While no living phytoplankton were present below 400 m, very low measurements of fluorescence were observed, assumed to be the background fluorescence of the water (see Sackmann et al., 2008 for further fluorescence considerations). A calibration curve (Figure 2.3.1) of profiled fluorescence and extracted discrete chl-a at concurrent depths was used to convert profiled fluorescence into chl-a units of µg l^{-1}. Fluorescence instrument sensitivity allowed for a minimum measurement of 0.02 µg Chl-a l^{-1}, thus all calculated concentrations below this were considered zero.

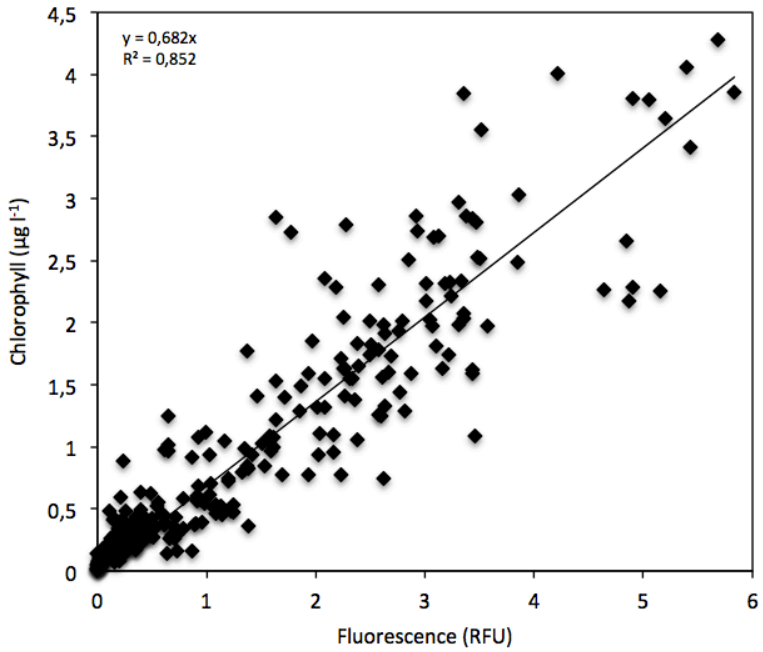

Figure 2.3.1 Calibration plot of raw fluorescence (RFU) and chl-a (µg l^{-1}) for all data pairs along the CTD Transect (n = 293). The trend line was forced through zero; the resultant equation and r^2 are shown. Fluorescence was corrected for surface quenching following Sackmann et al. (2008).

Surface fluorescence measurements during the day under-estimated chl-a concentrations as a result of cellular quenching under high light conditions (Falkowski and Kolber, 1995; Sackmann et al., 2008). Phytoplankton cells under high irradiances become light saturated and so disperse excess energy to avoid cell damage, thus reducing their measured fluorescence. Under these conditions, cellular fluorescence is not proportional to chl-a concentration. As a consequence, a quenching correction (QC) was applied as described by Sackmann et al., (2008), which employs the ratio between dark (below 300 m) fluorescence and backscattering ($fl:b_b$). The following equation was used to correct for quenching within the euphotic zone:

$$\text{QC-fluorescence} = b_{b(650)} \times fl:b_b \qquad (3)$$

where $b_{b(650)}$ is backscattering at 650 nm and $fl:b_b$ is the maximum fluorescence to $b_{b(650)}$ ratio in each profile. The equation was applied to all measurements shallower than the $fl:b_b$ to correct for surface quenching. This assumes that the

fluorescence to backscattering ratio is constant in surface waters and that variability due to cell size, cell shape and chl-a packaging are negligible compared to cell concentration (Sackmann et al., 2008).

2.3.6 Particulate Organic Carbon

POC samples were collected at five variable depths, which were chosen to capture the surf, chl-max, therm and bot. chl-max, as well as the export depth at ~100-250 m. Samples of 1 L were filtered onto pre-combusted 47 mm Whatmann GF/F filters, then frozen at -20 °C immediately after filtration. After drying and pelleting the filters (see details below), POC samples were analyzed using a CHN Analyzer in the UCT Archaeometry Laboratory within 12 months of collection.

In preparation for analysis, frozen filter samples were dried for 3 hours at 50 °C, acidified by fuming with 10% HCl for 24 hours to drive off inorganic carbon (e.g. carbonate shells of coccolithophores and foraminifera) and then re-dried in the oven for 3 hours at 50 °C. Because of the 47 mm size of the filters and constraints on the amount of filter material that could be run on the CHN analyzer, filters were sub-sampled by randomly punching out six small (4 mm in diameter) discs from the filtered sample area, which were then inserted and pelleted into 5×8 mm tin capsules. The proportion of particulates captured in this way was calculated from the ratio between the filtered area and the total area of the punched sub-samples. Due to the above restrictions only 21-40% of the total particulate filtered area per sample was captured by the pelleting procedure and analyzed.

The concentration of POC was determined by sample filter combustion via standard CHN analysis (Parsons et al., 1984; Knap et al., 1994). These concentrations were divided by the percentage area punched and the volume filtered to calculate total POC l^{-1} for each sample. Clearly, calculated POC l^{-1} will be subject to sampling errors associated with uneven distribution of particulate matter on the filter that forces biased sub-sampling during punching. The %

error involved in this procedure, however, was not quantified by carrying out repeat measurements of several samples, but it is recommended for future studies to do so.

Two sets of standards were used to calibrate the data and check for instrument drift. Pre-combusted filters through which no water had been filtered were used as blanks, which were run on the CHN analyzer after every 20 POC samples. To correct for possible background POC concentrations associated with the filters (see Bishop, 1999), an average blank value (3±0.4 μmol C l^{-1}) was subtracted from each POC sample to provide a blank-corrected concentration (μmol C l^{-1} = mmol C m^{-3}).

2.3.7 Phytoplankton Enumeration

Water samples (200 ml) for microscopy were collected at three depths (surface, chl-max and thermocline) at every CTD station. Sample depths ranged from 5-10 m (surface) to 60 m (deepest thermocline). Samples were placed into amber glass bottles with plastic lids to which 4 ml dilute alkaline Lugol's solution (see Appendix 1 for reagent list) was added as a preservative. Bottles were stored in the dark until examination was carried out ashore. The author counted and identified the phytoplankton assemblages for 17 selected samples within 18 months of collection. It is possible that some degradation of cells may have occurred between collection and analysis, which could have created quantitative errors. For example, soft-bodied cells (e.g. naked flagellates) and colonies (e.g. *Phaeocystis antarctica*) rapidly deteriorate or break apart in preservative (see Schoemann et al., 2005) and thus are not well represented in cell counts.

2.3.7.1 Microscopy Cell Counts and Size Calculations

Cell counts were made by inverted light microscopy. To do so, samples were gently inverted and mixed continuously for 2 minutes to evenly redistribute the cells. Sub-samples of 25 ml or 50 ml were then settled in settling chambers

(Hydro-Bios, Duncan and Associates, UK) for 24 hours and examined on an Olympus XI50 inverted light microscope at ×50 and ×100 magnification (after Hasle, 1978). Large and relatively rare cells were counted during a full examination of the chamber, while small and relatively abundant cells were counted in 2-3 transects (after Poulton et al., 2007). Species were identified as far as possible following Priddle and Fryxell (1985) and Tomas (1997). Cells < 5 µm, could not always be identified to species level or even functional group, while cells < 2 µm were not clearly visible and thus not counted.

Phytoplankton cells were counted, their dimensions measured and identified to species or functional group as far as possible. Cell concentration (cells l^{-1}) was calculated by accounting for the volume settled, the size of the settling chamber and the area counted. Cell dimensions included length, breadth and where possible depth (which was otherwise extrapolated from similar cell shapes that were accurately measured). These dimensions were used to calculate cell volume using either the equation for a cylinder or a sphere. It must be noted that this step has a high potential for error (~50%) as a result of applying simplified geometric shapes to a range of complex cell structures, but it has been successfully used to calculate cell size distributions from microscopy data in previous studies (Poulton et al., 2007).

Cell volume was converted to equivalent spherical diameter (ESD) for each cell to calculate the cell size distribution of each sample. To characterize each community by 'dominant cell size', a community size parameter, ESD_w, was calculated using the mean ESD weighted by cell concentration (cells l^{-1}). Previously, effective diameter (D_{eff}) has been applied as a community size parameter, calculated from Coulter Counter data using cell volume to area ratios and complex equations (Bernard et al., 2007). The weighted mean method of characterizing the community size, however, was considered more appropriate for this study due to small sample size, the limitations inherent in data collection methods and the errors present in calculating cell volumes from microscopy.

Cell counts were divided into four size-classes: <5 µm, 5-10 µm, 10-20 µm, 20-40

μm and 40-200 μm. Cells <5 μm were identified as far as possible, but due to the degree of damage of some sample populations, these smaller cells were often not accurately identified and thus classed as Un-identified (UI) cells. Due to the large number of species in these communities, the time constraints of this project and the uncertainty in identification down to species level, species were grouped by family name (e.g. *Rhizosolenia sp., Fragilariopsis sp*., *Chaetoceros sp*.) and placed in different functional groups (e.g. Diatom, Dinoflagellate, Heterotroph, Ciliate and the Prymnesiophyte *Phaeocystis antarctica*). Macro-zooplankton were counted and measured but removed from all analyses of the community structure.

Descriptive statistics of species abundance and diversity, dominant cell size and total bio-volume (estimated from cell concentration and size distribution), were carried out in Excel. Due to the small sample size (n = 17) of community structure data in this study, however, multivariate statistical analysis was not carried out.

2.3.8 Inherent Optical Properties

The inherent optical properties (IOPs) of the water column were defined using beam attenuation and backscattering measurements, in blue (470 nm) and red (650 nm) wavelengths, collected for all CTD casts by two WetLabs optical sensors mounted on the CTD frame.

2.3.8.1 Beam attenuation

Beam attenuation (c_p) was measured at 470 nm and 650 nm wavelengths (with a bandwidth of 20 nm) using a WetLabs C-Star Transmissometer (see Figure 2.3.2) with a path-length of 25 cm, acceptance angle of 1.2 degrees and an instrument sensitivity of 0.003 m^{-1}. The transmissometer consists of a light source (transmitter) and a light sensor (receiver). The distance between the two is the path-length, which is open to the ocean environment and continuously samples

as the CTD passes through the water column. The instrument output, transmittance (Tr), is a measurement of the percentage of light that is received by the sensor. Tr was converted to c_p (m^{-1}) using SeaSave software by taking into account the path-length (for details see WetLabs C-Star Transmissometer Manual, 2011).

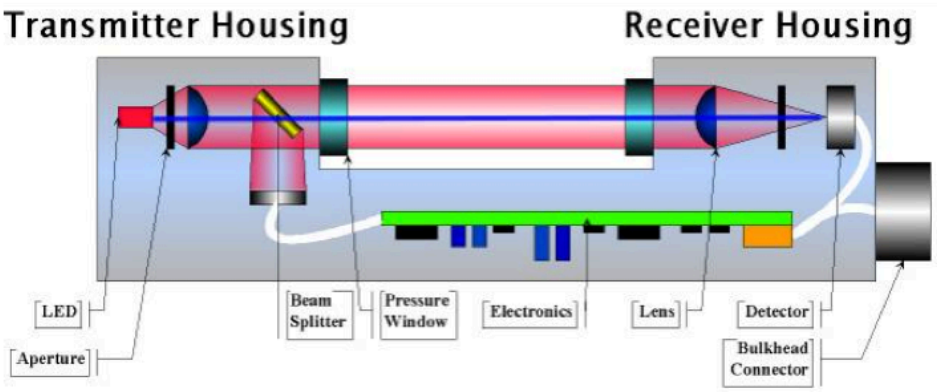

Figure 2.3.2 Functional illustration of the C-Star Transmissometer, showing the parts making up the Transmitter and Receiver units (reproduced from WetLabs Transmissometer Manual, 2011).

Based on increased standard variability at low values, a conservative threshold of 0.006 m^{-1} was chosen as the limit of accurate detection by the sensor and all values less than this were removed from the data set to maintain data accuracy. Instrument consistency was tested by assessing the deep (>400 m) anomalies for each CTD profile. The acceptable range in anomaly values due to natural variation was considered to be -0.01 to 0.01 m^{-1}. Values outside this range were assumed to be a result of instrument drift or offset due to factors associated with instrument sensitivity and/or sensor contamination. Data outside the acceptable range in anomaly were flagged, but were not corrected, due to the compounded detrimental effect of the correction on further analyses.

2.3.8.2 Backscattering

Backscattering (at 470 nm and 650 nm wavelengths) was measured by a WetLabs ECO BB Scattering Meter (see Figure 2.3.3) with a path-length of 12.7

cm and an instrument sensitivity of 0.003 m^{-1}. The instrument measures scattering at 124 degrees, which minimizes variation in the volume scattering function (VSF), due to the influence of suspended particles and water (WetLabs Manual, 2011). A single LED light source enters the water where it is scattered by particulate material and then detected by the sensor as a voltage value. The raw measurements of voltage were converted to VSF (m^{-1} sr^{-1}) and then backscattering (m^{-1}) using calibration equations applied by the ECO host program in SeaSave software (for details see WetLabs ECO Scattering Meter Manual, 2011).

With the removal of pure water during the SeaSave processing step, the remaining signal measured was primarily determined by the concentration of particles (with small contributions from detritus and Gelbstoff) and secondarily by their size and type.

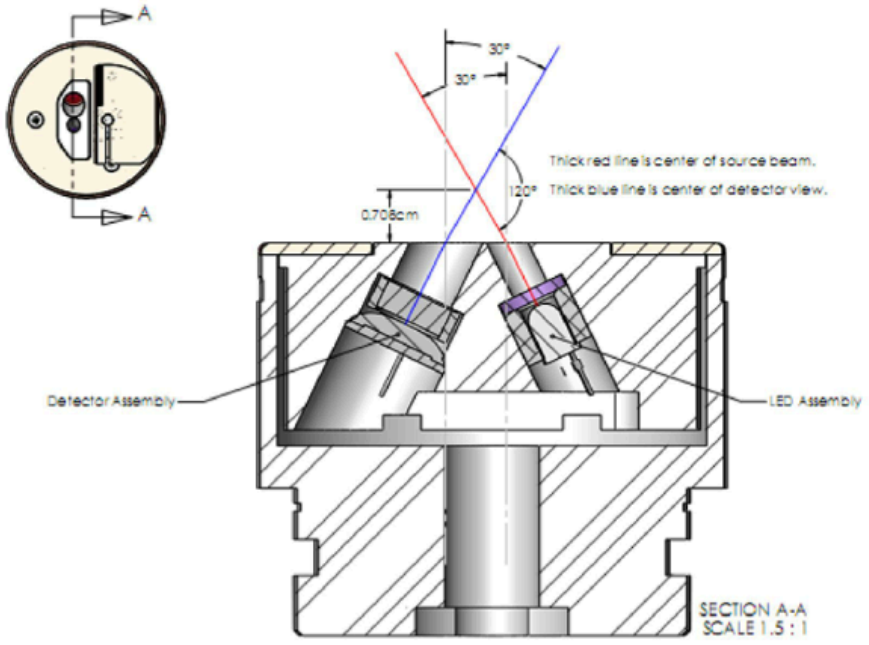

Figure 2.3.3 Optical configuration of the ECO Scattering meter (reproduced from WetLabs ECO Scattering Meter Manual, 2011).

2.3.9 Depth Integrated Nitrogen Uptake and Primary Production

2.3.9.1 Sampling methods

On-board phytoplankton incubation experiments using the ^{15}N-stable isotope technique (see Lucas et al., 2007) were conducted over a 24-hour period to capture both the light and dark phases of photosynthesis (see Table 2.3.1). This enabled the calculation of daily nitrogen (N) uptake rates for the euphotic zone (mmol N m^{-2} d^{-1}). These uptake rates were used to estimate rates of primary production (mg C m^{-2} d^{-1}) based on Redfield C:N (6:1) stoichiometry (Redfield et al., 1963; see Arrigo et al., 2002). The f-ratio was used as to estimate carbon export along the study.

Table 2.3.1. Primary production station positions and euphotic zone depths (Z_{eup}).

Station No.	Latitude (°S)	Longitude (°W)	Z_{euph} (m)
BR143	62.28	21.88	50
BR155	65.58	16.93	44
BR167	68.91	11.27	47
IS11	70.54	7.87	23

Incubation samples were collected from six defined light depths within the euphotic zone, using CTD-mounted Niskin bottles. Photosynthetic available radiation (PAR) was measured on the downward cast, and used to calculate the light depths (LD) that corresponded to 54%, 32%, 18.6%, 8.3%, 3.1% and 1.1% of surface irradiance. This was done by noting the PAR values on the down cast every 5 m to calculate the change in irradiance with depth ($\ln(E_z)$). The slope (k) of this regression was then used to calculate the corresponding depths for the six defined percent light levels (%LD):

$$\text{Light Depth (m)} = \ln(\%LD/100)*(-1/k) \qquad (4)$$

For example the 1.1% light depth at station BR167 was calculated as follows:

$$1.1\%\ LD\ (m) = \ln(1.1/100)*((-1)/(-0.0958)) = -47.05$$

Thus, the 1.1% LD sample was taken at 47 m below the surface.

Water was collected in 10 L carboys from each of the six defined depths. Sub-samples of 2-4 L were taken from each light depth to measure the uptake rates of NO_3-N, Urea-N and NH_4-N. Total euphotic zone uptake was calculated for 'new' (NO_3) and 'regenerated' (Urea + NH_4) forms of N by integrating across the whole euphotic zone. F-ratios were calculated by dividing NO_3-N integrated uptake by total integrated uptake in order to assess the relative dominance of either 'new' or 'regenerated' production.

2.3.9.2 Incubation Protocol

Sub-samples were measured into polycarbonate incubation bottles and spiked with ^{15}N-labelled nutrients at between 5% and 10% of ambient concentrations as follows:

NO_3: To measure nitrate uptake (ρNO_3), a 2 L sub-sample from each light depth was spiked with ^{15}N-NO_3 (1 µmol $K^{15}NO_3$ in 100 µl de-ionized water) at ~10 % of the ambient NO_3 concentration.

NH_4: To measure ammonium uptake (ρNH_4) and ammonium regeneration (rNH_4), a 4 L sub-sample from each light depth was spiked with ^{15}N-NH_4 (0.1 µmol ^{15}N H_4Cl in 100 µl de-ionized water) at ~10% of the ambient NH_4 concentration. This sample was then split into 2 x 2 L samples; one for ρNH_4 was measured into a 2 L polycarbonate bottle while the other 2 L was used for rNH_4 measurements.

To measure initial values for rNH_4, 2 L of inoculated water was filtered through a 25 mm Whatmann GF/F filter to provide the initial ^{15}N:$^{14}NH_4$ ratio for particulate N concentrations (R_0). From the R_0 filtrate, a 50 ml sub-sample was analyzed for time zero ambient NH_4 concentration (S_0), with a 50 ml sub-sample frozen as back up. 900 ml of the remaining filtrate was transferred into a 1 L glass Schotte bottle to which 400 µl of NH_4Cl 'carrier' solution (10 µmol ml^{-1}) was added to

ensure sufficient NH_4 concentrations for diffusion recovery and detection of the NH_4, before being frozen at -20 °C. This filtrate provided the initial ^{15}N:$^{14}NH_4$ ratio in the dissolved form (R_0 aqueous) to calculate ammonium regeneration rates (see Section 2.3.9.4 below).

Urea: To measure urea uptake, a 2 L sub-sample from each light depth was spiked with ^{15}N-Urea (0.1 µmol $CO(^{15}NH_2)^2$ in 100 µl de-ionized water) at ~10% of the ambient urea concentration.

After spiking, the 18 inoculated samples (3 x 6 light depths) were incubated in Perspex tubes covered in neutral density ('Lee') blue filters that simulated the light depths within the euphotic zone (see Figure 2.3.4, Table 2.3.2). It was assumed that this simulation of their natural light environment did not significantly affect phytoplankton uptake rates and every effort was made to reduce exposure to excessive light or shading by the ship (Figure 2.3.4). Samples were collected at night (~3 am) and placed into a dark container during spiking and transport to reduce light shock.

Figure 2.3.4 Photo of onboard primary production incubation set-up on the aft deck of the SA *Agulhas*. Tubes were covered in photographic filters to mimic the six light depths; from 54% to 1.1% (left to right) and cooled with a constant flow of surface seawater.

After the incubation bottles were 'spiked', they were transferred to the incubation tubes as quickly as possible (before dawn) and subsequently filtered in a reduced light environment (with the laboratory lights turned off) at the end of the experiment. Incubation tubes were cooled with a constant flow of surface seawater, however, it was not possible to account for possible temperature changes that may have occurred, due to the ship crossing different regions.

Table 2.3.2 Primary production light depths (% surface PAR – photosynthetically active radiance) and the neutral density 'Lee' filters used to simulate them.

% Surface PAR	Filter code	Description
54.0	117	Steel Blue
32.0	144	No Colour Blue
18.6	141	Bright Blue
8.3	132	Medium Blue
3.1	119	Dark Blue
1.1	120	Deep Blue

At the end of the 24-hour incubation period, all incubation samples were filtered onto pre-combusted 25 mm Whatman GF/F filters under low vacuum. Filters from each 2 L filtered sample were retained for later measurements of particulate N (ρN) for all three nutrients: NO_3 (ρNO_3), NH_4 (ρNH_4) and urea (ρUrea). All filters were rinsed with filtered (<0.2 µm) seawater to remove dissolved N and then frozen at -20 °C.

For NH_4 samples, 1 L of filtrate from each depth was collected after filtering and 50 ml was sub-sampled for immediate NH_4 analysis (and 50 ml frozen for back up) to determine post-incubation ambient NH_4 concentrations (S_t). 900 ml of the filtrate from each depth was measured into Schotte bottles and 400 µl carrier added as before. These (R_t) samples were frozen and later analyzed for the measurement and calculation of NH_4 regeneration (rNH_4) rates, which accounted for isotopic dilution of ^{15}N-NH_4 by excreted ^{14}N-NH_4 (see Sections 2.3.9.3 and 2.3.9.4 below).

2.3.9.3 Sample processing and calculations

All filters from primary production incubations were processed at UCT and analyzed with a Solid Phase Mass Spectrometer in the Archaeometry Department. In preparation for analysis, filters were dried for 3 hours at 50 °C, and then punched to capture all particulate material (possible due to the use of 25 mm, as apposed 47 mm filters) and pelleted in 5×8 mm tin capsules. Analysis was carried out within 6 months of sample collection, during which time samples were kept frozen or dried and stored in ziplock bags with silica crystals. It is important to note here that by capturing and analyzing all the particulate material we assume much higher accuracy in measurements, relative to the sub-sampling punching method used for POC (see Section 2.3.6).

Uptake rates were calculated using equations developed by Dugdale and Goering (1967) and Dugdale and Wilkerson (1986), as modified by Glibert et al. (1982a,b) and Laws (1984) to correct for rNH_4 and isotopic dilution during the incubation period.

The specific uptake rates (V) of nitrate and urea were calculated using the equations of Dugdale and Wilkerson (1986):

$$V = ({}^{15}N_p/(R)^* T)\ (h^{-1}) \qquad (5)$$

where ${}^{15}N_p$ is the particulate At%E, R is the aqueous At%E (corrected for natural abundance from machine standards) and T the incubation period in hours. To calculate absolute uptake rates (ρ), V was multiplied by the appropriate PON concentration:

$$\rho = V \times PN_T\ (\mu g\ N\ l^{-1}\ hr^{-1}) \qquad (6)$$

where PN_T (μg N l^{-1}) is the PON collected at the termination of the experiment. For ρNH_4, however, the equations of Glibert et al. (1982b) were used to calculate R, which accounts for isotopic dilution:

$$R_G = (R_0/\ln(R_0/R_t)) \times (1-(R_t/R_0)) \qquad (7)$$

where R_0 and R_t are aqueous At% at the start and end of the incubation, both corrected for natural abundance (see Section 2.3.9.4 below). The value R_G was then inserted into equation 5 to calculate ρNH_4, corrected for isotopic dilution.

This equation for NH_4 uptake calculates an exponential average value for aqueous enrichments (R) over the incubation period and assumes exponential decrease in R (Glibert et al., 1982b). An alternative equation for calculating NH_4 uptake, proposed by Laws (1984), follows the same principle but makes no assumption about the time dependence of R. The former equation is applicable when ambient nutrient concentrations (S_0 and S_t) differ, but if there is no change in S_0 and S_t, the model breaks down and the latter (Laws, 1984) must be used. For this study, however, the equation of Glibert et al. (1982b) was appropriate for all stations and a comparison with the equation of Laws (1984) yielded no significant differences. Consequently only the results from the Glibert et al. (1982b) model, have been presented here.

2.3.9.4 NH_4 diffusion technique and regeneration calculations

The diffusion method of NH_4 recovery as described by Glibert et al. (1982b) and modified by Probyn et al. (1985) allows recovery of 50-80% of the aqueous NH_4, which is considered sufficient to measure rNH_4. The method involves dangling an acid-soaked (potassium hydrogen sulfate, $KHSO_4$; 0.625g dissolved in 10 ml de-ionized water) GF/F filter from the inside of a Schotte bottle lid into the airspace above the aqueous sample. Pre-combusted 25 mm GF/F filters were halved, attached to paper-clips and wet with 20 µl of $KHSO_4$ solution (trapping capacity of 10 µmol NH_4) before being attached to the inside of the sample lid with Prestik. Sufficient (a heaped teaspoon) magnesium oxide (MgO) was added to the aqueous solution to increase the pH to >9, which caused the dissolved NH_4 to be liberated into the headspace as ammonia and absorbed by the filter.

The sample bottles were then left undisturbed for 14 days at room temperature before the filters were removed, dried and pelleted. The ratio of ^{15}N:^{14}N captured on the filters was determined by Mass Spectrometry to assess the degree of isotopic dilution due to the preferential regeneration (excretion) of ^{14}N-NH_4 over ^{15}N-NH_4 during the 24-hour incubation.

Calculations of ρNH_4 and rNH_4 rates were carried out according to the Blackburn-Caperone (BC) model (Glibert et al., 1982a,b):

$$r = (\ln(R_t/R_0)/\ln(S_t/S_0))*(S_t/S_0)/T \quad (8)$$

$$\rho = r - ((S_t/S_0)/T) \quad (9)$$

which estimates uptake (ρ) from the disappearance of ^{15}N from the aqueous phase as opposed to the appearance of ^{15}N in the particulate phase. It assumes that ρ and *r* are constant over the incubation period and that no regeneration of $^{15}NH_4$ occurs. For this study, however, only the equation for *r* was used as the calculation of ρ is considered to produce unrealistically high results (Glibert et al., 1982a).

2.4 Results

2.4.1 General Hydrography

The temperature (T) and salinity (S) sections along the study transect (Figure 2.4.1a,b) displayed strong contrasts between surface waters, which were generally cool (-1 to 0.5 °C) fresh (33.5-34.12 ppt) and of low density (26.9-27.4 kg m^{-3}), compared to deep waters (>150 m), which were generally warm (0.5-1.5 °C), salty (>34.5 ppt) and dense (>27.7 kg m^{-3}). While a temperature minimum (-1.5 °C) of sub-surface Winter Water (WW) was wedged between, at 50-150 m depth. Variations with latitude were highest within the surface layer (0-50 m) where surface temperatures varied between around 1.5 °C (60.5 °S) and -1 °C (62.5 °S). Between 58.5-63 °S, temperature decreased rapidly from north to south but then gradually increased towards the ice shelf (63-71.5 °S). The mixed layer depth (MLD) varied between 65 m (60.3 °S) and 19 m (62.3 °S), which reflected changes in surface temperature.

The most prominent feature was a temperature maximum (from here on referred to as the 'warm feature') between 60.2 °S and 61 °S associated with low salinity and density (ρ) values (T = 1.75 °C; S = 33.9 ppt; ρ = 27.1 kg m^{-3}). The warm feature extended below 500 m and formed a strong boundary separating the cool surface waters to the south (-0.5 °C) from the relatively warm waters to the north (0.5 °C). The position of the Southern Boundary of the ACC (SBdy) was placed at 61 °S – the southern edge of the warm feature – according to the defining characteristics described by Orsi et al. (1995). Highest temperatures (>1.5 °C) were observed in the upper 50 m and below 150 m separated by an intrusion of cold (-0.5 °C) water at around 100 m. Isopycnals dipped sharply in the warm feature as fresher surface waters penetrated down to 100 m (34.2 ppt), before rising again to the south of the feature.

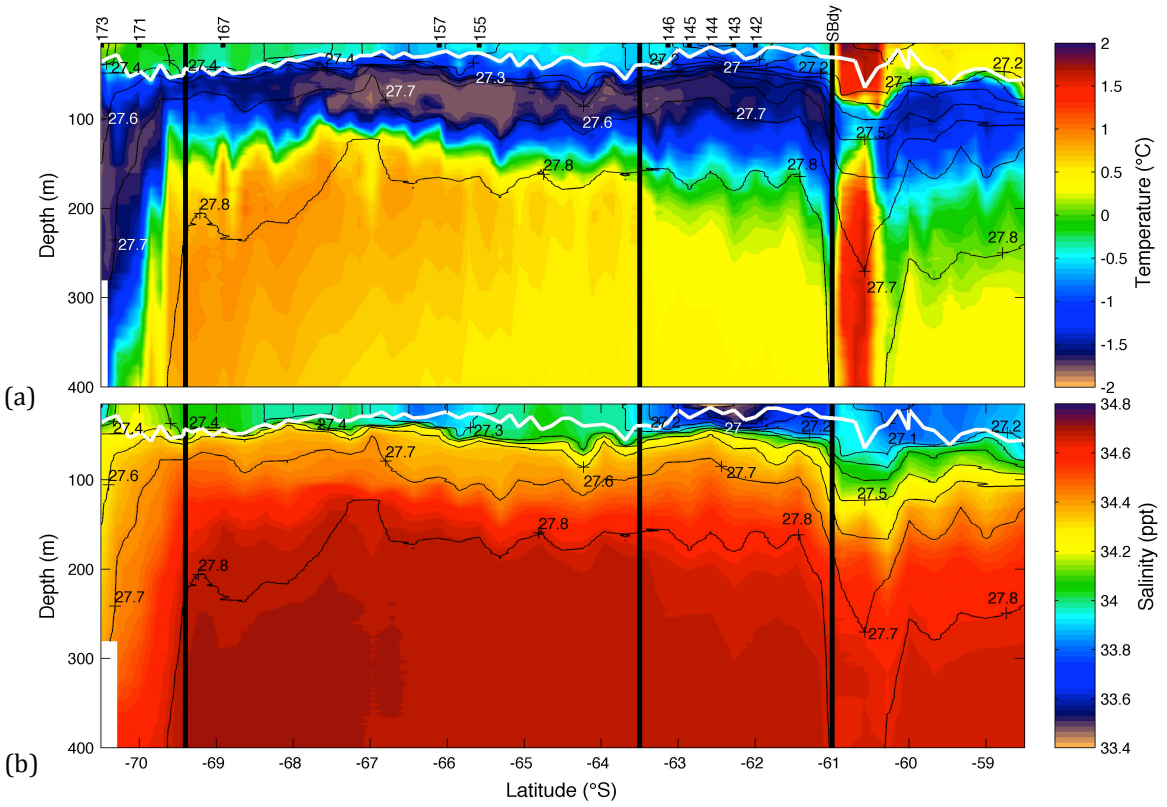

Figure 2.4.1 Section plots of a) Temperature (°C) and b) salinity (ppt) along the study transect (temperature from CTD and UCTD profiles combined). Conotours are isopycnals in kg m^{-3}. White line indicates the MLD calculated from temperature. Black lines are (from right to left): the Southern Boundary of the ACC (SBdy), the southern edge of the Northern Limb of the Weddell Gyre (NLWG) and the Antarctic Continental Shelf (ACS) margin; community structure stations included above.

South of 61 °S the temperatures in the upper layer (40-50 m) fluctuated between 0 °C and -1.5 °C. The -0.5 °C isotherm broke the surface between 62-63 °S and 66-66.8 °S, associated with shallow MLDs (15-20 m) and low salinities (33.5 ppt and 33.9 ppt, respectively). The strong surface ρ gradients south of the warm feature were associated with a cold (-1 °C), low density (ρ = 27 kg m^{-3}) salinity minimum (S = 33.4 ppt) at 62-63 °S (from here on referred to as the 'fresh pool'), with a strong horizontal gradient on either side that formed a 'salinity front'. The fresh pool formed a strong density gradient between surface and sub-surface waters corresponding to shallow MLDs (19-31 m) and strong stratification at 20-50 m (>5 $*10^{-5}$ s^{-1}, Figure 2.4.2). A doming of isopycnals was observed between 64 °S and 69 °S associated with colder, fresher waters and shallow MLDs found in the center relative to the warmer, saltier waters and deeper MLDs at either end.

From 67 °S southward, surface temperature and density increased (>0 °C and >27.5 kg m^{-3}) and isopycnals tilted sharply downwards, coinciding with the sinking of high-density cold water at the ice shelf. MLDs were closely associated with strong stratification in this region south of 67 °S. which deepened from 29 m (67 °S) to 57 m (69.8 °S), shoaling again at the ice shelf (28 m).

Water column stability was represented by the Brunt Väisälä (N^2) frequency in Figure 2.4.2. High values generally occurred within 10 m of the MLD indicating good agreement between MLDs and increased levels of stratification. Exceptions appeared at 60-61 °S and 64.5-66 °S where shallow MLDs were positioned up to 35 m above maximum N^2 values, indicating a de-coupling of the MLD with stratification.

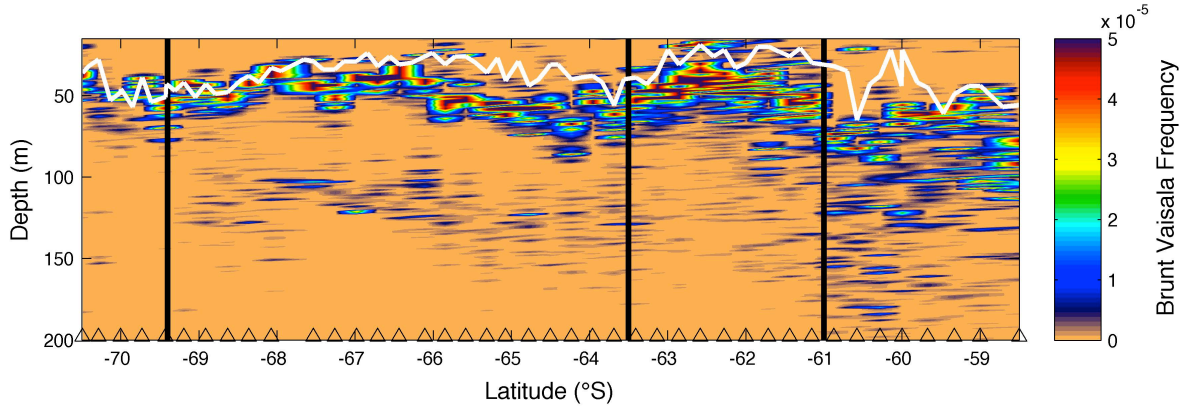

Figure 2.4.2 Water column stability and mixed layer depth (MLD): the Brunt Väisälä frequency calculated from density profiles for all stations along the CTD transect. White line indicates the MLD calculated from temperature. Black lines are (from right to left): the Southern Boundary of the ACC (SBdy), the southern edge of the Northern Limb of the Weddell Gyre (NLWG) and the Antarctic Continental Shelf (ACS) margin.

2.4.2 Biogeochemistry and Bio-optics

2.4.2.1 Fluorescence and Chlorophyll *a*

Discrete Chlorophyll *a* (chl-a) measurements showed strong correlation with quenching-corrected fluorescence (r = 0.91, df = 291). A regression analysis (Figure 2.3.1) revealed a good fit to a linear trend line forced through zero (y = 0.682x, r^2 = 0.85). Applying this equation to fluorescence data produced a high-resolution section of chl-a (Figure 2.4.3), with a standard error (SE) of 36.9%.

Highest chl-a concentrations were observed at 62.5 °S (4.28 µg l^{-1}) and 70.4 °S (3.41 µg l^{-1}), with maximum values at 25-30 m, which generally decreased with increasing depth (~0.05 µg l^{-1} by 100 m). At 70.4°S, however, elevated chl-a extended down to ~100 m (~ 1 µg l^{-1}) and notable concentrations (0.6 µg l^{-1}) were still evident at 200 m. Lowest surface chl-a concentrations were found north of the SBdy (0.23±0.11 µg l^{-1}) with minimum values around 59 °S. Between 63.5 °S and 69 °S surface chl-a was patchy, ranging from 1 to 2.5 µg l^{-1}, with no apparent connection to variations in MLD.

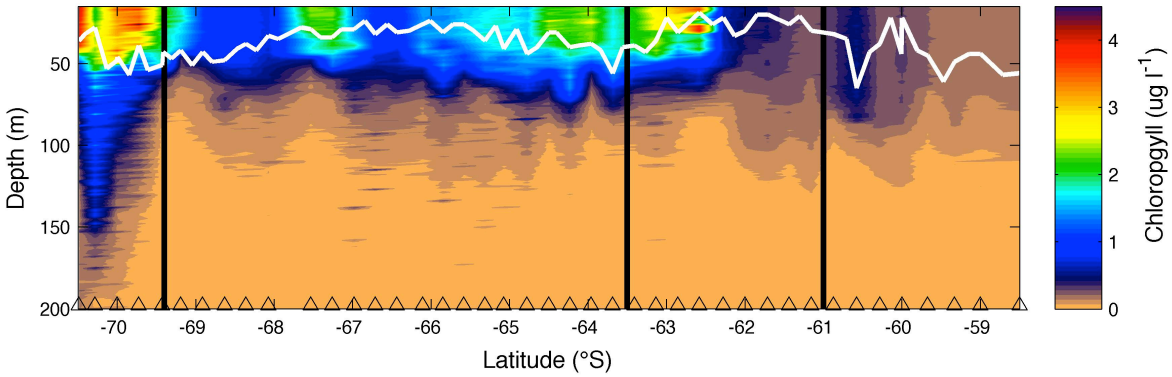

Figure 2.4.3 Chl-a section derived from fluorescence, corrected for surface quenching using the method described by Sackmann et al. (2008), for all stations along the CTD Transect. White line indicates the MLD calculated from temperature. Black lines are (from right to left): the Southern Boundary of the ACC (SBdy), the southern edge of the Northern Limb of the Weddell Gyre (NLWG) and the Antarctic Continental Shelf (ACS) margin.

2.4.2.2 Bio-optics

Beam attenuation at 650 and 470 nm

Beam attenuation (c_p) measurements at 650 nm ($c_{p(650)}$, Figure 2.4.4a) were lower and showed less variation (range = 0.007-0.921 m^{-1}) than measurements at 470 nm ($c_{p(470)}$, range = 0.1-1.286 m^{-1}, Figure 2.4.4b), but both followed the general pattern of chl-a decreasing rapidly below ~50 m. Highest values of $c_{p(650)}$ (0.6-0.92 m^{-1}) were found in the surface waters south of the SBdy, associated with the bloom at 62.5-64.5 °S. North of the SBdy surface waters were characterized by low c_p, with lowest $c_{p(650)}$ measurements observed at 59 °S (~0.1 m^{-1}).

Below 75 m both $c_{p(650)}$ and $c_{p(470)}$ measurements were low (< 0.1 m^{-1} and <0.2 m^{-1}, respectively) and generally varied little with depth. An exception was at the ice shelf where elevated c_p values (~0.2 m^{-1} and ~0.4 m^{-1}, respectively) extended down to 150 m, compared to the low average values (~0.08±0.04 m^{-1} and ~0.15±0.03 m^{-1}, respectively) observed in deep water (100-200 m).

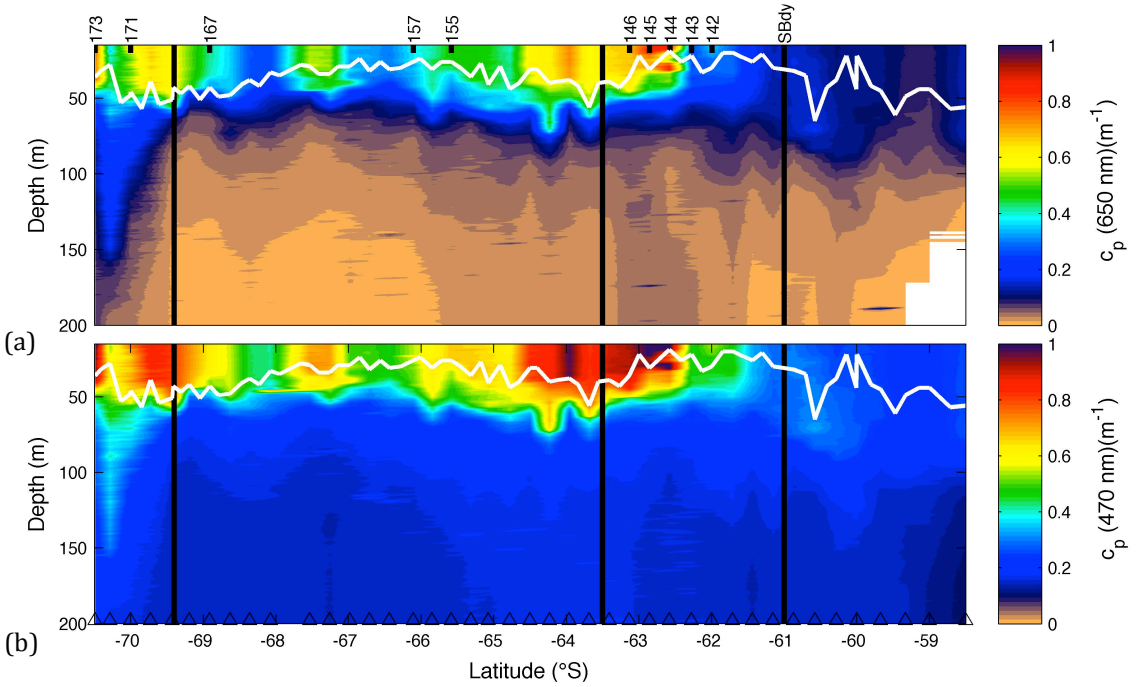

Figure 2.4.4 Sections of beam attenuation (c_p m^{-1}) at 650 nm (a) and 470 nm (b) down to 200 m along the CTD Transect. White line indicates the MLD calculated from temperature. Black lines are (from right to left): the Southern Boundary of the ACC (SBdy), the southern edge of the Northern Limb of the Weddell Gyre (NLWG) and the Antarctic Continental Shelf (ACS) margin; community structure stations included above.

Backscattering at 650 and 470 nm

Backscattering at 650 nm ($b_{b(650)}$, Figure 2.4.5a) and 470 nm ($b_{b(470)}$, Figure 2.4.5b) similarly followed the general pattern of chl-a and measurements showed similar variation for both wavelengths (0.42-1.8 $*10^{-3}$ m^{-1} and 0.36-1.7 $*10^{-3}$ m^{-1}, respectively). Highest b_b measurements (>1.5 $*10^{-3}$ m^{-1}) were observed at the surface at 62.5-64.5 °S and ~69.5°S, associated with elevated chl-a (2-4 µg l^{-1}). Lowest surface values were recorded north of the SBdy with a minimum at 59 °S (~0.5 $*10^{-3}$ m^{-1}). At 60.5 °S, however, slightly elevated b_b (~0.7 $*10^{-3}$ m^{-1}) extended to ~80 m and coincided with the deep MLD (65 m) in the warm feature.

Below 75 m both $b_{b(650)}$ and $b_{b(470)}$ were generally low (<0.5 $*10^{-3}$ m^{-1}) with the exception of patches of elevated values (0.6-1.3 $*10^{-3}$ m^{-1}) scattered throughout the transect, which were more noticable for $b_{b(470)}$ (Figure 2.3.6b). At the ice shelf elevated b_b was observed down to 150 m with slightly higher values observed for $b_{b(650)}$ (~0.7 $*10^{-3}$ m^{-1}) compared to $b_{b(470)}$ (~0.6 $*10^{-3}$ m^{-1}).

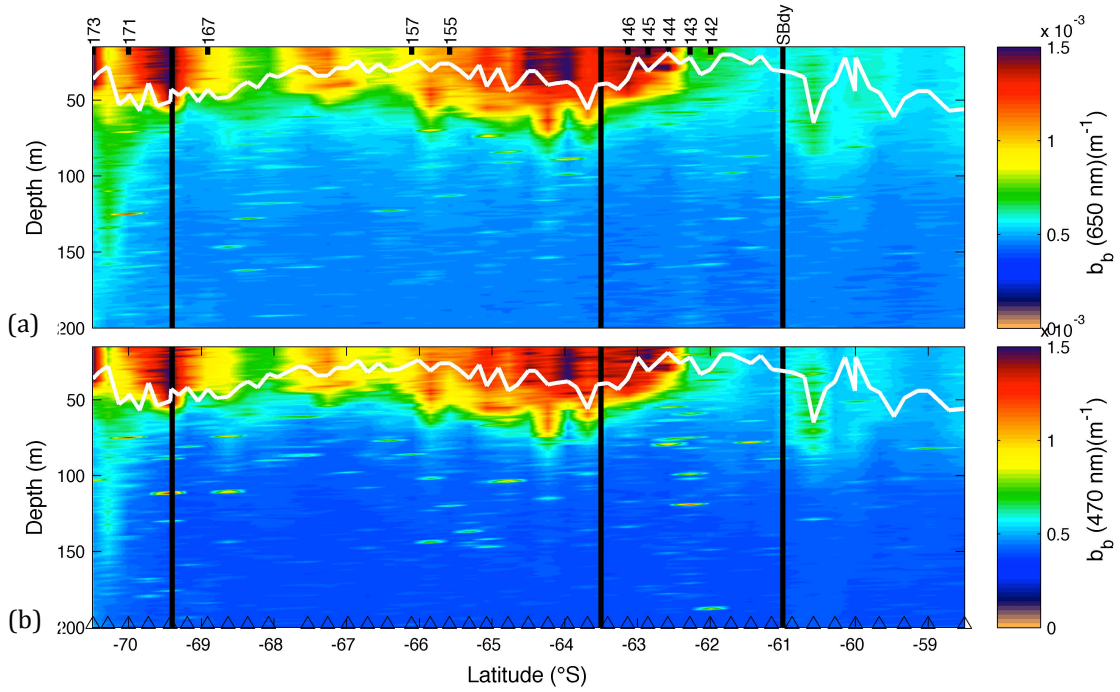

Figure 2.4.5 CTD b_p ($*10^3$ m^{-1}) at 650 nm (a) and 470 nm (b) down to 200 m along the CTD Transect. White line indicates the MLD calculated from temperature. Black lines are (from right to left): the Southern Boundary of the ACC (SBdy), the southern edge of the Northern Limb of the Weddell Gyre (NLWG) and the Antarctic Continental Shelf (ACS) margin; community structure stations included above.

2.4.2.3 Nutrients

Nitrate (NO_3) and silicate (SiO_3) concentrations from discrete CTD samples varied substantially with latitude and generally increased with depth (Figure 2.3.7a.b). NO_3 surface minima (<19 µmol l^{-1}) occurred at 61.5-67 °S and at the ice shelf (Figure 2.4.6a). While relatively low NO_3 concentrations persisted below 500 m between 65 °S and 66.3 °S. the expected deep (200-500 m) NO_3 maxima (>29 umol l^{-1}) was observed at ~67-68.5 °S and ~59-60.5 °S. Relatively low surface SiO_3 concentrations (< 90 µmol l^{-1}) were fairly consistent throughout the transect, except at 63-61 °S where higher concentrations (>100 µmol l^{-1}) were observed (Figure 2.4.6b). While the 100 µmol l^{-1} SiO_3 isoline fluctuated within ~100 m of the surface along much of the transect, it tilted down steeply to ~175 m at the ice shelf.

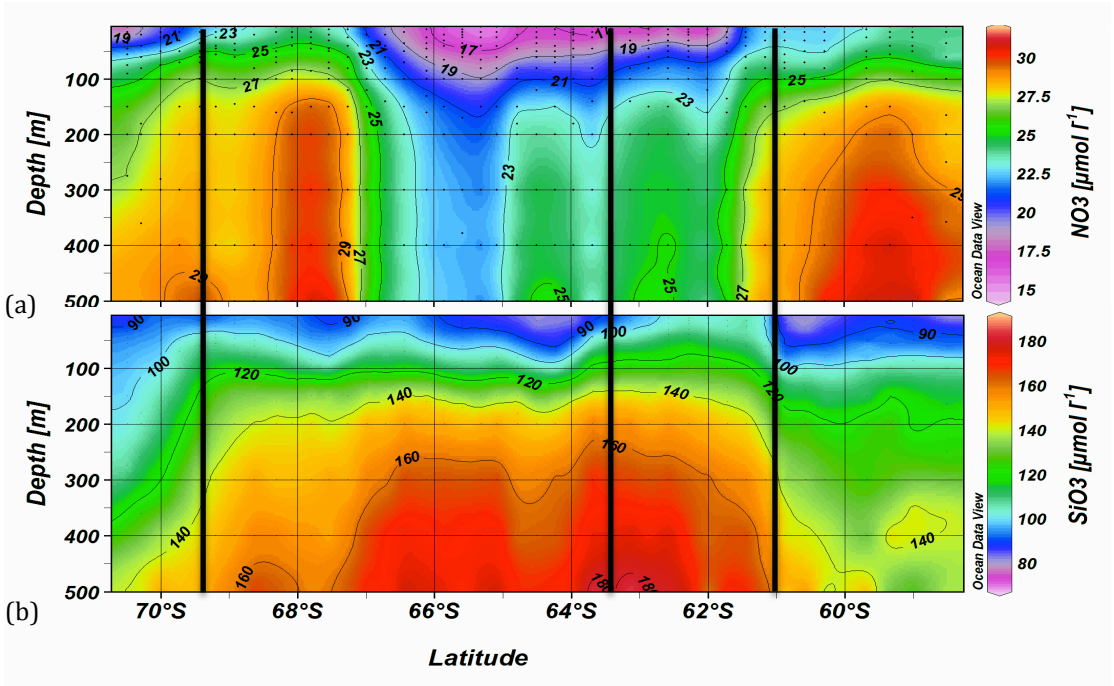

Figure 2.4.6 ODV section of Nitrate (a) and Silicate (b) concentrations with depth, from discrete samples collected along the CTD Transect. Black lines are (from right to left): the Southern Boundary of the ACC (SBdy), the southern edge of the Northern Limb of the Weddell Gyre (NLWG) and the Antarctic Continental Shelf (ACS) margin.

2.4.3 Community Structure from Microscopy

Results for phytoplankton size distribution and species composition are presented for all 17 samples at 10 stations along the CTD Transect. Community structure data is summarized in Table 2.4.1, together with sample position, chl-a and POC concentrations and cell specific carbon and chl-a. The positions of community structure samples are also displayed on the chl-a and bio-optics sections above (Figures 2.4.3-5).

Cell size distribution and cell concentration varied greatly between samples (see Table 2.4.1), resulting in a large variation in community cell size (5.6-23.0 µm) – estimated using ESD_w (mean equivalent spherical diameter weighted by cell concentration). Variations in community cell size were accompanied by large variations in bio-volume (220-4331 $mm^3\ l^{-1}$), chl-a concentration (0.35 to 4.28 µg l^{-1}), POC (52.7 to 266.9 µg l^{-1}) and Chl:POC ratios (0.48-1.80 $*10^2$ g:g) but showed little or no correlation to cell size ($r^2 < 0.3$ for all figures not shown). In general, the smallest ESD_w was associated with the highest recorded chl-a concentrations (2-4 µg l^{-1}, highlighted in dark green), POC concentrations (158.1-266.8 µg l^{-1}, highlighted in light orange) and Chl:POC ratios (1.4-1.8 $*10^2$ g:g, highlighted in blue), which generally decreased with increasing size. Conversely, largest ESD_w (highlighted in purple) were observed in the upper layer (~5-35 m) at BR155 (65.6 °S) and BR167 (68.9 °S), where chl-a was low (1-1.26 µg l^{-1}) and bio-volume was variable (594-3415 $mm^3\ l^{-1}$). At BR142 (62 °S) and BR143 (62.3 °S), however, large ESD_w values (11.5-20.2 µm) were observed at depths of 50-60 m.

Table 2.4.1 Summary of community structure sample data: chlorophyll (Chl-a) and particulate organic carbon (POC) per liter (µg l^{-1}), Chl:POC (g:g *10^2), chl-a and POC per cell (µg $Cell^{-1}$), cell concentration (cells l^{-1}), bio-volume (mm^3 l^{-1}), equivalent spherical diameter weighted by cells l^{-1} (ESD_w). The bold highlighted cells indicate the values greater than the average (included) calculated for each variable.

Station (#)	Latitude (°S)	Depth (m)	Chl-a (µg l^{-1})	POC (µg l^{-1})	Chl:POC (g:g*10^{-2})	Chl-a $Cell^{-1}$ (µg $Cell^{-1}$*10^{-9})	POC $Cell^{-1}$ (µg $Cell^{-1}$*10^{-6})	Total Cells (cells l^{-1})	Total Bio-volume (mm^3 l^{-1})	ESD_w (µm)
BR142	-61.995	5	0.98	115.63	0. 5	1. 4	0.15	07.9E+888	906	7.7
		20	0.97	95.57	1.01	0.64	0.06	15.2E+8	**2 15**	6.4
		60	0.35	72.99	0.48	1.1	0. 3	03.1 8	552	**11.400**
BR143	-62.276	30	0.61	NaN	NaN	1.07	NaN	05.7E+8	514	6.9
		50	0.56	52.70	1.06	**15.88**	**1.49**	35.3E+6	220	**17.72**
BR144	-62.571	10	**3.65**	**266.88**	**1.37**	0.43	0.03	**85.1E+8**	**5 374**	6.0
		30	**4.28**	**237.68**	**1.80**	0.75	0.04	**56.8E+8**	1 804	5.6
		40	**2.74**	**158.17**	**1.73**	**5.00**	0.29	05.5E+8	1 397	9.1
BR145	-62.855	5	**3.81**	**255.95**	**1.49**	1.50	0.10	**25.4E+8**	**2 218**	7.4
BR146	-63.131	5	**3.02**	**180.81**	**1.67**	2.17	0.13	13.9E+8	**4 331**	9.0
BR155	-65.584	10	1.26	**196.23**	0.64	2.21	**0.34**	05.7E+8	**2 189**	**13.28**
		35	1.71	88.74	**1.93**	**8.78**	**0.45**	02.0E+8	**3 435**	**19.43**
BR157	-66.106	10	1.06	94.25	1.13	0.36	0.03	**29.4E+8**	908	6.5
BR167	-68.911	6	1.00	NaN	NaN	**7.58**	NaN	01.3E+8	1 513	**23.01**
		36	1.07	127.14	0.84	**8.73**	**1.03**	01.2E+8	594	**17.71**
BR171	-70.002	5	**2.11**	151.55	**1.39**	1.80	0.13	11.7E+8	**2 157**	8.2
BR173	-70.489	35	**3.41**	**246.98**	**1.38**	2.49	0.18	13.7E+8	1 177	6.6
Average Values			1.92	156.08	1.25	3.63	0.31	16.7E+8	1 850	10.7

2.4.3.1 Community Characteristics: Size, Concentration, Diversity and Cell Specific Carbon and Chlorophyll

The range of community cell sizes (5.6-23.0 μm) was plotted against various community structure and physiological characteristics (i.e. cell concentration, species diversity, cell specific chl-a and cell specific POC; Figure 2.4.7a-d). All relationships showed good agreement (r^2 >0.75) but were associated with high standard errors (SE). Cell specific POC (POC*, Figure 2.4.7a) and cell specific chl-a (chl-a*, Figure 2.4.7b) increased with increasing ESD_w, both fitted to power regression lines (r^2 = 0.82. SE = 37.9% and r^2 = 0.72. SE = 75.6%, respectively), with highest values observed at 18 μm (0.15 μg C 10^{-12} $cell^{-1}$ and 0.016 μg Chl 10^{-9} $cell^{-1}$). Cell concentration (Figure 2.4.7c) decreased with increasing ESD_w, fitted to a power regression (r^2 = 0.77. SE = 65.3%), with highest concentrations observed at 6 μm (8.5 *10^9 cells l^{-1}). The diversity index, fitted to a natural log regression, showed the strongest positive relationship with size but also the highest SE (r^2 = 0.85, SE = 0.87%). Values ranged from 0.5 to 3.2 with highest values observed at 19.4 μm, which indicates that relative species richness (species number) increased with community cell size.

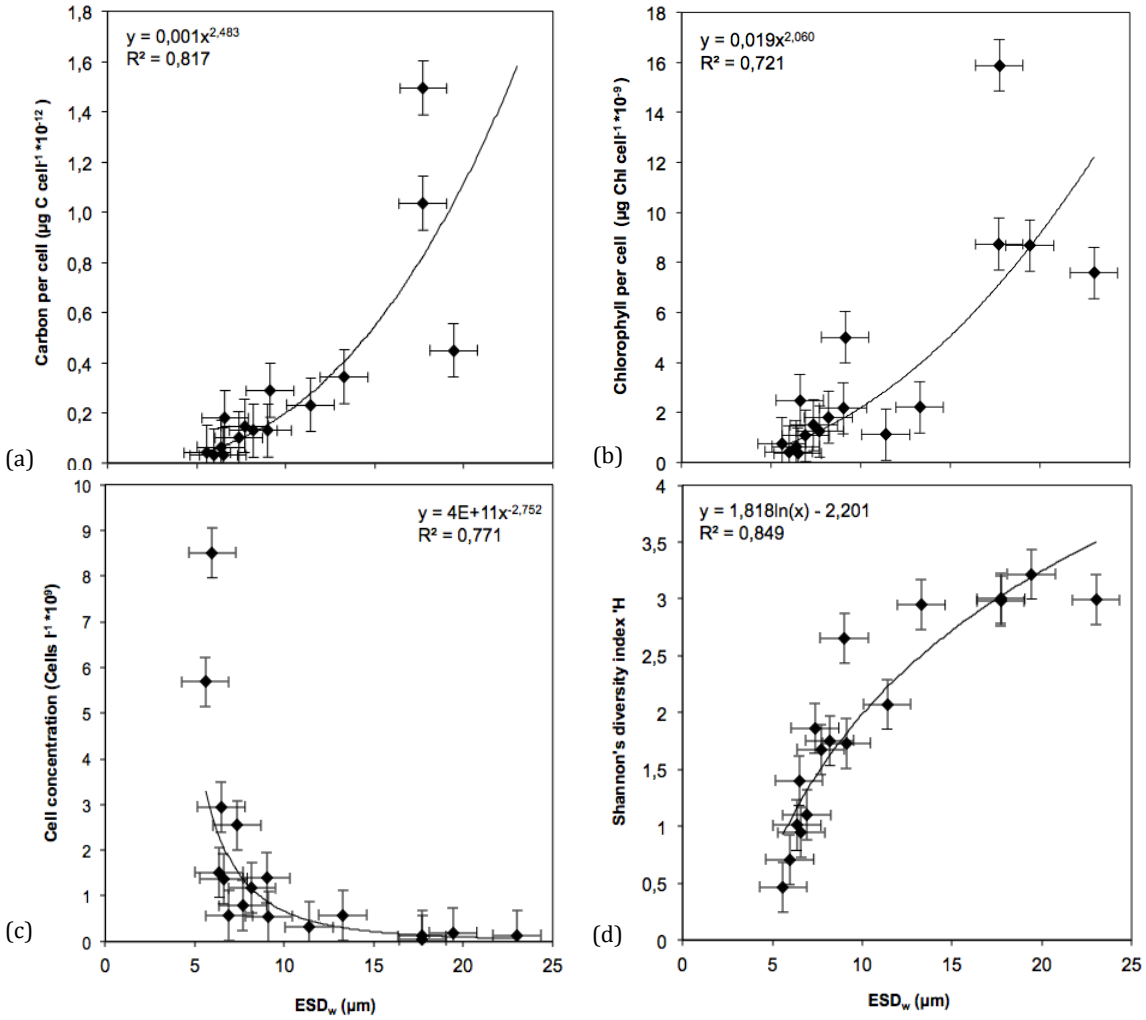

Figure 2.4.7 Scatter plots of community size parameter ESD_w (mean equivalent spherical diameter weighted by cell abundance) with (a) Cell specific chlorophyll (µg Chl cell^{-1} *10^{-9}); (b) Cell concentration (cells ml^{-1}); (c) Cell specific carbon (µg C cell^{-1} *10^{-9}); (d) Shannon diversity index *H'* ($\log_e$). Vertical and horizontal error bars represent standard errors calculated for each variable.

2.4.3.2 Size distribution

Of the 17 community samples analyzed, 11 were dominated by cells <10 µm (60-95%), while 6 samples (where *Phaeocystis antarctica* was absent or present at very low concentrations) consisted of varying proportions of cells in the 5-10 µm and >20 µm ranges.

Figure 2.4.8 displays the proportion that each size class makes to total cell

concentration (cells l^{-1}), for each community sample. Samples were divided into three categories and highlighted in Figure 2.4.8 accordingly: 1) blue - dominance (>60%) of small cells (<5 µm), 2) green - mixed small cells (<10 µm), 3) yellow - mixed large cells (5 to >20 µm). Eight samples were dominated by small cells <5 µm (highlighted in blue), which made up 63-93% of total cells l^{-1}. These <5 µm communities were observed in shallow (5-35 m) samples at stations BR142-144 (62-62.6 °S), BR157 (66.1 °S) and BR171-173 (70-70.5 °S). The remaining nine samples consisted of a mix of size classes with no clear dominance. Three were small (<10 µm) mixed communities and corresponded to surface (5 m) samples at BR145-146 (62.9-63.1 °S) and a deep (40 m) sample at BR144 (62.6 °S). The remaining six were large (5 to >20 µm) mixed communities and corresponded to deep (50-60 m) samples at BR142-143 (62-62.28 °S) and all samples at BR155 (65.6 °S) and BR167 (68.8 °S). Large cells (>20 µm) contributed between 5% (BR142, 60 m) and 62% (BR167, 6 m) in these six mixed samples.

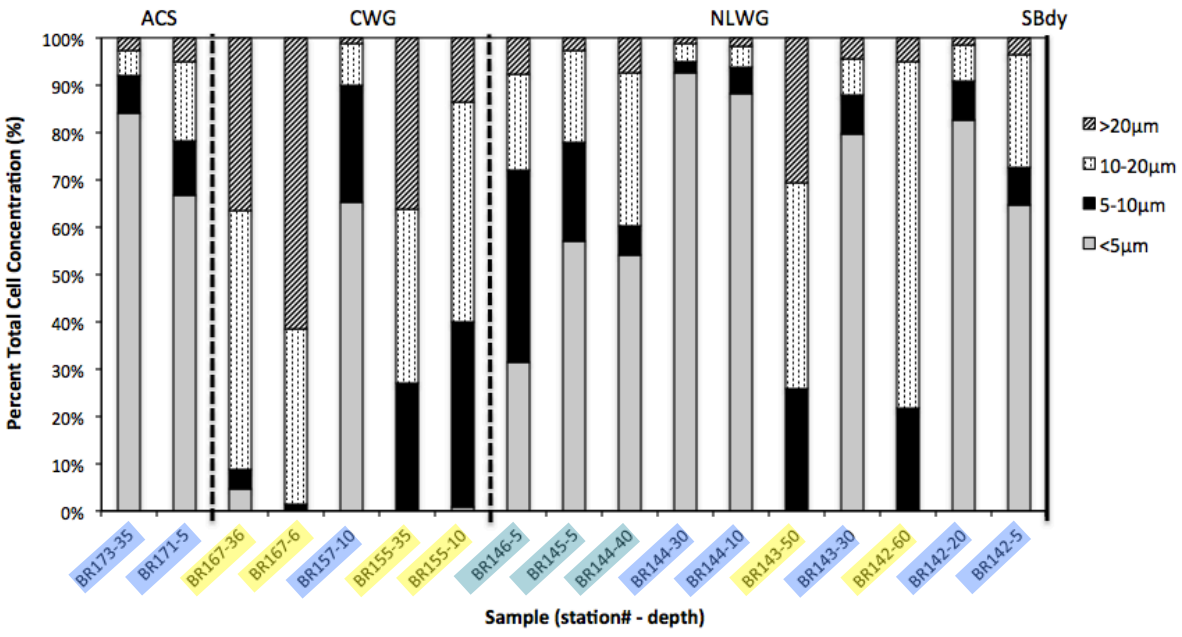

Figure 2.4.8 Cumulative percent bar graph of relative concentrations of cell sizes for microscopy samples, showing the contributions of four cell size categories: <5 µm (grey), 5-10 µm (black), 10-20 µm (black dots) and >20 µm (black lines). Lines indicate the Southern Boundary of the ACC (SBdy)(solid) and mark the boundaries (dotted) between the Northern Limb of the Weddell Gyre (NLWG), Central Weddell Gyre (CWG) and Antarctic Continental Shelf (ACS)(see Discussion section 2.4 for definitions).

2.4.3.3 Species composition

Species cell count data were grouped into four main phytoplankton types (i.e. *P. antarctica*, Diatoms, Dinoflagellates and Other – ciliates, silicoflagellates and heterotrophs) and are presented in Table 2.4.2. Based on cell concentration (cells l^{-1}) *P. antarctica* was the most consistently dominant species, contributing 69.5±18.4% to total cells l^{-1} (n = 11 samples where *P. antarctica* was present). In eight of these samples, corresponding to the small cell dominated communities (<5 µm, Figure 2.4.8), *P. antarctica* made up >60% of cells (bold values in Table 2.4.2). In the mixed communities, where *P. antarctica* abundance was <60%, diatoms and dinoflagellates made up the majority of the remaining population, with the exception of one sample (BR142, 60 m) where hererotrophs dominated (67.5%). Diatoms were observed at all stations, contributing 20.5±17.9% to total cells l^{-1} (n = 17) but varied greatly in their contribution, ranging from ~3% (BR144, 30 m) to ~78% (BR155, 35 m). The most common diatoms were the chain forming species *Pseudonitzschia. Fragilariopsis, Rhizosolenia, Chaetoceros* and *Leptocylindrus*. Dinoflagellate distribution was similarly variable (20.1±20.9%. n = 17), ranging from ~2% (BR144, 30 m) to ~69% (BR143, 50 m).

Table 2.4.2 Relative contributions (%) of phytoplankton types for cell count data (cells l^{-1}). Un-identified cells have been labelled as 'Other'. Bold values indicate dominant contributions and 0% contributions are indicated (-).

Station No.	Latitude (° S)	Depth (m)	Diatoms	*P. antarctica*	Dinoflagellates	Heterotrophs	Ciliates	Silicoflagellates	Other
BR142	-61,995	5	12,27	**64,77**	7,80	14,73	0,22	0,22	-
		20	9,50	**82,66**	5,18	2,25	0,19	0,23	-
		60	11,21	-	18,99	**67,45**	2,17	-	0,18
BR143	-62,276	30	3,51	**79,82**	13,45	2,91	0,30	-	-
		50	9,68	-	**69,35**	16,13	4,84	-	-
BR144	-62,570	10	7,48	**88,27**	2,46	0,11	0,06	0,03	1,58
		30	3,13	**92,70**	2,24	0,12	0,05	0,05	1,71
		40	7,66	54,07	10,21	3,35	0,32	0,16	24,24
BR145	-62,860	5	20,36	56,95	5,56	0,72	0,14	0,38	15,89
BR146	-63,131	5	40,15	29,33	8,56	4,47	0,63	3,40	13,47
BR155	-65,580	10	48,56	-	25,07	0,90	1,49	0,70	23,28
		35	**77,81**	-	15,85	3,75	0,86	1,73	-
BR157	-66,106	10	23,36	**65,09**	6,52	0,27	0,29	0,04	4,43
BR167	-68,911	6	32,90	-	**61,04**	5,63	0,43	-	-
		36	35,65	-	47,22	11,57	2,31	-	3,24
BR171	-70,002	5	15,71	**66,54**	12,99	0,68	0,83	0,29	2,97
BR173	-70,489	35	11,41	**84,15**	3,98	0,08	0,37	0,00	-

2.4.4 Primary Production & Size Fractionated Chlorophyll

The results for the four primary production stations that were carried out along the CTD Transect (Table 2.3.1) are displayed in Figure 2.4.9a-b, Figure 2.4.10a-d and Table 2.4.3 (see also Table in Appendix 2).

Total daily Nitrogen (N) uptake for the euphotic zone (Figure 2.4.9a, Table in Appendix 2) generally increased southward from 7.0 mmol N m^{-2} d^{-1} at BR143, where NH_4-N uptake dominated (f-ratio = 0.11), to 30.0 mmol N m^{-2} d^{-1} at IS11, where NO_3-N uptake dominated (f-ratio = 0.68) (see Table 2.4.3 for nutrient specific uptake rates).

Total daily euphotic zone chl-a specific N uptake (N uptake normalized to chl-a concentration (mg m^{-3}), Figure 2.4.9b) was highest at stations BR143 and BR167, where NH_4-N uptake was highest. Conversely, lowest chl-a specific N uptake was recorded at IS11, where NO_3-N uptake was highest.

Figure 2.4.10 displays total N uptake rates (mmol m^{-3} d^{-1}, hatched area), total chl-a concentration (mg m^{-3}, bars) and size-fractionated chl-a (% <2 µm, 2-20 µm and 20-200 µm, pie charts) at different light depths (LD, 1.1-54%). N uptake generally increased with depth from the surface, with highest uptake rates recorded at the 18% LD (~20 m) and lowest at the 1.1% LD (~ 47 m). Station IS11 was an exception, where highest N uptake was observed at the 3.2% LD (17 m) and lowest nearer the surface at 32% LD (see Table 2.4.3).

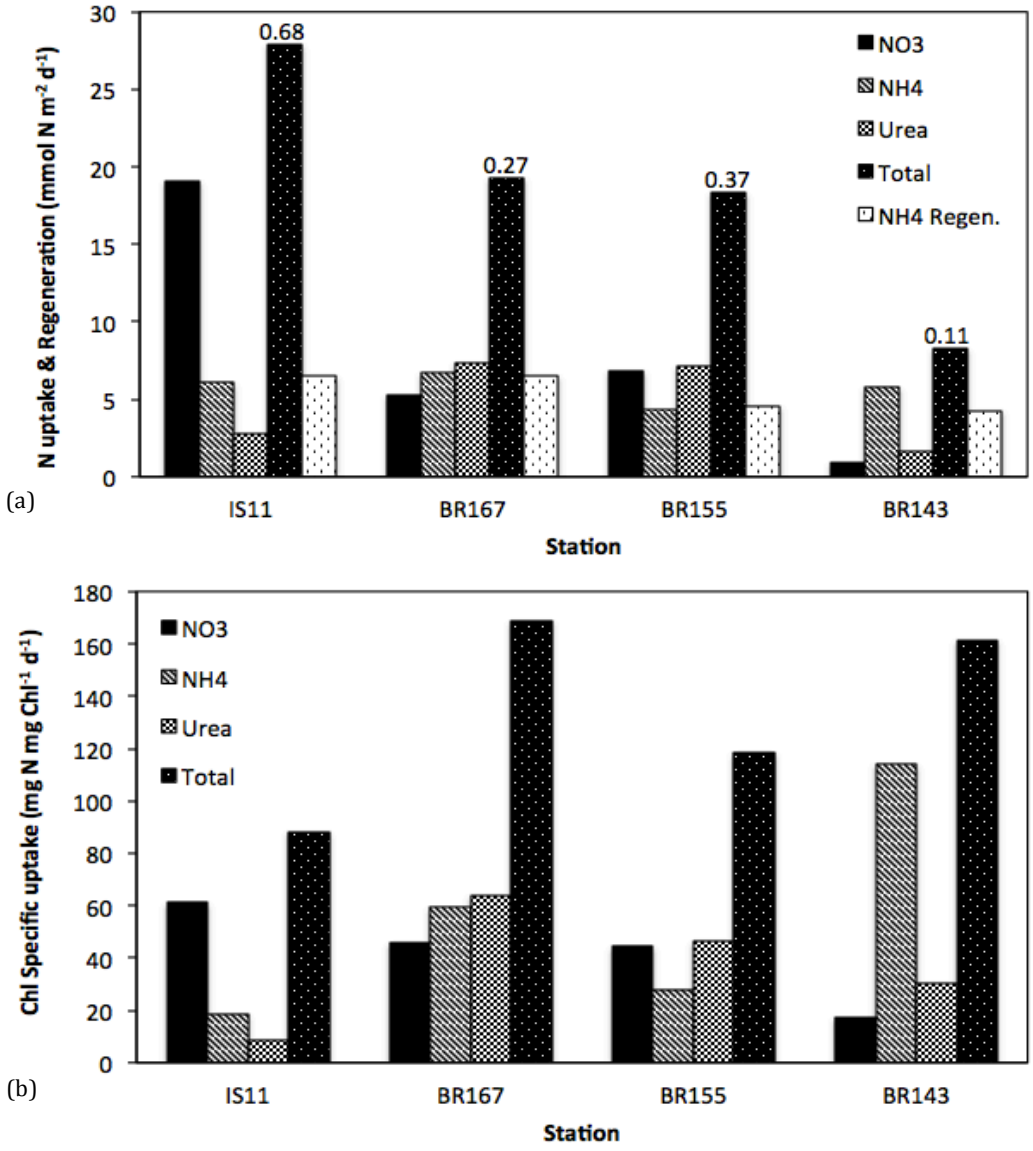

Figure 2.4.9 Euphotic zone integrated uptake rates for ^{15}N-Primary Production incubation stations along the CTD Transect (see Table 2.3.2 for station positions). (a) Nutrient specific (NO_3-N, NH_4-N, Urea-N) and Total uptake rates (mmol N m^{-2} h^{-1}) and NH_4 regeneration rates, (b) chlorophyll specific nitrogen uptake (mg N mg Chl^{-1} d^{-1}) (see Table in Appendix 2).

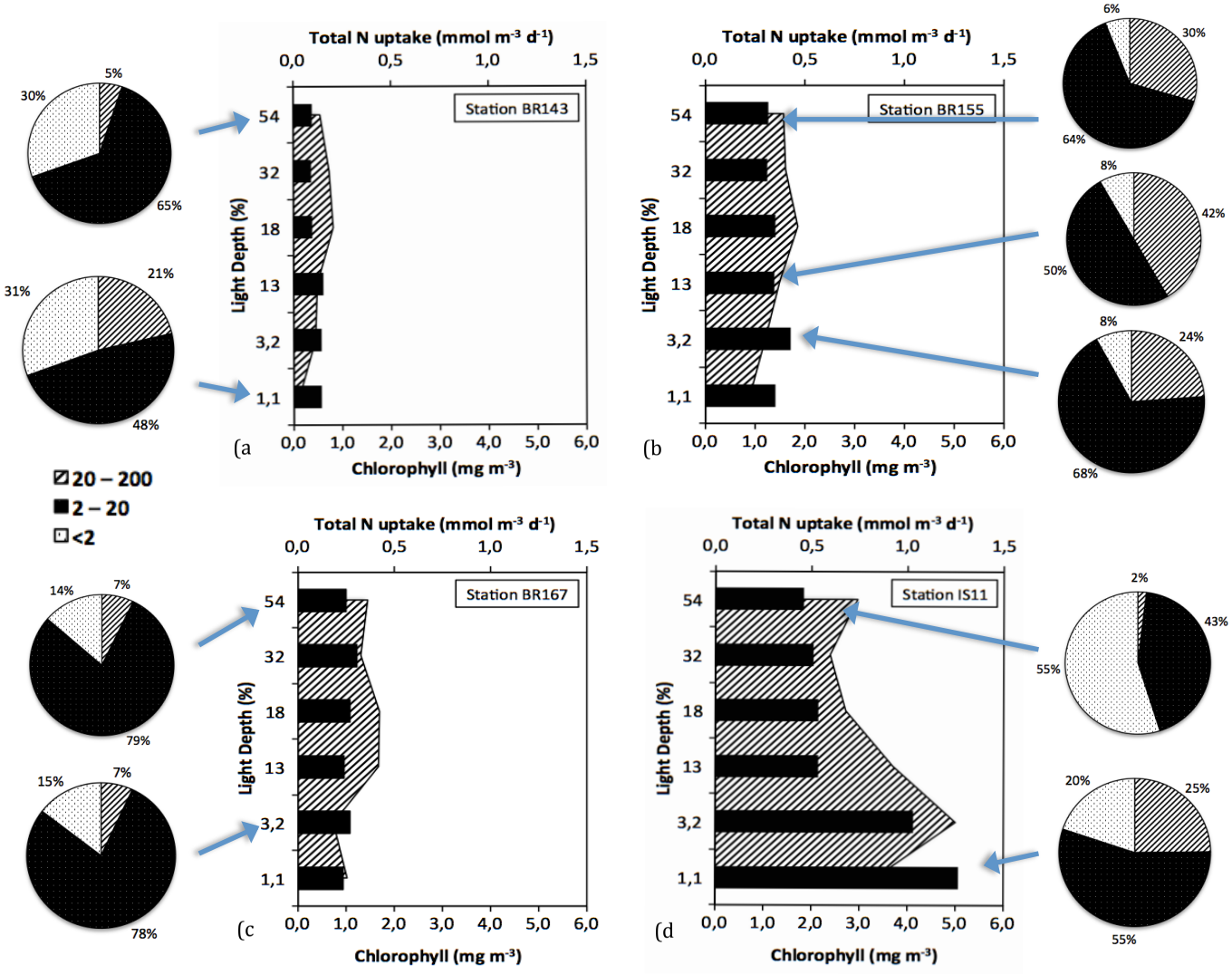

Figure 2.4.10 Production stations at (a) 62.3 °S, (b) 65.6 °S, (c) 68.9 °S and (d) 70.5 °S, showing total N uptake (mmol m^{-3} d^{-1}, hatched area) and chlorophyll concentration (mg m^{-3}, solid bars) for the six light depths (see Table 2.3.2 for actual depths). Pie charts indicate size fractionated chlorophyll proportions at selected light depths indicated. Fractions correspond to: Picoplankton (<2 µm, dots), nanophytoplankton (2-20 µm, solid black) and micro-phytoplankton (20-200 µm, stripes)(see legend inserted).

Table 2.4.3 Nitrate, ammonium and urea concentrations (mmol m^{-3}), uptake rates (mmol m^{-3} d^{-1}), f-ratios and total chlorophyll (mg m^{-3}) at the different light depths for productivity stations of the CTD Transect.

Station No.	% Light	Depth (m)	Ambient [NO_3] (mmol m^{-3})	Ambient [NH_4] (mmol m^{-3})	Ambient [Urea] (mmol m^{-3})	NO_3 Uptake (mmol m^{-3} d^{-1})	NH_4 Uptake (mmol m^{-3} d^{-1})	Urea Uptake (mmol m^{-3} d^{-1})	f-ratio	Total Chlorophyll (mg m^{-3})
BR143	54	10	24.19	1.94	0.40	0,015	0,080	0,031	0,122	0.39
	32	15	25.21	2.51	0.49	0,012	0,096	0,031	0,084	0.37
	18	20	24.44	2.38	0.31	0,017	0,113	0,027	0,106	0.39
	13	30	23.05	2.23	0.34	0,012	0,069	0,028	0,108	0.61
	3.2	40	22.47	1.72	0.51	0,021	0,057	0,027	0,196	0.58
	1.1	50	21.50	1.01	0.51	0,009	0,015	0,010	0,274	0.56
BR155	54	10	22.70	0.45	0.51	0,152	0,141	0,156	0,339	1.26
	32	15	22.96	0.43	0.51	0,167	0,100	0,153	0,397	1.25
	18	20	22.12	0.43	0.51	0,184	0,101	0,191	0,387	1.41
	13	25	21.98	0.37	0.51	0,152	0,103	0,139	0,386	1.38
	3.2	35	19.73	0.50	0.51	0,090	0,100	0,117	0,292	1.71
	1.1	44	18.84	0.49	0.51	0,069	0,065	0,095	0,302	1.40
BR167	54	6	27.72	0.51	0.51	0,115	0,115	0,150	0,303	1.00
	32	12	26.99	0.48	0.51	0,095	0,122	0,130	0,274	1.22
	18	18	27.48	0.53	0.50	0,107	0,167	0,166	0,243	1.08
	13	21	27.27	0.58	0.64	0,097	0,171	0,170	0,221	0.97
	3.2	36	27.37	0.72	0.25	0,065	0,074	0,050	0,342	1.07
	1.1	47	26.22	0.61	0.51	0,054	0,123	0,101	0,193	0.93
IS11	54	3	15.31	0.68	0.65	0,542	0,185	0,070	0,680	1.84
	32	6	26.45	0.64	0.51	0,427	0,163	0,065	0,652	2.04
	18	9	22.48	0.76	0.39	0,486	0,189	0,059	0,662	2.15
	13	10	28.70	0.57	0.51	0,658	0,277	0,076	0,651	2.14
	3.2	17	25.06	0.97	0.86	0,815	0,383	0,126	0,616	4.12
	1.1	23	21.62	0.96	0.27	0,551	0,213	0,116	0,627	5.06

Total chl-a concentrations showed little variation with depth at stations BR143-167, but there was evidence of a sub-surface chl-a maxima at 18% LD (Figure 2.4.10a,b,c). Conversely, at the ice station IS11 chl-a concentrations increased with depth reaching a maximum at the 1.1% LD (5 µg l^{-1}, Figure 2.4.10d). Size fractionated chl-a varied with depth for the three size fractions (pie-charts), with greatest variation observed at stations BR143 (Figure 2.4.10a) and IS11 (Figure 2.4.10d). At both stations the 20-200 µm fraction increased substantially from the surface to the 1.1% LD (5 to 21% and 2 to 25%, for each station respectively). This coincided with substantial decreases in the <2 µm fraction at station IS11 (55 to 20%) and the 2-20 µm fraction at BR143 (65 to 48%). The remaining two stations (Figure 2.4.10b,c) showed weaker variation between size fractions with depth, however, BR155 (Figure 2.4.10b) had the highest proportion of the 20-200 µm fraction (24-42%), while BR167 had the highest proportion of the 2-20 µm fraction (78-79%).

2.5 Discussion

The Southern Ocean plays a vital role as a net 'sink' for atmospheric CO_2 (Metzl et al., 1999) taking up ~50% of the ocean anthropogenic CO_2 flux (Takahashi et al., 2002). A key player in the effectiveness of the Southern Ocean CO_2 sink is the biological carbon pump (Eppley and Peterson, 1979) driven by phytoplankton primary production. In the Southern Ocean, primary production is characterized by high variability (Pollard et al., 2002; Seeyave et al., 2007; Thomalla et al., 2011), however the mechanisms driving this variability are not well understood. Consequently, the regional sensitivity of biological production to likely changes in the Earth's climate is hard to predict. Part of our limited understanding of the Southern Ocean's biological seasonal cycle, and its sensitivity to various physical forcing mechanisms, lies in operational limitations to resolving these questions at the required *in situ* spatial and temporal scales. This highlights the need for high-resolution hydrographic and biogeochemical measurements that address the temporal and spatial scale gaps in our knowledge of an under-sampled ocean.

Over the past twenty years satellite imagery has provided a unique tool for observing many surface ocean processes at unprecedented scales in space and time. This tool has enabled the link between synoptic scale measurements of surface chlorophyll (Sathyendranath and Platt, 1987; Mitchell, 1992) and physical variables such as sea surface temperature (Nalli and Smith, 1998; Dong et al., 2006) and sea surface height (Shum et al., 1995; Blinken and Koch, 2001; Sokolov and Rintoul, 2009). Other biogeochemical parameters have more recently been investigated through the application of inversion radiometry algorithms and include estimates of particulate organic carbon (POC) (Stramski et al., 1999; Babin et al., 2003; Martinez-Vincente, et al., 2013), particulate inorganic carbon (PIC) (Balch et al., 2005), particle size distributions (Loisel et al., 2006; Kostadinov et al., 2009) and phytoplankton community structure (Uitz et al., 2006; Alvain et al., 2008; Dierssen et al., 2006; Sathyendranath et al., 2009). Limitations inherent in these remotely-sensed observations are that they rely on model-derived measurements and are limited to observing processes in the surface layer only. *In situ* validation using high-density physical, biogeochemical

and bio-optical data is thus essential for refining bio-optical algorithms, supporting the development of biogeochemical models and enabling the implementation of novel investigative strategies (e.g. autonomous platforms) in marine biogeochemistry (IOCCG, 2011).

An example is the use of inherent optical properties (IOPs), which are easily measured *in situ* or may be derived from remote sensing, as a proxy for phytoplankton biomass (Gardner et al., 2001), community structure (Stemman and Boss, 2012) and physiology (Behrenfeld et al., 2009). The application of these proxies to autonomous platforms (i.e. floats and gliders) and remote sensing data enables the inference of phytoplankton dynamics over broad spatial and temporal scales. This use of IOPs in conjunction with ancillary data (e.g. hydrography, nutrients, community structure) may contribute to a more comprehensive understanding of the mechanisms driving phytoplankton variability; ultimately assisting to identify biologically driven CO_2 'source' and 'sink' regions in the Southern Ocean, and shedding light on how they may be expected to adjust to climate forcing.

This discussion of the results presented in Section 2.4 is structured within the context of the three aims of this study. Beginning with an investigation of the relationships between IOPs and POC, phytoplankton cell size, species composition and physiology (Section 2.5.1). Followed by the application of these relationships, to produce high resolution sections of POC, cell size, and Chl:C ratios (Section 2.5.2), to explore the variability of POC, community structure and physiology across the study region. Finally, these sections were interpreted within the context of four defined regions and their different hydrographic and nutrient environments (Section 2.5.3), with the aim of investigating the causative factors driving the observed phytoplankton variability. Concurrent discussion of these section plots with N uptake measurements enabled the inference of carbon export potential for different regions.

This study makes a valuable contribution to *in situ* bio-optical and biogeochemical data collection in an acutely under sampled region of the world's

oceans. As such, it adds to the growing database that will improve *in situ* Southern Ocean empirical relationships, which can be applied to data from remote sensing ocean colour and autonomous platforms (e.g. gliders and floats), thus improving the use of these observational tools for biogeochemistry in this globally important region.

2.5.1 Aim 1: Investigating the variability in IOPs that may be explained by changes in POC and phytoplankton community structure (with regard to cell size, species dominance and physiology)

2.5.1.1 *IOPs and POC*

In the Southern Ocean, IOPs are largely determined by phytoplankton particulates, the concentration of which influences IOPs to the first order (Stemman and Boss, 2012). Relationships between IOPs and POC thus enable the use of both particulate beam attenuation (c_p) and backscattering (b_b) as proxies for POC (Gardner et al., 2001; Stramski et al., 1999, Dall'Olma et al., 2009). The development of a linear regression relationship between IOPs and POC is of particular interest in the Southern Ocean because of the scarcity of ship based *in situ* measurements and increasing use of remotely sensed apparent optical properties (AOPs) and autonomous IOP platforms (e.g. floats and gliders) to explore the particle structure of the ocean (Stramski et al., 2008).

Increasing evidence suggests that significant regional differences exist between base-line optical properties of open ocean waters. As a result, the retrieval of bio-optical and biogeochemical properties in globally under-represented regions is likely to be biased (Claustre and Maritorena, 2003), thus highlighting the need for region specific data. A focus of this study was to develop Southern Ocean specific relationships between IOPs and the particle field that would improve the products derived from satellite and autonomous observation platforms. Although previous studies have utilized the more abundant b_b data and found good agreement with POC concentrations (Babin et al., 2003; Martinez-Vincente, et al., 2013), this study placed more emphasis on the stronger c_p-POC relationship. It must be noted, however, that b_b is easier to determine from satellites and b_b sensors are more easily attached to autonomous platforms than bulky c_p sensors, highlighting the continued importance of the b_b-POC relationship.

In this study, the respectable linear relationship between c_p at 650 nm ($c_{p(650)}$) and POC, shown in Figure 2.5.1a (r^2 = 0.65, n = 162, standard error (SE) = 28%), lies well within the range of regional variability reported by Gardner et al., (2006). Methodological and instrumental differences between datasets, may play an important role in the observed variability. For example, Bishop and Wood (2009) found that differences in acceptance angle between instruments (0.5-1.5°) contributed to part of this variability, while further uncertainty has been associated with the blanks for discrete POC samples (Bishop, 1999). When correct calibration procedures are carried out, the reliability of the c_p-POC relationship improves (IOCCG, 2011), typically varying by about 10% (Bishop, 1986; 1999; Bishop and Wood, 2009).

The weaker relationship between b_b at 650 nm ($b_{b(650)}$) and POC (r^2 = 0.56 , n = 170, SE = 45.7%) is shown in Appendix 3. While c_p is strongly determined by total particle concentration and thus POC, b_b is sensitive to particle size and composition and is thus not as reliable a proxy for POC. In a comparison between c_p and b_b measurements versus POC in the upper water column, Bishop and Wood (2009) found a good correlation for both. The relationship between b_b and POC, however, did not hold below the euphotic zone, where the proportion of POC exported to the deep ocean is important to quantify. Although backscattering sensors are smaller, simpler to use and attach easily to gliders, transmissometers are more stable and less affected by changes in particle composition. Despite their different strengths and limitations, both provide valuable tools for estimating POC and particle properties (IOCCG, 2011). By comparing *in situ* ship-based c_p and b_b measurements with b_b measurements retrieved from gliders over the seasonal cycle these relationships may be further tested and improved.

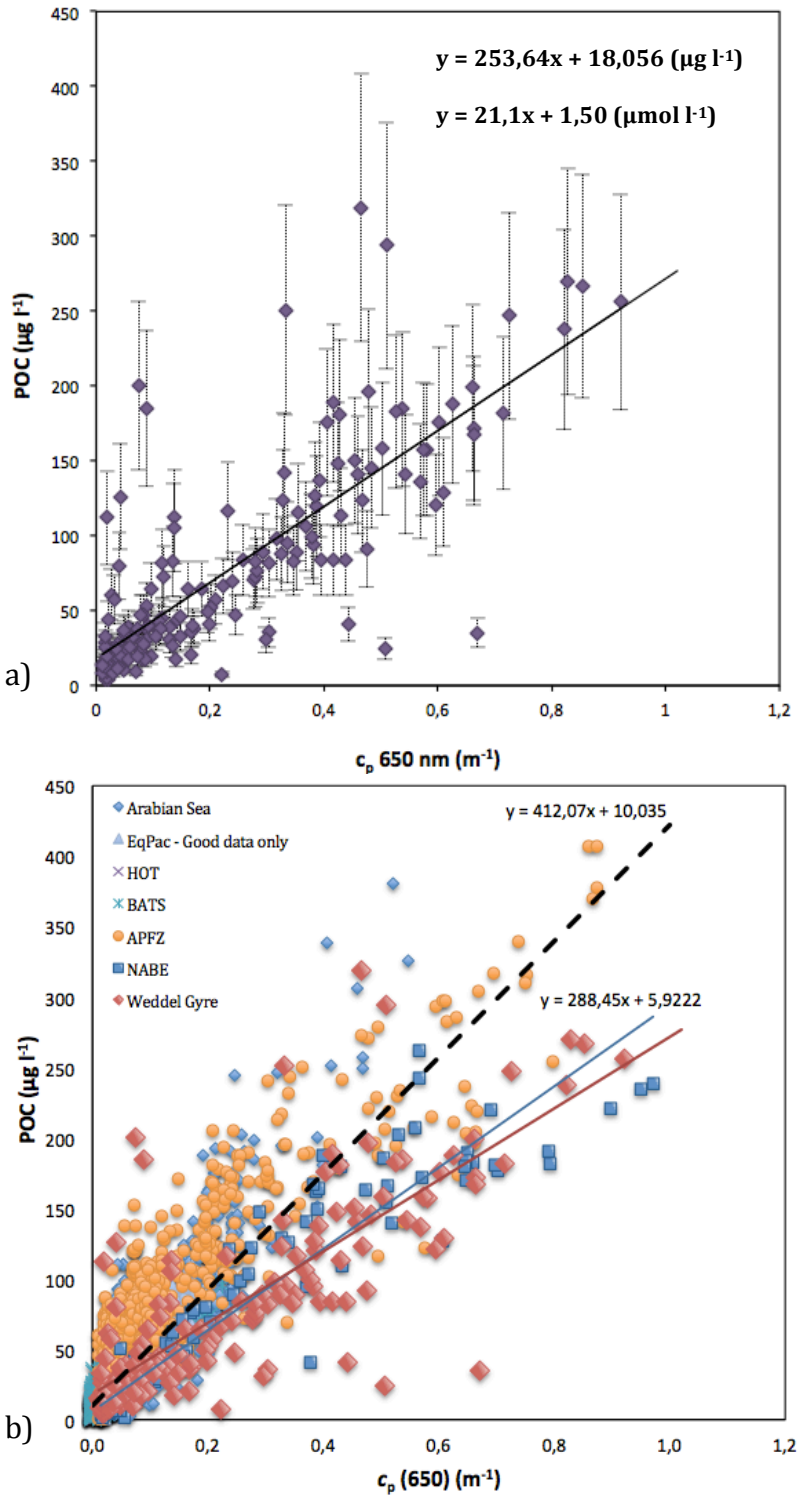

Figure 2.5.1 Regressions of POC and c_p (650 nm) data: (a) for this study in the Weddell Gyre (Error bars represent a standard error of 28%) and (b) a comparison with a global dataset from six different surveys. Global datasets are from: the Arabian Sea, Equatorial Pacific, North Pacific (HOT), North Atlantic (BATS and NABE) and the Antarctic Polar Frontal Zone (APFZ). Regression lines are fitted to this study Weddell Gyre (red), NABE (blue, equation shown) and all data (dashed, equation shown). Data re-plotted from Gardner et al. (2006). (Data source: Particle Dynamics Group, http://oceanography.tamu.edu/~pdgroup/TAMU-SMP.html)

Within a global context, the c_p-POC regression equation for this study (POC = 21.1*c_p + 1.50 for POC converted to µmol l^{-1}) is in good agreement with the equation developed for the global dataset by Gardner et al. (2006)(POC = 31.7*c_p + 0.785, see Figure in Appendix 4). These results show convincing evidence for the use of IOPs, particularly c_p, as a proxy for POC in the Southern Ocean. A direct comparison of the present data with the global dataset for the Indian, Atlantic and Pacific oceans (Figure 2.5.1b), reveals an interesting observation: namely, that the data for this study (Weddell Gyre, red triangles) and the North Atlantic (NABE, blue squares, n = 165) show striking similarities with regard to data scatter and regression line slope (304 versus 288, for this study). This is surprising when you consider how different these two systems are. Primary production in the oligotrophic North Atlantic is limited year round by macronutrients (Mills et al., 2004) and iron (Moore et al., 2009), and prone to spring blooms commonly associated with high concentrations of coccolithophores, which have a dominant impact on IOPs (Gitelson et al., 1996). Furthermore, there are differences in optical instrument specifications between the present dataset and that of Gardner at al. (2006). While the c_p measurements for the global dataset were all collected using a SeaTech Transmissometer with a 1.03 degree acceptance angle, the present study used a C-star Transmissometer with a 1.2 degree acceptance angle (see Section 2.3.8.1). A more recent study in the North Atlantic carried out in the open ocean during spring of 2008, showed strong differences in the c_p-POC relationship (Cetinić et al., 2012). While measurements of c_p were taken using the same instrumentation as the present study, they reported a much steeper slope (391±19) and a negative y-intercept (-5.8±5.5). Thus, it becomes clear that while regional-specific c_p-POC relationships are important to clarify, differences in instrument specifications (particularly acceptance angle; see review by Boss and Behrenfeld, 2000; Boss et al., 2009) need to be taken into account when comparing datasets. Ideally, the acceptance angle should be standardized for all instruments used in c_p data collection to ensure accurate comparisons between datasets and reduce the uncertainty of background variability.

In addition to instrument differences, observed variations in slope and y-intercept between datasets (Figure 2.5.1a,b; see Table in Appendix 4) were likely the result of regional differences in the particle structure, with regard to cell size distribution and particle composition (organic, siliceous, carbonate), as well as differences in background signal (water and dissolved components) (Stemman and Boss, 2012). By increasing the size of the Southern Ocean IOP-POC dataset, using data from multiple seasonal cruises (as well as from gliders, which measure b_b) we may begin to establish a more robust empirical relationship for this region.

In the following section (Section 2.5.2.1) the c_p-POC regression equation will be applied to the $c_{p(650)}$ transect across the Weddell Gyre and the subsequent POC section discussed in context.

2.5.1.2 *IOPs and Size*

In the open ocean, where phytoplankton are considered the dominant constituent influencing optical properties (Bricaud and Morel, 1986), the effect of suspended particles on light attenuation varies greatly with wavelength. The spectral shape is largely defined by chl-a concentration and cellular packaging, which produce absorption (and thus beam attenuation) peaks at ~440 nm (blue) and ~670 nm (red)(see Figure 1.5 in Section 1.6.3.1), while absorption by detritus steadily increases from red to blue. Large variations in the attenuation spectra are associated with variations in phytoplankton communities (Sathyendranath et al., 1987; Bricaud et al., 1998), due to cellular differences in size, shape, internal structure and non-POC components (e.g. silica cell walls; Vaillencourt et al., 2004), as well as variations in accessory pigments between dominant species (Yentsch and Phinney, 1989).

If we consider a typical Jungian particle size distribution (a population of particles where small particles occur at the highest concentrations, decreasing rapidly with increasing size, following a logarithmic curve.), consisting of

spherical particles, the strongest influence on c_p is by particles within the 0.5 to 10 μm range (Stramski and Kiefer, 1991). This size range generally corresponds to that of living (pico- and nanophytoplankton, pico- and nano-zooplankton and heterotrophic bacteria) as well as non-living particles (detritus) within this size range (IOCCG, 2011). As cell size increases we expect c_p to decrease as a result of the lower backscattering efficiency of larger cells (Morel and Bricaud, 1981; Vaillencourt et al., 2004). While variations in cell specific backscattering were primarily attributed to POC it appeared to be secondarily related to cell size, such that by accounting for changes in cell concentration, "per-cell" backscattering appeared to increase with increasing cell size or POC content (Vaillencourt et al., 2004).

IOPs have been successfully related to cell size, based on the variation in spectral shape (e.g. Coitti et al., 2002; Bricaud and Stramski, 1990). This is because small cells (<5 μm), when compared to large cells; occur at greater concentrations, have higher surface area to volume ratios and generally higher pigment concentrations relative to their size, and thus are more effective at absorbing light (DuRand and Olson, 1996). Furthermore, the variations in intra-cellular pigment densities linked to changes in cell size are particularly prevalent when light is limiting (see Ciotti et al., 1999; Sathyendranath et al., 2001). This "pigment packaging" (Morel and Bricaud, 1981) has a stronger influence on c_p in the blue compared to the red wavelengths (Bricaud and Stramski, 1990). As a consequence, small cells are associated with a higher peak in the blue wavelengths, resulting in a steeper slope between blue and red wavelengths.

In this study, the IOP-size relationship in the Southern Ocean was tested using c_p at two narrow wavebands (460-480 nm and 640-660 nm). Although the two-wavelength approach significantly limits the accuracy of cell size estimates when compared to the use of spectrally resolved absorption data (described in Section 1.6.3.1, see Figure 1.5), based on the impact of cell size on spectral slope, we still expected to see a steeper slope between the red and blue wavelengths for smaller cells (pico-phytoplankton) than for larger cells (micro-phytoplankton) as has been previously observed (Baker and Lavelle, 1984; Ciotti et al., 2002;

Oubelkheir et al., 2005).

While ESD_w (Equivilent Spherical Diameter weighted by cells ml^{-1}) performed well when compared to cell concentration, cell specific Chl and POC and species diversity (Figure $2.4.7_{a-d}$), it did not show any significant relationship with the spectral slopes of, c_p (Figure 2.5.2) or b_b (see Figure in Appendix 5). Possible errors may have incurred in the slope calculations due to the c_p and b_b data being limited to two spectral measurements, both of which fell short of the two main spectral peaks thus reducing the magnitude and sensitivity of the slope to changes in cell size. A number of other factors related to the cell size calculations likely contributed to the absence of any relationship between ESD_w and these two optical measurements. Firstly, the small ESD_w sample size of this study (n = 14) was possibly insufficient to drive a statistically significant relationship. Secondly, there are limitations inherent to microscopy in characterizing community size; for example the method does not accurately account for cells <2 μm, which are known to significantly contribute to cell concentration and have a dominant impact on IOPs (Morel, 1974; Stramski and Kiefer, 1991). Thirdly, the estimates of size were based on equivalent spherical diameters (ESDs), derived from cell volume estimates using two microscope measurements applied to simple geometric shapes. This estimation of size assumes that all phytoplankton cells are spherical, which is rarely the case, and thus does not account for the impact of non-spherical shapes and surface irregularities. This is important to consider because irregular cell shape and surface roughness, which increase surface area to volume ratios, have been shown to contribute to variations in backscattering efficiency (Vaillencourt et al., 2004) as well as increasing the optical size of a cell (Morel and Ahn, 1990). In addition, sampling and sub-sampling bias (~10%), cell deterioration due to preservation (~5%), microscope size limitations (~5%), human error (~15%), accurate match-ups of data (~10%) and instrument error (generally <1%), must also be taken into account when using microscopy to characterize the community structure by size. Finally, the two wavebands (460-480 nm and 640-660 nm) occur just off the two distinct chl-a absorption peaks at ~440 nm and ~680 nm (Figure 1.5), further limiting the probability of establishing a reliable IOP-size relationship given this limited

dataset.

We anticipate that with a larger sample size and more robust measurements of particle size (through automated techniques) the expected IOP-size relationship will hold. A superior method for characterizing the dominant size-classes of a phytoplankton community, for example, would be through the use of a Coulter Counter and/or Flow Cytometer, which are both able to capture particle sizes of ~0.2 µm. Neither of these instruments, however, was available at the time of this study. A Beckman Multisizer-4 has since been purchased, which will more accurately measure the size distribution of the phytoplankton community and account for the presence of small particles (<2 µm), thus improving the relationship between size and IOPs in future surveys. Measurements of increased spectral resolution for beam attenuation, absorption and scattering using a recently acquired WETLabs AC-S and ECO BB9 are further expected to improve the IOP-size relationship for this region.

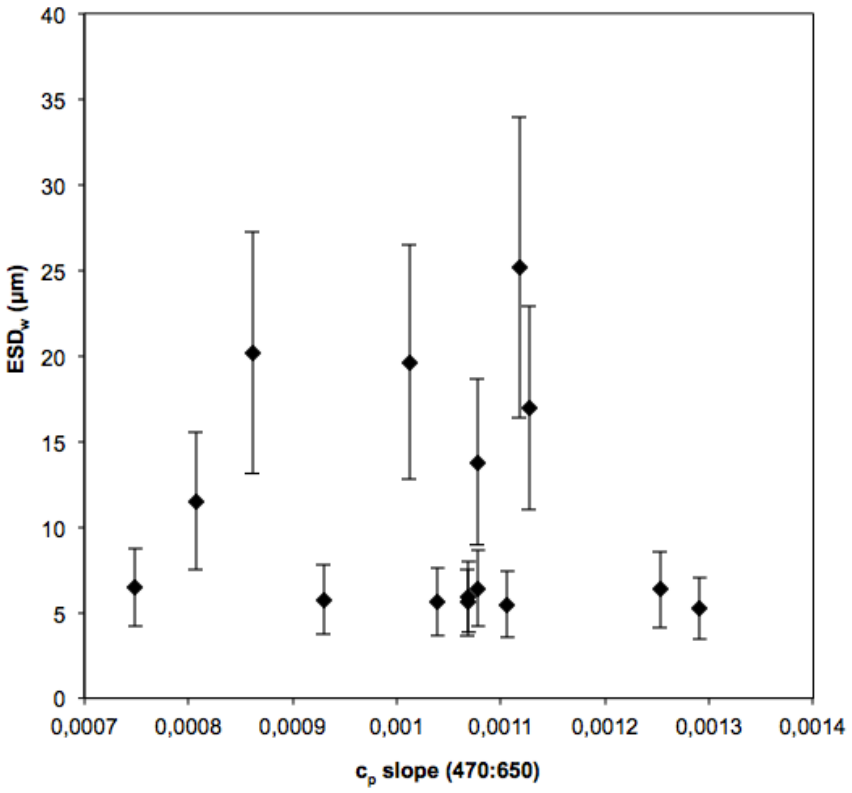

Figure 2.5.2 Estimated Spherical Diameter (ESD_w) versus c_p (470/650) spectral slope. Error bars show accumulated error estimate of 35% for size calculations (n = 14).

It must be noted here however, that ESD_w showed good agreement with variations in cell concentration, species richness and cell specific values of carbon (POC*) and chl-a (chl-a*) (Figure 2.4.7a-d). These variables that appear to co-vary with cell size, are all likely to contribute to the impact on the IOPs and further complicate the IOP-size relationship. On the other hand, these relationships also emphasize the suite of ecological and physiological information that may be inferred from measurements of community cell size.

Although no significant relationship between size and c_p (or b_b, Figure in Appendix 5) spectral slope was measured in this study, the theory is considered to be robust (Baker and Lavelle, 1984; Ciotti et al., 2002; Oubelkheir et al., 2005). Thus the optical slope is assumed to reflect adjustments in dominant particle size and can be applied to an array of optical instruments (e.g. CTDs, gliders and floats). In the following section (Section 2.5.2.2) c_p slope will be applied to the transect data across the Weddell Gyre and discussed in terms of variations in relative community cell size.

2.5.1.3 *IOPs and Physiology*

If we are to improve predictions of marine ecosystem responses to environmental and climate change, we need to quantify and parameterize the key physiological responses of plankton that will in turn affect marine food webs and the carbon-climate system. To achieve this, one needs to assess not only variability in primary productivity, but also to routinely provide information on phytoplankton functional types and physiology. The significance of establishing relationships between optical properties and physiology lies in the development of new methods to investigate broad-scale changes in phytoplankton physiology. Such broad-scale changes will provide insight into the environmental drivers of the observed variability, with possible indications of physiological responses to future environmental changes (Finkel et al., 2010). A recent focus on solar stimulated fluorescence has provided a new source of physiological information from ocean colour data (Behrenfeld et al., 2009). Under high nutrient low

chlorophyll (HNLC) conditions, for example, iron stress was associated with elevated satellite fluorescence as a result of physiological adjustments in photosystem stoichiometry (Behrenfeld et al., 2009). These physiological adjustments in turn affect carbon to chl-a (C:Chl) ratios. The ability to observe physiological responses using remotely sensed optical properties thus allows us to identify areas of possible resource abundance and limitation. It is however, essential that these satellite-based observations be validated with *in situ* optical data to ensure that the accuracy of these relationships holds for different regions. For example, in a field-based study, Behrenfeld and Boss (2003) showed that chl-a normalized c_p (c_p*, a proxy for C:Chl ratio) was sensitive to changes in photosynthetic rates, as a result of acclimation to low light. While variations were observed between several regions, due to cell size and taxonomic differences, the relationship was surprisingly consistent.

The subtle variability in Chl:c_p ratios (the ratio between fluorescence-derived chl-a and c_p) was used in this study as a proxy for Chl:C ratios to provide insight into the adaptive strategies of phytoplankton communities to light and iron limited environments through cellular chl-a packaging. In the Southern Ocean where both iron and light co-limit phytoplankton growth (De Baar, 1994; Moore et al., 2007), we expect to see strong responses in the physiological parameter of the Chl:C ratio. Changes in Chl:C ratios are strongly influenced by changing light, temperature and nutrient environments (Behrenefeld and Boss, 2003). As such, under light limiting conditions phytoplankton respond by increasing the amount of chl-a packed into their cells, in order to increase their light harvesting ability (Behrenfeld and Milligan, 2013), thus we expect Chl:C ratios to increase under low light conditions. Similarly high Chl:C ratios are expected to be associated with high temperatures and nutrient replete conditions (Gieder et al., 1998), while the opposite is true for low Chl:C (i.e. low temperature, high irradiance and nutrient limiting conditions). Thus, for the Southern Ocean, where surface temperatures are often below 0 °C, light is highly variable and iron is limiting, low Chl:C ratios are expected to coincide with shallow mixed layer depths (De Baar, 1994). Conversely, increased Chl:C ratios are expected to be associated with regions of surface warming, light limitation at depth and high iron

availability (e.g. Moore et al., 2007), for example near the ice shelf. It must be noted, however, that while phytoplankton are considered the primary drivers of particle concentration, and thus POC, in the Southern Ocean, contributions by zooplankton, detritus and bacteria, which have not been accounted for here, may also play an important role in driving the variability of Chl:C ratios.

The strong agreement between chl-a concentration (mg m^{-3}) and c_p (m^{-1}) observed in Figure 2.5.3a (c_p = 0.23Chl + 0.06; r^2 = 0.90, SE = 24.1%) indicates that changes in chl-a were dominated by changes in phytoplankton biomass, rather than by photo-acclimation. This is consistent with previous work by Behrenfeld and Boss (2006), who report a similar relationship for the Joint Global Ocean Flux Study (JGOFS) Southern Ocean Program dataset (c_p = 0.24Chl + 0.02; r^2 = 0.91). An equally strong relationship between chl-a concentration and b_b (m^{-1} *10^{-3}) was observed (b_b *10^{-3}= 0.33Chl + 0.50; r^2 = 0.87, SE = 27.6%, see Figure in Appendix 6) and suggests that Chl:b_b is equally suitable as a proxy for investigating Chl:C ratios, and thus can be successfully applied to glider data. The scatter in both relationships that is not accounted for by phytoplankton biomass (~10%), may be a result of either; 1) the physiological responses of cells to light and/or iron limitation (Behrenfeld and Boss, 2003; 2006), 2) changes in phytoplankton abundance, community size structure and composition (Bricaud and Stramski, 1990; Bricaud et al., 2004) or, 3) a combination of the above, as all of these factors influence the cellular chl-a content per unit carbon (c_p) (e.g. Behrenfeld and Boss, 2003; 2006).

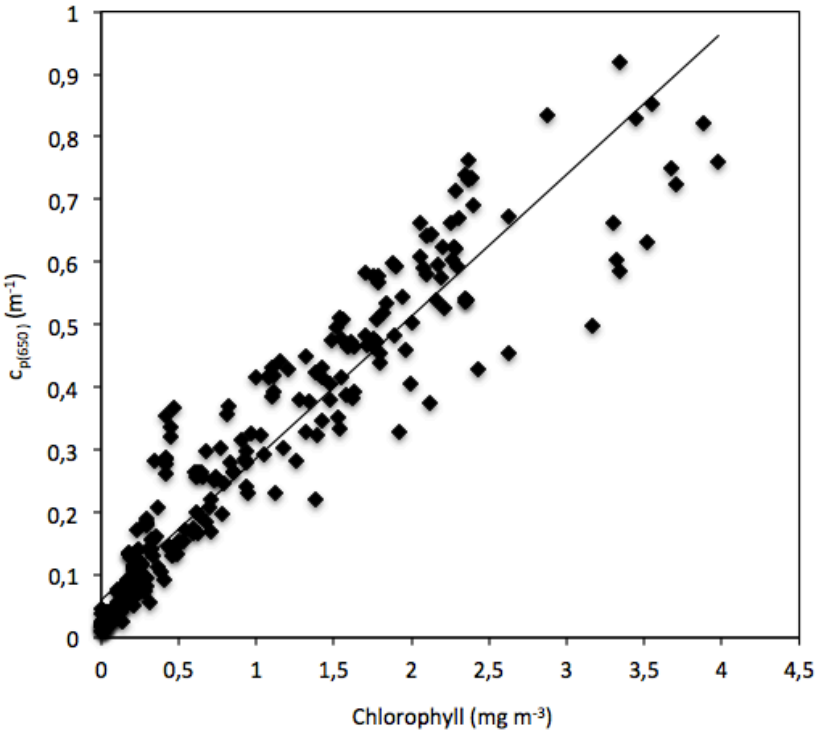

Figure 2.5.3 A regression plot of chl-a concentration (mg m^{-3}) against $c_{p(650)}$ (m^{-1}), fitted to a linear trend line (y = 0.227x + 0.060, r^2 = 0.896, n=271) representing the variability in Chl:C ratios.

In the following section (Section 2.5.2.3) Chl:c_p ratios are applied to the entire Weddell Gyre dataset and the relative variations investigated in conjunction with co-located environmental and biological parameters (e.g. light, temperature, cell size and species composition) to tease out potential physiological responses to different environmental conditions along the transect.

2.5.2 Aim 2: Applying the relationships developed in Aim 1 to explore the variability in POC, phytoplankton cell size and physiology in the Weddell Gyre

To improve our understanding of biogeochemical responses to physical forcing, we need to overcome current limitations in observing physical and biogeochemical properties. Ship-based platforms, which are not able to resolve variability over large temporal and spatial scales, are currently the dominant means of studying biogeochemical processes. As a result, these limitations restrict our understanding of biogeochemical processes and the functioning of the oceans as a whole. High-resolution measurements of biogeochemical properties over appropriate time and space scales are required to resolve the current poorly described processes, which are essential for improving biogeochemical-modeling capabilities and associated predictions of future changes (IOCCG, 2011). Optical properties (*in situ* and satellite-derived) have the ability to capture biogeochemical information over broad spatial and temporal scales, and are thus instrumental in resolving these gaps in our understanding.

In this section, the relationships investigated in Aim 1 are applied to a high resolution CTD transect across the Weddell Gyre to explore variations in POC, cell size, species dominance and physiological responses to environmental conditions.

2.5.2.1 *High resolution POC from $c_{p(650)}$*

While fluorescence-derived chl-a has long been used as a proxy for phytoplankton biomass, it is strongly influenced by changes in nutrients and light, which impact intracellular pigment concentrations as well as levels of chlorophyll-fluorescence (Behrenfeld et al., 2009). POC derived from c_p, in comparison, is largely unaffected by these physiological changes in cellular pigment concentration and thus theoretically provides a superior measure of phytoplankton biomass, but only if non-living detrital POC can be accounted for (Behrenfeld and Boss, 2003; 2006; Siegel et al., 2005; Huot et al., 2007; Dall'Olmo

et al., 2009). It is worth noting here that for this reason, the IOP data in this study (in this case the b_b but c_p is also suitable) was used to correct fluorescence measurements for surface quenching (see methods section 2.3.5).

The c_p-POC empirical relationship developed in section 2.5.1 was applied to the $c_{p(650)}$ CTD transect to produce a high-resolution section of POC across the Weddell Gyre (Figure 2.5.4a). The conversion of IOP data into POC highlights the efficacy of this method in providing a means to measure POC at high resolution and over broader spatial (horizontal and vertical) scales, which is particularly prevalent when applied to Southern Ocean glider and float data with equivalent optical sensors. It also provides an *in situ* IOP-POC link that may be used to develop and improve regional specific satellite algorithms that advance estimates of POC from remotely sensed AOPs (Stramski et al., 1999). The POC (µg l^{-1}) section (Figure 2.5.4a) illustrates that POC generally followed the pattern of chl-a (µg l^{-1}, Figure 2.5.4b), however regions of high POC were not always associated with high chl-a. The enhanced POC relative to chl-a in certain areas may be either due to a higher proportion of non-living particulate (detritus), or possible changes in pigment packaging due to variations in cell size and species composition (Finkel et al., 2010). This decoupling of POC and chl-a highlights the importance of POC, and thus c_p, as additional measurements of phytoplankton biomass distribution (Behrenfeld and Boss, 2003; 2006). In the open ocean, phytoplankton are the dominant contributor to POC (Eppley et al., 1992; Green and Sosik, 2004), thus we assume here that c_p-derived POC, as apposed to fluorescence-derived chl-a, is a superior proxy for estimating algal biomass (Behrenfeld and Boss, 2006). It is important to note here, however, that the sensitivity of c_p to suspended particles is dominated by the influence of small particles (0.5-20 µm), which peaks at 1-2 µm (Stramski and Kiefer, 1991; Boss et al., 2001). Thus, measurements of c_p-derived POC may display bias towards the dominance of small cells.

The range in POC measured along the Weddell Gyre transect (4.6-319.0 mg m^{-3}) is comparable to that seen in the Antarctic Polar Frontal Zone (0.5-407.1 mg m^{-3}, Gardner et al., 2006) but much lower than that measured in the Ross Sea (7.4-

1869.0 mg m^{-3})(see Figure 2.5.1b). Highest POC (~319 mg m^{-3}) was observed at the surface between 62.5 °S and 64.5 °S and south of the Southern Boundary (SBdy), strongly constrained by the MLD, while lowest surface POC (<5 mg m^{-3}) was associated with the low chl-a region north of the SBdy.

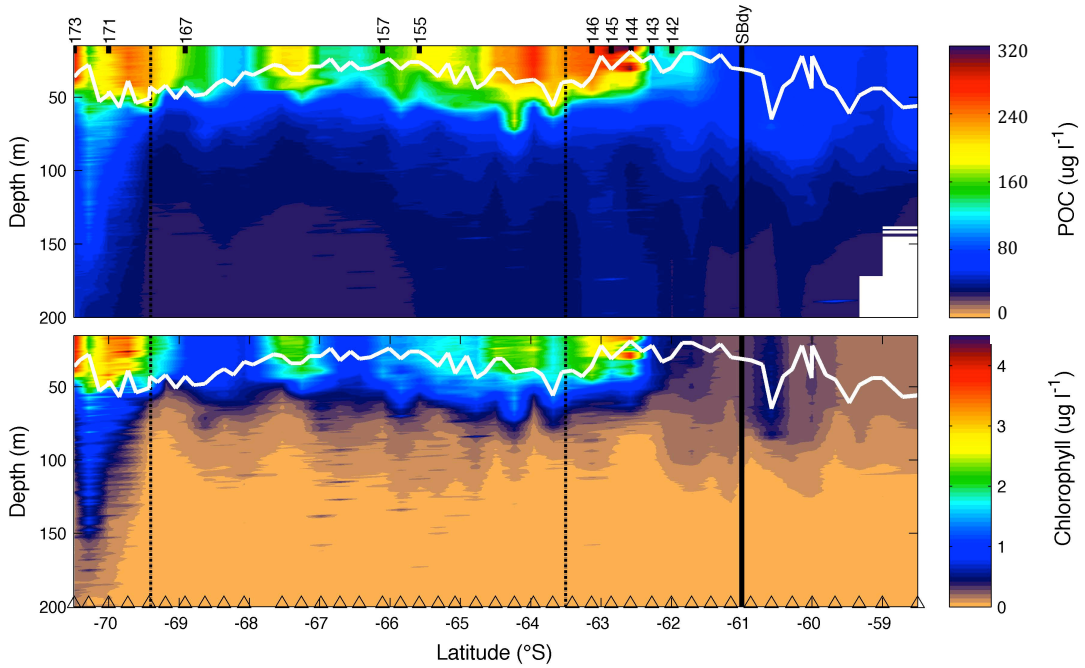

Figure 2.5.4 High resolution sections for the upper 200 m of the CTD Transect of (a) POC derived from $c_{p(650)}$, through the application of the linear regression equation developed in section 2.5.1.1, (b) Chlorophyll concentration derived from fluorescence. The temperature derived MLD (white line). Black lines mark the position of (from right to left): the Southern Boundary of the ACC (SBdy, solid line), the southern extent of the Northern Limb of the Weddell Gyre (NLWG, dashed line) and the beginning of the Antarctic Continental Shelf (ACS, dashed line); phytoplankton community structure stations are labelled above.

2.5.2.2 *Cell size from c_p spectral slope*

Establishing a relationship between dominant cell size and optical properties provides valuable insight into changes in community structure, which may determine higher trophic levels, and the potential for carbon export (Finkel et al., 2010). Providing a broad-scale view of phytoplankton size distributions will thus assist in identifying regions with a higher or lower potential for efficient carbon

export. When examined in conjunction with physical and biogeochemical data, the IOP-size relationship may provide additional insight into the environmental mechanisms driving variability in phytoplankton community structure over broad spatial and temporal scales.

The absence of a coherent statistical relationship between community cell size data (ESD_w) and $c_{p(470:650)}$ slope for this data set, however, meant that $c_{p(470:650)}$ slope could not be converted to community cell size. Instead, following previous studies (Bricaud and Stramski, 1990; Boss et al., 2001; Ciotti et al., 2002; Oubelkheir et al., 2005), $c_{p(470:650)}$ slope is used as an effective "size index" for investigating relative changes in community cell size along the CTD transect.

To clarify the spectral relationship with size; high $c_{p(470:650)}$ values correspond to steep slopes, suggesting the dominance of small cells, while low values correspond to flatter slopes and imply the presence of large cells (Figure 2.5.5a). Focusing on the regions of enhanced chl-a (Figure 2.5.5b) along the transect from north to south, the communities were characterized by the following size structure:

The first bloom region (62.5 °S and 64.5 °S) with predominantly high yet variable chl-a concentrations (1.8-3.5 mg m^{-3}, Figure 2.5.5b), was associated with the smallest cells ($c_{p(470:650)}$ = 1.1-1.4 *10^{-3}, Figure 2.5.5a) and consistently high POC (14-18 mg m^{-3}, Figure 2.5.4a). Microscopy observations revealed that small solitary cells of *Phaeocystis antarctica* generally dominated around 62.5 °S (88-93%), where ESD_w ranged between 5.6 and 6.9 µm (Table 2.4.1), but their dominance decreased southward (30-57%) from 63 °S, where diatoms contributed 20-40% (see Figure 2.4.8 and Table 2.4.2). and ESD_w increased (7.4-9.1 µm; Table 2.4.1). The majority of these cells appeared to be evenly distributed within the mixed layer, generally increasing in size with depth below the MLD. An exception was at 63.4 ° S where the smallest cells were observed at ~35 m ($c_{p(470:650)}$ >1.5 *10^{-3}). While no microscopy data was available for this region, microscopy observations at station BR144 (62.6 ° S) reveal smallest cells (ESD_w = 5.6 µm) at 30 m, which then increased in size at 40 m (ESD_w = 9.0 µm),

corresponding to a decrease in *P. antarctica* dominance (93 to 54%) and an increases in the proportion of both dinoflagellates (2.2 to 10.2%) and other un-identified cells >5 µm (1.7 to 24.2%; see Figure 2.4.8, Table 2.4.2).

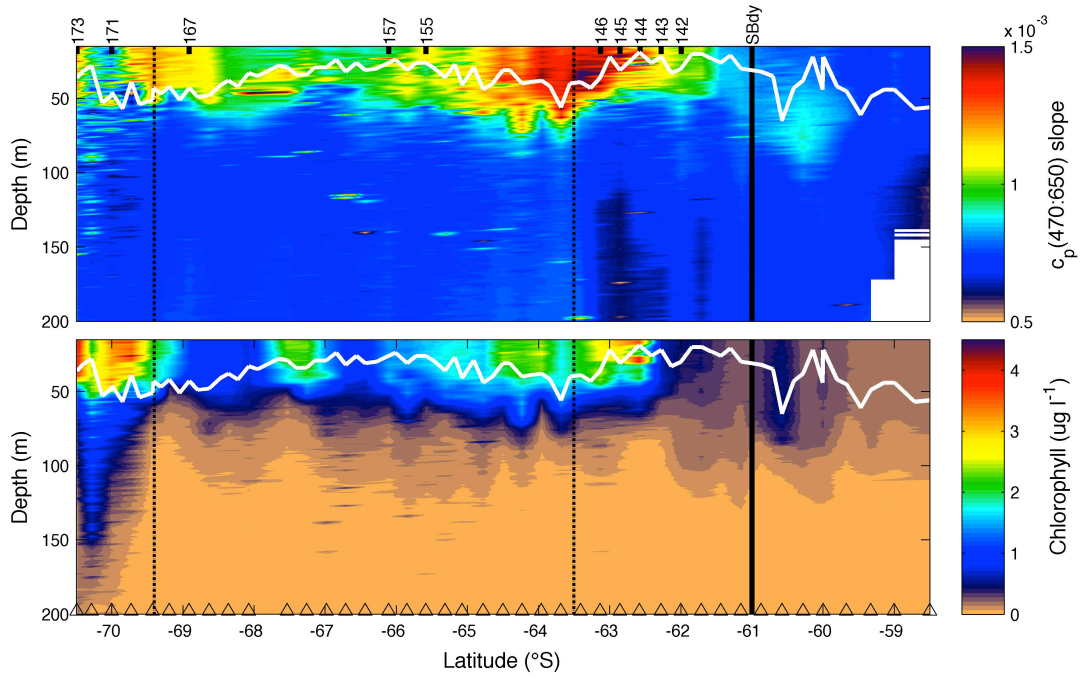

Figure 2.5.5 High resolution sections for the upper 200 m of the CTD Transect of (a) the spectral slope of beam attenuation between 470 nm and 650 nm ($C_{p(470:650)}$), (b) Chlorophyll concentration derived from fluorescence. The MLD calculated from temperature is indicated (white line). Black lines mark the position of (from right to left): the Southern Boundary of the ACC (SBdy, solid line), the southern extent of the Northern Limb of the Weddell Gyre (NLWG, dashed line) and the beginning of the Antartic Continental Shelf (ACS, dashed line); phytoplankton community structure stations are labelled above.

The second bloom (67-67.9 °S) had moderately high chl-a (~2 mg m^{-3}) and POC (~12 mg m^{-3}) concentrations, which appeared to be associated with a surface community of mixed or moderately sized cells ($c_{p(470:650)}$ = ~1 *10^{-3}), decreasing in size below the MLD ($c_{p(470:650)}$ = 1.2-1.3 *10^{-3}). While no microscopy data was available for this bloom, observations from 68.9 °S revealed a mixed community, which varied between the surface (6 m) and 36 m, where diatoms increased (33 to 36%) and dinoflagellates decreased (61 to 47%, respectively) with depth. Largest ESD_w values were recorded at this station ranging from 23.0 µm at the surface and 17.7 µm at 36 m (Table 2.4.1). An interesting feature was observed at ~48 m, where a prominent band of even smaller cells ($c_{p(470:650)}$ = ~1.5 *10^{-3})

extended across the bottom of the bloom. This feature, located below the MLD could represent a community of small cells, which are better able to adapt to low light conditions (Strzepek et al., 2012), but insufficient microscopy data means that this could not be confirmed.

The ice shelf bloom had the highest chl-a concentrations (3.5-4 mg m^{-3}) and was characterized by a varying community that shifted from small ($c_{p(470:650)}$ 1.2 *10^{-3}) cells in the north (69-69.7 °S) to large ($c_{p(470:650)}$ = 0.7-0.8 *10^{-3}) cells in the south (~70 °S), with evidence of small cells right against the ice shelf (70.5 °S). The presence of relatively enhanced chl-a associated with the sinking water mass below this ice shelf bloom (Figure 2.5.5b) appeared to be dominated by large cells or perhaps large aggregates ($c_{p(470:650)}$ = 0.8 *10^{-3}), which has important implications for carbon export (discussed further in Section 2.5.3 below). Microscopy data appeared to partly contradict these size indexes, revealing a mixed diatom/dinoflagellate community of cells >10 μm at the edge of the northern community (~69 °S) and a dominance of small cells (<5 μm) in the southern community (see Figure 2.4.8 and Table 2.4.2). However, analysis of fresh (un-preserved) samples, revealed that *P. antarctica*, (<5 μm when solitary), was present in large colonies (50-100 μm) at the ice shelf, along with large colony-forming diatoms (e.g. *Rhizosolenia* and *Chaetoceros* species). This reveals the complex effect of cells in colony formation and differences in species structure on the spectral slope (and thus effective "size index"). In addition, it highlights the importance of having good quality community structure data (preferably including some observations of un-preserved samples) and a sound understanding of the impact that cellular formation (i.e. solitary vs colonial) has on spectral slope.

These results provide intriguing evidence for how $c_{p(470:650)}$ slope may be used as a "size index" for resolving variations in size distribution at high-resolution. This "size index", however is complicated by other phytoplankton morphological traits, such that increased and improved community structure sampling efforts, which take into account not only cell size (e.g. from a Coulter Counter), but also cell formation and dominant species type (e.g. by assessing fresh samples on

board), will help to improve the empirical relationships between IOPs and community structure.

The importance of this relationship may ultimately be realized when this "size index" is applied to autonomous data sets (e.g. gliders and floats) as it will allow us to investigate temporal changes in dominant functional types, which will give us a better idea of species succession over the seasonal cycle.

2.5.2.3 *Chlorophyll to c_p ratio: a proxy for physiology and species dominance*

The complex influence of nutrients, light and temperature on phytoplankton in the euphotic zone results in a non-linear relationship between phytoplankton chl-a concentration and carbon biomass (Geider et al., 1997; Behrenfeld and Boss, 2003; Armstrong, 2006). For example, it is commonly accepted that as light decreases with depth phytoplankton respond by increasing their chl-a concentration (and as such their cross sectional area available for light absorption) (Behrenfeld and Boss, 2003). This process of photo-adaptation results in an increase in Chl:C ratio with depth. Conversely, under high light conditions cells exhibit photo-inhibition, whereby they respond by reducing the amount of chl-a within their cells, as well as actively dispersing the excess energy to avoid damage to their photosynthetic apparatus (Behrenfeld et al., 2008; 2009). The physiological responses of phytoplankton to macro-nutrients and iron, however, are more complex and difficult to observe. Model simulations (e.g. Wang et al., 2010) and iron fertilization experiments (e.g. Gall et al., 2001, Moore et al., 2007a) have played an important role in improving our understanding of the physiological responses of phytoplankton to nutrient limitation. In the Equatorial Pacific for example, it has been suggested that the spatial and temporal variations of Chl:C ratios are controlled by iron availability (Wang et al., 2010). Similarly, in the HNLC waters of the Southern Ocean iron enrichment has been shown to increase cell size and cellular chl-a, and thus result in increased Chl:C ratios (Gall et al., 2001; Moore et al., 2007a).

In this study, variations in the Chl:c_p ratio was used as a proxy for exploring physiological responses to light and iron limitation (Behrenfeld and Boss, 2003; Behrenfeld et al., 2008) as well as changes in species composition (Vaillencourt et al., 2004) across the Weddell Gyre. In the absence of iron measurements carried out for this survey, reference is made to recently published iron data (Klunder et al., 2011; Tagliabue et al., 2012), in order to establish the drivers of the observed differences in phytoplankton physiological responses and species composition.

The effect of species dominance on the relationship between c_p–derived POC and chl-a has previously been used to identify species shifts between diatoms and *P. antarctica* (Behrenfeld and Boss, 2003), however, Chl:c_p ratios in the latter, have also been shown to vary depending on cell formation (i.e. solitary vs colonial) (Strzepek et al., 2002). Thus, both the impact of species dominance and cell formation are expected to contribute to variations in Chl:c_p ratios, in addition to physiological responses to resource limitation.

The Chl:c_p ratios in Figure 2.5.6a show large variation (1-6) in the upper water column decreasing with depth below 100 m, where living cells are unlikely to be found. Highest Chl:c_p ratios (~6) were associated with the high chl-a bloom (2.5-4 mg m^{-3}, Figure 2.5.6b) at the ice shelf, while patches of elevated Chl:c_p ratios (5-6) observed below 50 m near the ice shelf and around 67 °S, provide evidence for photo-adaptation to low light conditions. The slightly elevated Chl:c_p ratios (~3.5) in the warm, low chl-a (0.5 mg m^{-3}) feature at 60.5 °S, compared to the surrounding water mass (1-2), suggests the presence of very few cells with increased chl-a concentration, possibly in response to the higher temperature (Gieder et al., 1998).

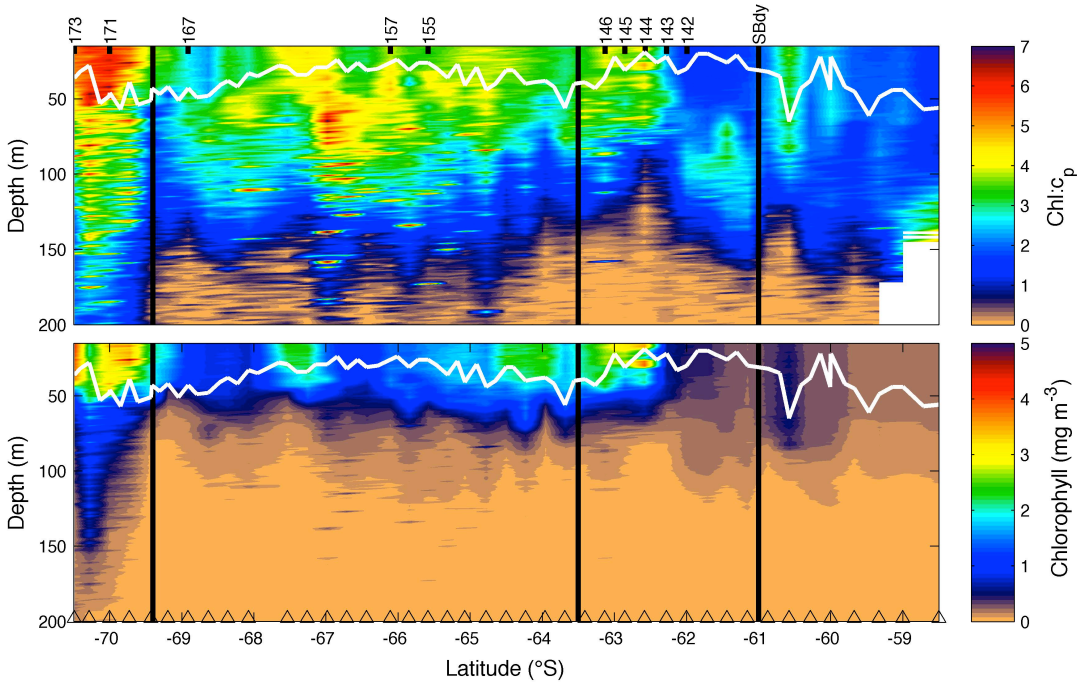

Figure 2.5.6 High resolution sections for the upper 200 m of the CTD Transect of (a) the physiology parameter, Chl:c_p, (b) Chlorophyll concentration derived from fluorescence. The MLD calculated from temperature is indicated (white line). Black lines mark the position of (from right to left): the Southern Boundary of the ACC (SBdy, solid line), the southern extent of the Northern Limb of the Weddell Gyre (NLWG, dashed line) and the beginning of the Antarctic Continental Shelf (ACS, dashed line); phytoplankton community structure stations are labelled above.

The different Chl:c_p ratios observed between the two *P. antarctica* blooms (chl-a >3mg m^{-3}) at the ice shelf (5-6) and at ~62.5 °S (3-4), is likely indicative of physiological responses to different nutrient environments. For example, the high Chl:c_p ratios at the shelf suggest relief of iron stress (Gall et al., 2001), which may be supported by the high iron concentrations generally associated with this region due to melting sea-ice (Klunder et al., 2011) and possible re-suspension of iron from the continental shelf (Tagliabue et al., 2012). However, while intra-cellular iron concentrations and iron:carbon ratios in temperate diatom species tend to increase in response to decreasing light (Strzepek et al., 2011), Southern Ocean species tend to employ adaptive strategies to deal with low ambient iron concentrations showing little change with decreasing light (Strzepek et al., 2012). Thus, Southern Ocean diatoms are able to maintain lower cellular iron concentrations and iron:carbon ratios at comparable growth rates to those of temperate species. By increasing the size rather than number of photosynthetic

units under low light conditions, these polar species exhibit an acclimation strategy to iron-light limitation that does not increase their cellular iron requirements (Strzepek et al., 2012). The ice shelf bloom varied between a dominance of *P. antarctica* colonies (84%, Table 2.4.2) at the surface and a mixed community of large diatoms and *P. antarctica at* 35 m, likely supported by increased iron input from melting sea-ice (Klunder et al., 2011). At ~62.5 °S, the community was also dominated by *P. antarctica* (88-93%, Table 2.4.2), however these were solitary cells. This difference could possibly reflect adaptation to iron limitation (Strzepek et al., 2012) as solitary cells infer a competitive advantage of increased surface area to volume ratio and are known to dominate in iron limited waters (Moor et al., 2007b). On the other hand, iron relief associated with melting ice at the ice shelf, (Grotti et al., 2005; Klunder et al., 2011) is thought to be responsible for the presence of *P. antarctica* colonies, the formation of which is associated with iron replete conditions (Hutchins et al., 2002; Strzepek et al., 2012). An additional explanation for the difference in Chl:c_p ratios between these blooms, characterized by different cell formations, is that colonies are thought to have a lower impact on the optical signal, relative to their size, specifically with regard to backscattering (Stramski, 1999). This is because the refractive index of the mucilage that forms these colonies is closer to that of the surrounding medium (Strzepek et al., 2012), and thus corresponds to lower backscattering and attenuation coefficients. Higher Chl:c_p ratios would thus be expected from colonies of *P. antarctica* compared to solitary cells.

Conversely, the two regions of comparably enhanced chl-a (~2.5 mg m^{-3}) at 63.8-64.7 °S and 67-67.7 °S had distinctly different Chl:c_p ratios of 3 and 4 respectively, that likely reflected both physiological and taxonomic differences. Previous iron measurements across the Weddell Gyre indicate that, while dissolved iron maxima were associated with salinity minima (due to melting sea-ice) there was a high degree of variability in iron concentrations (0.15-0.25 nM) within these regions (Klunder et al., 2011). Thus, the higher Chl:c_p ratios (4) in the southern bloom may possibly indicate iron relief due to slightly elevated iron concentrations, which is supported by the presence of larger cells (see Figure 2.5.5a). While the lower Chl:c_p ratios (3) in the more northern bloom were

associated with small cells (see Figure 2.5.5a), possibly due to limitation by lower iron concentrations and subsequent control by grazing (Smetacek et al., 2004).

The lower chl-a patches (1-2 mg m^{-3}) across the rest of the transect were characterized by highly variable Chl:c_p ratios ranging from 2 to 5. But while variations in Chl are driven by phytoplankton alone, variations in POC and thus c_p are also driven by detritus, zooplankton and bacteria, which have not been accounted for here. The limited microscopy sample data for these regions showed a mixed phytoplankton community made up largely of diatoms and dinoflagellates, but true dominance by any single phytoplankton group was rare (see Table 2.4.2). An exception was at 65.6 °S (BR155), where diatoms made up 49-78% of the community and Chl:c_p ratios were 3.5-4. However, this being the only station showing a diatom dominance it is not possible to make inferences about Chl:c_p ratios for diatoms in general. Yet, with more data these types of applications ought to become possible. Similarly, one needs to be careful about interpreting the low Chl:c_p ratios (~2) found in surface waters at 68.6 °S as photo-inhibition, however it is possible that this patch of particularly low ratios in a region surrounded by similarly low chl-a concentrations may reflect reduced packaging of cellular chl-a as a photo-inhibition response to high light. Worth noting is that within this patch of low surface ratios (2), Chl:c_p ratios increased to ~3 below the mixed layer.

In summary, variations in Chl:c_p may give us insight into physiological responses of phytoplankton to low light (photo-adaptation), high light (photo-inhibition) and community adaptation (reduction in cell size) to iron limitation. Due to the varying dominance of *P. antarctica* and subsequent lack of distinct communities between samples the impact of species dominance on Chl:c_p ratios remains unclear. Rather, it appears that a combination of 1) changes in the composition of organic material (i.e. colony-forming mucilage versus opaline frustules) associated with varying proportions of different species, 2) shifts in cell size distribution (i.e. solitary cells versus colonies) and 3) associated changes in pigment packaging (Sosik and Olson, 2002), was responsible for variations in the

Chl:c_p ratio. With the collection of more bio-optical, community structure and ancillary data, it is anticipated that we may begin to establish more robust relationships between IOPs and physiological indicators (both *in situ* and remotely sensed) that will allow us to tease apart the dominant factors contributing to the optical signal and in so doing increase the scope of bio-optics as a valuable biological tool.

2.5.3 Aim 3: Investigating some of the factors driving the observed variability in POC, phytoplankton cell size, community structure, physiology, primary production and carbon export

The intricate spatial (and seasonal) patterns of chl-a distribution in the Southern Ocean reflect the complex nature of the mechanisms controlling primary production in this region (Boyd et al., 2002). In these HNLC waters, the patchwork of high seasonal productivity is largely driven by ocean fronts, sub-Antarctic islands and ice-edge regions, which are often dominated by diatoms (De Baar et al., 2005; Cochlan, 2008). The overall impact of these productive hotspots results in the export of ~3% of total production into the deep ocean, which is among the highest rates for the world's oceans (Honjo et al., 2000). For this reason, it is vital to identify the regional characteristics of variability in physical drivers and the associated bloom dynamics in order to understand the sensitivity of ocean productivity to climate change.

The physical and chemical characteristics of the Weddell Gyre observed in this study, have lead to a division of the transect into four distinct regions. These are defined from North to South as: the Antarctic Zone (AAZ) – north of the Southern Boundary of the ACC (SBdy) at 61 °S; the Northern Limb of the Weddell Gyre (NLWG) – from the SBdy to 63.5 °S; the Central Weddell Gyre (CWG) – from 63.5 °S to 69.5 °S; and the Antarctic Continental Shelf (ACS) – from 69.5 °S to the ice shelf (see Figure 2.5.4-6 and Table 2.5.1). In the following sections, the observed variability in POC and phytoplankton community structure, physiology and primary production will be investigated in the context of the distinct physical and chemical drivers that characterize each region.

Using Table 2.5.1 below, which displays the hydrography, biogeochemistry and optical proxies of community cell size and physiology averaged within the mixed layer for each region, the potential drivers of phytoplankton variability will be examined. To begin with, MLD is generally shallow and varies little between regions, ranging between 32 and 45 m, which implies that light was not limiting in any of the regions. Variability in temperature, however, may play a part in

controlling phytoplankton biomass, as low temperatures are known to affect phytoplankton growth through reducing photosynthetic efficiency (Tilzer et al., 1986). The two Weddell Gyre regions for example, had the lowest average surface temperatures (-0.43 and -0.64 °C) and moderate chl-a concentrations (47.85 and 44.27 mg m^{-2}). While polar species are generally well adapted to cold conditions (Boyd et al., 2010), these low temperatures may be a contributing factor controlling the upper limit of phytoplankton growth in these two regions.

Table 2.5.1. Regional summary of hydrographic, biogeochemical and bio-optical properties averaged within the MLD for all stations in each region.

	AAZ	NLWG	CWG	ACS
Latitude (°S)	North of 61	61-63.5	63.5-69.5	South of 69.5
MLD (m)	45	32	36	38
Temperature (°C)	0,646	-0,643	-0,432	-0,087
Salinity (ppt)	33,84	33,74	33,99	34,10
Chl-a (mg m^{-2})	9,27	44,27	47,85	102,11
POC (mg m^{-2})	152,42	323,90	338,50	443,04
NO_3 (mmol l^{-1})	29,11	24,95	25,91	28,11
SiO_3 (mmol l^{-1})	131,08	165,56	160,89	126,13
PO_4 (mmol l^{-1})	1,98	2,20	2,11	2,01
Chl:c_{p650}	2,05	2,92	3,41	5,53
$c_{p(470:650)}$ slope *10^{-3}	0,75	1,19	1,07	1,00

High variability in chl-a (9.3-102.1 mg m^{-2}), POC (152.4-443.04 mg m^{-2}) and the proxies for Chl:C (Chl:c_p = 2.05-5.53) and community size index (c_p slope = 0.75-1.19) was visible between regions. Values generally increased from north to south, with the exception of the size index, which suggests that the smallest cells occurred in the two Weddell Gyre regions. In the HNLC Southern Ocean, phytoplankton are generally not limited by macro-nutrients (Boyd et al., 2007; Moore et al., 2007b; Arrigo et al., 2008). It is not surprising then that NO_3, SiO_3 and PO_4 concentrations vary little between regions, and thus along with the hydrography, fail to explain the observed variability in the biology. Other factors, which have not been measured here, are suggested to be the primary drivers of this variability. Iron concentration, for example, is one such factor that is known to be a dominant driver of phytoplankton growth and distribution in the

Southern Ocean (De Baar et al., 1990; Coale et al., 2004; Boyd et al, 2007; Pollard et al., 2007, 2009). Due to the lack of iron data available for this study, iron data from the literature (e.g. Tagliabue et al., 2012; Klunder et al., 2011) has been drawn upon to discuss the possible role of this essential micro-nutrient in controlling phytoplankton distribution, community structure, physiology and primary production across the different regions of this study.

Figure 2.5.7 is a schematic designed to consolidate all the physical and biogeochemical and bio-optical properties across the study transect. It aims to provide a visual summary that highlights the characteristics of each region with regards to phytoplankton community (biomass, cell size, species structure and physiology), bio-optical properties (c_p slope and Chl:c_p ratio), estimates of carbon export (f-ratio) and the potential driving factors of the variability observed between regions.

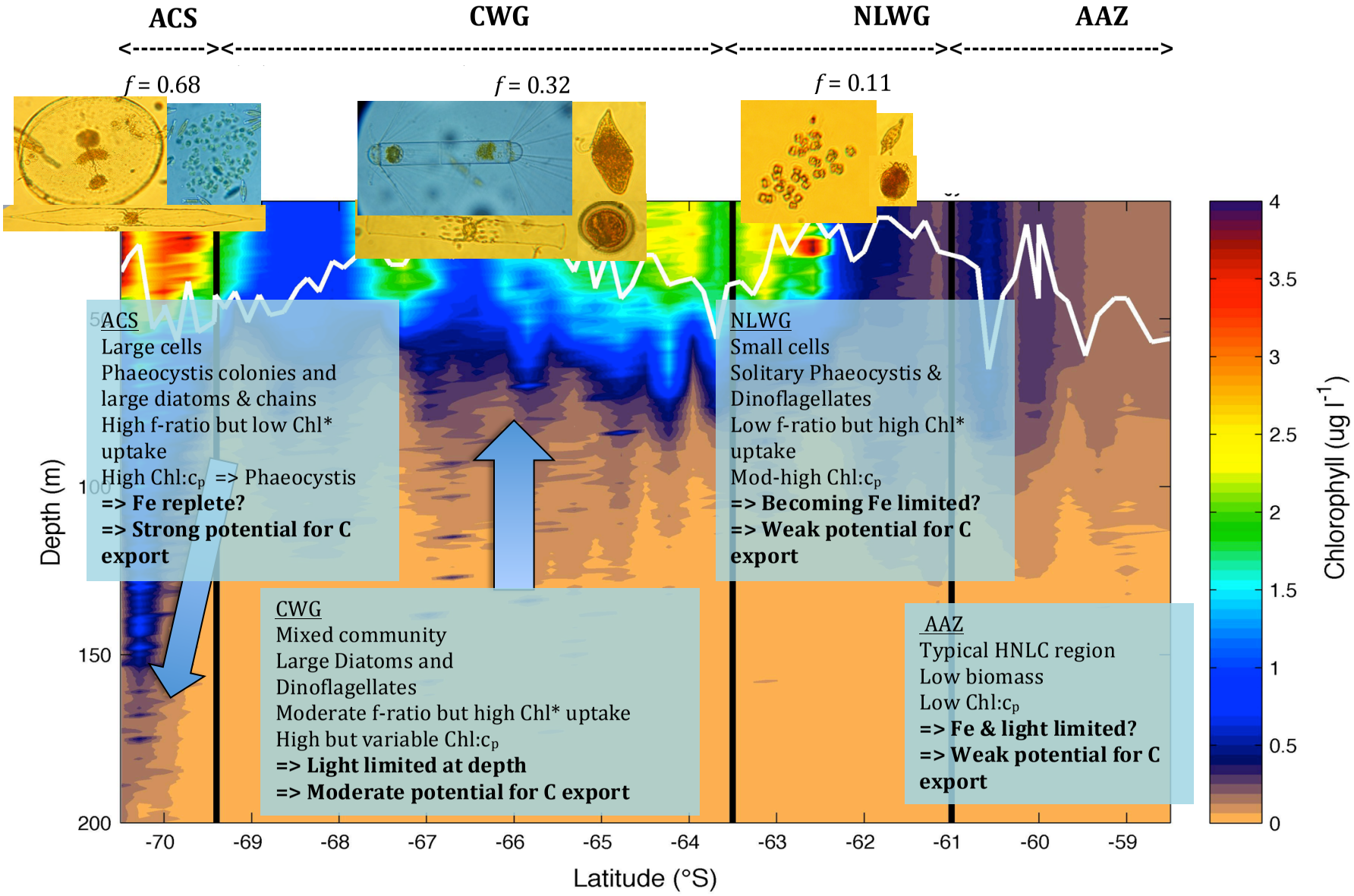

Figure 2.5.7 A summary schematic of chlorophyll concentration (ug l^{-1}) across the four regions of the study transect, overlaid with the MLD (white line), upwelling and subduction processes (arrows), images of typical phytoplankton cells (displayed as relative sizes), f-ratios (above) and text boxes (inset) listing key features and likely driving processes for each region.

2.5.3.1 *The Antarctic Zone*

The AAZ constituted the waters from the Antarctic Polar Front (APF, not shown) to the Southern Boundary of the ACC (SBdy)(61 °S). The SBdy forms a sharp retroflection in this region (Garabato et al., 2002; see Figure in Appendix 7) and separates the warm, salty and weakly stratified AAZ surface waters, from the cooler, fresher Antarctic surface waters to the south. This first region was dominated by a warm feature at 60.5 °S (Figure 2.4.1a), associated with the SBdy, which appeared to be a permanent feature as observed in annual sea-ice plots and previous surveys (see Figure in Appendix 8; personal communication with Sebastiaan Swart who identified the feature on previous cruises). This feature was likely the result of an intrusion of ACC water that formed due to retroflection of the SBdy.

Despite high nutrients (NO_3, SiO_3 and PO_4) the AAZ had consistently low phytoplankton biomass (chl-a = 9.3 mg m^{-2}; POC = 152.4 mg m^{-2}), which is typical of the HNLC region, driven by a combination of light, iron and silicate limitation (Boyd, 2002; Arrigo et al., 2008). Given the relatively shallow MLD's and high macro-nutrients, both light and SiO_3 were not limiting, thus iron limitation remains the likely factor controlling phytoplankton growth in this region (Cochlan, 2008). This suggestion is further supported by previous studies in the area, which report low iron concentrations (~0.2 nM) north of the SBdy (Klunder et al., 2011; Tagliabue et al., 2012). These low concentrations typically observed in the latter part of the growing season, lead to the dominance of small cells, which are able to scavenge iron more efficiently (Boyd et al., 2012) but are maintained at low biomass levels by grazing (Smetacek et al., 2004).

The low average Chl:c_p ratio (2.05) and flat c_p slope ($0.75*10^{-3}$), however, imply the previous bloom of large cells, likely diatoms, which may explain the slightly lower SiO_4 concentrations (131 mmol l^{-1}) relative to the Weddell Gyre regions (161-165 mmol l^{-1}). The accuracy of these optical proxies for inferring physiology and cell size, however, appears to break down at very low chl-a concentrations (9.3 mg m^{-2}). Furthermore, the lack of microscopy observations

and primary production measurements for this region, inhibit our ability to make any further assumptions regarding the phytoplankton community.

The low biomass of this region and likely iron limitation of NO_3 uptake (e.g. Lucas et al., 2007; Cochlan, 2008) would imply a community of small cells based on regenerated production and therefore low associated export (Lucas et al., 2007; Cochlan, 2008; see Figure 2.5.7). The warm feature at 61-60.5 °S, however, may potentially represent a region of increased productivity relative to the surrounding waters of the AAZ. Here, elevated chl-a concentrations (~150% higher) and increased Chl:c_p ratios (~50% higher) were likely driven by the increased temperature and deeper MLD's (69 m) (not too deep so as to be light limiting but potentially deep enough to access a subsurface regenerated nutrient supply). The persistence of this warm feature, providing an area of enhanced productivity in an otherwise low productivity region, may make a notable contribution to carbon export in the AAZ region, particularly over extended time periods. Potential evidence for carbon export was seen in the subsurface (~60 m), where a patch of higher $c_{p(470:650)}$ ratios may be indicative of larger particles or aggregates of cells sinking below the MLD. The relative loss of silicate from surface waters also implies prior diatom growth and possible export. Further work is required to examine the seasonal variability in primary production, community structure and carbon export in this region to enhance our understanding of the role of these meso-scale features in driving the Southern Ocean biological carbon pump (e.g. Smetacek et al., 2012).

2.5.3.2 *The Weddell Gyre*

The barotropic (wind-driven) cyclonic circulation of the Weddell Gyre comprises a large body of water between the AAZ and ACS regions. Two regions have been defined within the Weddell Gyre as a result of the characteristics of circulation. These are the Northern Limb of the Weddell Gyre (NLWG) and the Central Weddell Gyre (CWG).

Northern Limb of the Weddell Gyre

The eastward flowing current of the NLWG region extended from the SBdy to 63.5°S (following Garabato et al., 2002) and was characterized by cold, fresh, low-density surface water, a strong salinity gradient and thus strong surface stratification (Figure 2.4.2) with shallow MLDs (32±11 m, Table 2.5.1, Figure 2.5.7). The broader layer of WW in the NLWG (~150 m), relative to the CWG (~80 m, see Figure 2.4.1a), was indicative of deep winter mixing in this region. This was observed as the extension of sub-zero temperatures down to 200 m and little apparent influence of Warm Deep Water (WDW) (Orsi et al., 1995) on the upper layers. Chl-a characteristics of the NLWG were unusual in that they did not follow obvious physical boundaries of the region, but were rather separated at 62.5 °S, where salinities reached a minimum. Low chl-a concentrations were found to the north (0.69±0.27 mg m^{-3}) and higher chl-a concentrations to the south (3.5±0.62 mg m^{-3}).

The cause of this separation is uncertain, as no significant change in macro-nutrients was observed, but could possibly be explained by the apparent salinity front set up by the fresh surface pool, which created a strong highly stratified density gradient south of 62.5 °S (Figure 2.4.1b, Figure 2.4.2). Alternatively, the separation visible in the chl-a may have been driven by other factors such as differences in iron concentration. The observed surface freshening was likely due to melting sea-ice, which has been shown to provide an important source of iron to surface waters (Sedwick and DiTullio, 1997; Grotti et al., 2005; Lannuzel et al., 2008; Klunder et al., 2011). For example, iron measurements taken at similar latitudes just east of this survey (along the 0° meridian) by Klunder et al. (2011), found that while surface dissolved iron maxima coincided with salinity minima (<34ppt), iron values within these salinity minima varied between 0.26 and 0.15 nM. This variability in iron concentration, which may explain the observed differences in chl-a, may also represent different rates of productivity (gain) and grazing (loss), related to changes in community structure with regards to cell size and species dominance.

The low chl-a (higher SiO_4) region to the north was associated with larger cells

($c_{p(470:650)}$ = 0.8-1.1 *10^{-3}, Figure 2.5.5) and lowest recorded surface Chl:c_p ratios (~1.5, Figure 2.5.6), possibly due to the lower pigment packaging of large cells to reduce self-shading. Alternatively, the low Chl:c_p ratios were driven by iron limitation, resulting in low concentrations of small cells, which have a higher iron uptake efficiency at low iron concentrations than larger cells (Boyd et al., 2011). However, at low chl-a concentrations the phytoplankton-optical relationships become less robust it is increasingly difficult to draw conclusions about community cell size and physiology. Microscopy observations however, revealed two distinct communities which changed with depth: at the surface small cells (<5 μm) of *P. antarctica* dominated (65-80%) and large cells (>10 μm) contributed 10-20%; while at 50-60 m larger cells, made up of dinoflagellates, heterotrophs and ciliates, dominated the community (~75%) and small cells were barely present (<2%, Figure 2.4.8). This is consistent with previous studies that have observed larger heterotrophic cells gathering at the base of the mixed layer, scavenging on particles as they sink (Smetacek et al., 2004).

The high chl-a, lower SiO_4 (80-90 μmol l^{-1}) bloom to the south on the other hand, was associated with smaller cells ($c_{p(470:650)}$ = 1.4-1.5 *10^{-3}) and higher Chl:c_p ratios (~3, Figure 2.5.6), possibly due to increased pigment packaging, but more likely driven by the higher proportion of chl-a relative to total particulate (which includes phytoplankton, zooplankton, bacteria and detritus). Microscopy data revealed surface communities that ranged in species dominance from small solitary cells of *P. antarctica* (~90%) at 62.5 °S to a mixed community (~63 °S) of *P. antarctica* (30-57%) and diatoms (20-40%, Table 2.4.2) associated with a higher proportion (40-60%) of larger cells (>5 μm). The dominance of solitary *P. antarctica* was indicative of iron limitation (Strzepek et al., 2012), which was possibly relieved at ~63 °S where diatom abundance increased. Here, small (<5 μm) cells were able to out-compete larger cells due to their large surface area relative to their small volume, and hence are able to reach reasonable concentrations in spite of iron limitation (see Sunda and Huntsman, 1997; Twining, 2004; Lucas et al., 2007; Strzepek et al., 2011; Boyd et al., 2012).

Given the distinct differences in chl-a distribution and community structure, the

single primary production station in the low chl-a region was not representative of the whole NLWG region and thus an estimate of potential carbon export for the NLWG region is not possible, but it has been included in this discussion for completeness. As expected, in this low chl-a region, nitrogen (N) uptake rates at station BR143 were low (~0.11 mmol N m^{-3} d^{-1}, Table in Appendix 2) and dominated by NH_4 uptake (Table 2.4.3), but chl-a specific uptake was surprisingly high (~0.25 mmol N mg Chl^{-1} d^{-1}). The low f-ratio (0.11, Figure 2.4.9a, Table 2.4.3) suggested the dominance of regenerated production by small cells, which in turn implied low carbon export (Lucas et al., 2007). This further supports the suggestion of iron limitation in this region. The total euphotic zone integrated N uptake rate (7.2 mmol N m^{-2} d^{-1}, Figure 2.4.10a, Table in Appendix 2) was comparable to those reported by Waldron et al., (1995) for similarly low chl-a concentrations in the Bellingshausen Sea (10.28 mmol N m^{-2} d^{-1}, 0.22 mg Chl m^{-3}, f-ratio = 0.27) and those during CROZEX (6.0±1.5 mmol N m^{-2} d^{-1}, f-ratio = 0.28±0.07; Lucas et al., 2007). The higher f-ratios in the Bellingshausen Sea (Waldron et al., 1995) and the HNLC waters south of the Crozet Islands (Lucas et al., 2007) may be indicative of higher iron concentrations that facilitated NO_3 assimilation and thus increased production rates (Lucas et al., 2007; Boyd et al., 2012). While the low f-ratio may imply low potential export it is interesting to note that total integrated chl-a specific uptake rate for the NLWG was among the highest for all regions (15.3 mmol N mg Chl^{-1} d^{-1}), suggesting that phytoplankton cells were photosynthesizing efficiently but were perhaps maintained at low concentrations by grazing (Smetacek et al., 2004). It must be noted here, however, that in this study the NH_4 uptake rates measured at station BR143 were likely over estimated due to errors incurred in the measurement of NH_4 regeneration (see Section 2.2 for uptake calculations), thus under-estimating the f-ratio.

Central Weddell Gyre

The largest and most variable region defined here was the CWG (64.2-69.5 °S), where the doming of WDW (Figure 2.5.7) in the center has been shown to enrich the surface with macronutrients (Bakker et al., 2008). Shallow and less variable

MLDs (36±6 m), coupled with strong stratification (Figure 2.4.2), were associated with this region. Nutrient concentrations across the CWG were highly variable, and while surface SiO_3 (~90 µmol l^{-1}) was generally depleted relative to deep waters (140 µmol l^{-1} at 200 m, Figure 2.4.6b), concentrations were never limiting (Boyd et al., 1999; Brzezinski et al., 2003). This is evident from the elevated chl-a concentrations (~2.5 mg m^{-3}) associated with surface SiO_3 minima (<90 µmol l^{-1}) at ~64.2 °S and 67.3 °S.

The two regions of elevated chl-a in this region both coincided with a slight deepening of the MLD but varied in their nutrient concentrations, community structure and Chl:c_p ratios. The chl-a bloom at ~64.2 °S (~2.6 mg m^{-3}) was associated with relatively low NO_3 (~17 µmol l^{-1}, Figure 2.4.6a) but the highest SiO_3 (>100 µmol l^{-1}) concentrations, which suggests relative absence of diatoms. Here the community was characterized by small cells ($c_{p(470:650)}$ ratio ~ 1.4 *10^{-3}), likely dominated by *P. antarctica*, but without microscopy data this could not be confirmed.

Conversely, the bloom at 67.3 °S (~2.5 mg m^{-3}) was associated with higher NO_3 (>23 µmol l^{-1}) and slightly lower SiO_3 (~90 µmol l^{-1}) concentrations found in the middle of the CWG, which may suggest that an injection of nutrients (possibly including iron) from the WW layer was responsible for driving this bloom. Here the community was characterized by larger cells ($c_{p(470:650)}$ ratio ~ 1 *10^{-3}), which may have been made up of a mixed community of diatoms and dinoflagellates, as seen at 65.6 °S and 69 °S, where community structure data was available (Figure 2.4.8, Table 2.4.2). Alternatively, a possible increase in iron could have lead to the formation of large *P. antarctica* colonies (50-100 µm), as seen at the ice shelf (see discussion below). Without microscopy data for this bloom, however, this discussion regarding community structure is largely speculative, but nevertheless highlights the value of spectral slope as a tool for observing variations in community structure between blooms.

Higher POC concentrations were observed at the northern bloom (~17 mg m^{-3}), relative to the southern bloom (~12 mg m^{-3}), which resulted in different Chl:c_p

ratios (~3.2 and ~4.2, respectively). These differences support the suggestion of two distinctly different phytoplankton communities, but could also indicate a physiological response to iron limitation (Sosik and Olson, 2002; Behrenfeld et al., 2009). For example, the higher Chl:c_p ratios in the southern bloom were likely driven by the physiological response to iron relief, as a result of an injection of nutrient-rich WW.

Evidence of photo-adaptation to low light (Mitchell and Holm-Hansen, 1991; Fennel and Boss, 2003) was visible below 50 m depth in the CWG, as seen at ~67 °S for example, where patches of high Chl:c_p ratios (~6) suggest that cells increased their chl-a concentration in response to light limitation.

The shallow MLDs associated with this area, coupled with the timing of this study at the end of Summer, when surface iron concentrations were likely depleted but not replenished, as described in the CROZEX study (Pollard et al., 2009), supports late season iron limitation driving the decline in phytoplankton growth rates (Timmermans et al., 2001; Smith et al., 2000; see also Sosik and Olson, 2002). NO_3 concentrations were variable but not limiting in the CWG, however, the uptake of NO_3 may have been limited by insufficient bioavailable iron required for NO_3 uptake. This is supported by the relatively low f-ratios observed at 65.6 °S (0.37) and 68.9 °S (0.27). When compared to the NLWG, however, total N uptake rates were almost 3-fold higher at both these stations (19.2 mmol N m^2 d^{-1} and 20.3 mmol N m^2 d^{-1}, respectively, Table in Appendix 2), but low f-ratios again indicated the dominance of regenerated production. This could be linked to a dominance of microbial uptake and recycling of iron by small cells, which due to their size have more efficient uptake rates and a higher affinity for recycled nutrients, thus outcompeting diatoms (Boyd et al., 2012), while their biomass is controlled by grazing (Smetacek et al., 2005). The N uptake rates reported here were substantially higher than previously reported by Savoye et al. (2004) at similar latitudes (61-65 °S) in the Australian sector of the Southern Ocean (9.6±2.2 mmol N m^2 d^{-1}), while f-ratios were ~50% lower (0.61±0.08, compared to 0.31±0.07 for this study). Perhaps more interesting to note here is that highest total chl-specific uptake (Figure 2.4.9b, Table in

Appendix 2) was measured at 68.9 °S (31-86% higher than other production stations), which suggests that while chl-a concentrations were low (~1 mg m^{-3}), cells displayed high photosynthetic efficiency. Furthermore, the phytoplankton community at 68.9 °S was dominated by large cells (~95% of cells >10 μm, Figure 2.4.8), which package less chl-a per cell than small cells to avoid self-shading. Smaller cells were likely maintained at low concentrations by grazing, as a result of the similar growth rates between small phytoplankton (<5 μm) and those of micro-zooplankton (Smetacek et al., 2004). This community of efficiently photosynthesizing large cells has important implications for energy transfer through the food web (Jennings and Warr, 2003) and export of carbon to the deep ocean (Smetacek, 1985). While the low f-ratio for this community implied very little potential for carbon export (Savoye et al., 2004; Lucas et al., 2007; Cochlan 2008), the dominance of large cells, which escape grazing pressure and have faster sinking rates than small cells (Asper and Smith, 2003; Fischer and Karakas, 2009), suggests a higher proportion of organic carbon would potentially sink below the mixed layer and effectively be removed from the surface.

2.5.3.3 *Antarctic Continental Shelf*

The ACS was defined as the region closest to Antarctica, which extended from the ice shelf to the edge of the continental slope (~69.6 °S). The relatively shallow (~500-1000 m) bathymetry of the continental shelf (see Figure 2.2.1) and the sinking of sub-zero WW from 100 m to 500 m (Figure 2.5.7), coincided with the southern most extent of WDW. The combination of these features lead to the placement of the northern boundary of the ACS at 69.6 °S.

The ACS region was characterized by warm, relatively fresh surface waters, which overlaid the cold, high salinity WW that extended below 200 m (Figure 2.4.1). The warm fresh surface waters produced shallow MLDs (25-29 m near the ice shelf) and moderate stratification (Figure 2.4.2), while the cold salty water of the deep WW layer invoked sinking (Figure 2.5.7). Nutrient concentrations (NO_3 and SiO_3) decreased towards the ice shelf where concentrations were ~19 μmol l^{-}

^{1} and ~90 µmol l^{-1}, respectively (Figure 2.4.6a,b), but again neither were limiting.

Chl-a concentrations reached a maximum in the ACS (~4 mg m^{-3}), where larger cells ($c_{p(470:650)}$ ratio ~1 *10^{-3}, Figure 2.5.5) generally characterized the community. Given that the spatial distribution of surface chl-a blooms in the Southern Ocean in summer is consistent with iron limitation (De Baar et al., 1995; Boyd et al., 2000; Blain et al., 2007; Pollard et al., 2009), the high biomass, large cell characteristics of this ice shelf community could possibly be explained by increased iron supply through melting sea-ice (Sedwick and DiTullio, 1997; Grotti et al., 2005) and the re-suspension of shelf waters (Klunder et al., 2012). While the lack of iron measurements make it difficult to draw any conclusions about the drivers of this high biomass bloom, however, previous studies show that surface water iron concentrations generally increase towards the continental shelf (Klunder et al. 2011; Tagliabue et al., 2012), with shelf water measurements increasing more than 2-fold higher (0.61-0.7 nM) relative to open ocean waters (~0.31 nM). These elevated concentrations would thus provide sufficient iron enrichment to induce rapid diatom growth, which may be moderated by the efficient uptake rates of bacteria and pico-phytoplankotn (Boyd et al., 2012).

This particular bloom in the ACS, however, was divided into two distinct populations (one at 69-69.7 °S and the other at~70 °S) associated with shallow MLDs (~45 m and ~50 m, respectively) but different euphotic zone depths (~45 m and ~20 m, respectively, Table 2.4.2), and varied in their community structure and optical properties. The mixed diatom/dinoflagellate community at 69-69.7 °S, at the edge of the bloom, was associated with small cells ($c_{p(470:650)}$ ratio ~1.2* 10^{-3}) and lower chl-a concentrations (1.8-2.5 mg m^{-3}), which implied the onset of iron limitation (Pollard et al., 2009). In contrast, the chl-a maximum (~4 mg m^{-3}) at ~70 °S, associated with the dominance of *P. antarctica* colonies (68-84%) and the presence of large (10-20 µm) chain-forming diatoms (11-16%), produced a community characterized by large cells ($c_{p(470:650)}$ ratio ~0.7 *10^{-3}), likely driven by sufficient iron supply (Karsh et al., 2003). This high biomass bloom of large cells, associated with high cell specific values for POC and chl-a (Figure 2.4.7a,b)

as well as high species diversity (Figure 2.4.7d), implies high carbon export potential (Lucas et al., 2007; Pollard et al., 2009) and efficient energy transfer through the food web (Jennings and Warr, 2003). Although relatively low in abundance, the presence of large chain-forming diatoms such as *Rhizosolenia* and *Chaetoceros* sp. appeared to have a disproportionate impact on the optical signal. This is consistent with previous work on cultured species (Ciotti et al., 2002), where increases in chl-a were generally associated with the addition of relatively few large cells to a background of small cells, resulting in a disproportionally large impact on the absorption spectrum (Ciotti et al., 2002).

Large cells (with low surface to volume ratio) have a competitive advantage over small cells under nutrient (iron) replete conditions, because they allow space for storage vacuoles (which may substantially impact on the optical signal) while also reducing grazing pressure (Smetacek et al., 2004), resulting in a higher proportion of cellular carbon exported to the deep ocean (Lucas et al., 2007). Community shifts between diatoms and *P. antarctica* observed in the Ross Sea, have been shown to strongly impact nutrient cycling and potential carbon export estimates due to species differences in stoichiometry and cellular carbon content, which have significant impacts on the food web through trophic cascades and the transfer of energy across trophic levels (Arrigo et al. 1999). *P. antarctica* is well adapted to variable light conditions (see Boyd et al., 2002; Boyd et al., 2010), and thus can out-compete diatoms when MLDs are deep (Arrigo et al., 1999). This has important implications for carbon fixation and subsequent export because, comparisons between cultured species (Strzepek et al., 2012) have revealed that carbon content for the largest diatom was substantially lower (3-8-fold) than *P. antarctica* under iron replete conditions. While in the Ross Sea these shifts in community structure appeared to be driven by substantial differences (~50 m) in the depth of the MLD (Arrigo et al. 1999), the MLDs for this study differed by less than 10 m (~45 m versus ~50 m) between the two blooms in the ACS, however the euphotic zones were significantly different (45 m versus 20 m). Thus observed differences between these two communities may have been driven by variable iron concentrations (Strzepek et al., 2002; Moore et al., 2007), associated with the patchiness of iron concentrations due to melting

sea-ice and icebergs (Klunder et al., 2011) at ~69 °S, while surface shading by *P. antarctica* colonies at ~70 °S, caused shallow euphotic zone depths (~20 m), and limited diatom abundance due to their lower photo-adaptation ability (Arrigo et al., 1999).

Despite differences in community structure, high POC concentrations (14-16 mg m^{-3}) were associated with both blooms, and high surface Chl:c_p ratios (~6) were observed across the whole ACS region (Figure 2.4.6). This uniformity in the high Chl:c_p ratios implies that cells displayed increased pigment packaging relative to cellular carbon, likely driven by a combination of community structure and physiological responses. While cell specific concentrations of chl-a and POC were both shown to increase with increasing community cell size (Figure 2.4.7a,b), the high Chl:c_p ratios were likely due to a combination of iron relief (Gall et al., 2001) and community species composition. The presence of large chain-forming diatoms, which have substantially lower carbon content (Strzepek et al., 2012) and lower tolerance for reduced light conditions (Arrigo et al., 1999; Boyd et al., 2002) relative to *P. antarctica*, resulted in a substantial increase in chl-a concentration with relatively little increase in total carbon.

Elevated Chl:c_p ratios (4-5) associated with the sinking of WW at the ice shelf, provide evidence of photo-acclimation to the low light conditions (Behrenfeld et al., 2009) extending well below 100 m. This suggests that viable phytoplankton cells were sinking below the MLD and effectively being exported to the deeper layers, increasing their chl-a content as light levels decreased. The patches of elevated $c_{p(470:650)}$ ratios below 100 m (~0.7 $*10^{-3}$) relative to surrounding water (~0.4 $*10^{-3}$), suggest that these cells were large, or possibly were in the form of aggregates of mineral and organic matter heavy enough to sink towards the shelf floor (Armstrong et al., 2002).

The dominance of large, efficiently photosynthesizing cells in the ACS was strongly supported by N uptake measurements, which were the highest at the ice shelf (30.0 mmol N m^{-2} d^{-1}, Figure 2.4.9a, Table in Appendix 2) out of all production stations for this study. The high f-ratio (0.68), indicated the

dominance of new production based on NO_3 and further supports the assumption that phytoplankton were not limited by iron at the ice shelf (Sedwick and DiTullio, 1997; Grotti et al., 2005, Klunder et al., 2011). These rates compare well to those reported by Lucas et al., (2007) during the Crozet Iron Experiment (30.1±7.5 mmol N m^{-2} d^{-1}; f-ratio = 0.67±0.08). Highest uptake rates were observed at 17 m despite significantly reduced light levels (3.2% LD; Figure 2.4.10; Table 2.4.3), further supporting the dominance of *P. antarctica*, which is well adapted to variable light conditions (Strzepek et al., 2002) and thus able to out-compete diatoms at low light.

In summary, high chl-a concentrations, large cells and the dominance of new production in the ACS, indicated that phytoplankton growth was not limited by either light or iron in this region. Variations in community structure, however, were observed with depth, possibly in response to species-specific adaptations to lower light levels below the surface bloom. The dominance of large *P. antarctica* colonies, coupled with high N uptake rates based on NO_3 and the strong prevalence of sinking particles at the ice shelf, provide compelling evidence for significant carbon export in this region.

2.6 Conclusions

This study used relationships between bio-optical properties and biogeochemistry to explore the variability of phytoplankton particulate organic carbon, phytoplankton community structure, physiology and primary production in the Weddell Gyre. The application of these relationships produced high-resolution section plots of POC, beam attenuation spectral slope ($c_{p(470:650)}$) and chlorophyll (chl-a) to beam attenuation (Chl:c_p) ratios, (i.e. light and iron) across the region. By interpreting this information within the context of distinct hydrographic regions and their associated nutrient environments, some of the causative environmental drivers of the observed phytoplankton variability were explored. A significant caveat in this study is that no iron data was available for this cruise and discussions of iron as a driving factor are based only on previous findings in this region. The interpretation of these patterns of variability, in combination with estimates of carbon export from ^{15}N primary production experiments, enabled regions of high and low carbon export potential in the Weddell Gyre, to be identified. As such, we observed that the high biomass blooms in the Northern Limb of the Weddell Gyre (NLWG) and Antarctic Continental Shelf (ACS) regions, were generally associated with the dominance of *Phaeocystis antarctica* but had different Chl:c_p ratios, cell sizes and potential for carbon export. These differences suggest that iron relief drove the dominance of colonial *P. antarctica* at the ice shelf, which together with strong sinking of surface waters and high f-ratios, result in the identification of the ACS as an important region for carbon export. Conversely, the dominance of *P. antarctica* as solitary cells in the NLWG, coupled with strong surface stratification and low f-ratios, suggests that this region has a lower potential for carbon export. The lower biomass blooms in the Central Weddell Gyre (CWG) region were associated with mixed communities of diatoms and dinoflagellates, variable stratification and moderate f-ratios. High chl-a specific primary production rates and the dominance of large cells with high Chl:c_p ratios in the southern region of the CWG, suggest high photosynthetic efficiency due to iron relief and a higher potential for carbon export, compared to that inferred from f-ratios. While the more northerly bloom, associated with small cells and lower Chl:c_p ratios

suggests iron limitation and subsequent control by grazing, driving the dominance of regenerated production and resultant low export potential. These results highlight the importance of comprehensive investigations such as this, which combine bio-optical, biogeochemical and community structure data, to explore fine-scale phytoplankton variability over regional scales.

The results presented in this study provide strong evidence for the potential of bio-optics as an investigative approach for exploring the variability of phytoplankton biomass, community structure and physiology across different hydrographic regions in the Southern Ocean. Despite the large uncertainties related to the community structure data, which limited the development of an IOP-size relationship, this preliminary assessment, application and interpretation of empirical relationships between IOPs and phytoplankton variability, has much potential. It is believed that with improved data collection techniques, the support of more ancillary data and a growing dataset of *in situ* collocated biogeochemical and bio-optical data, more robust empirical relationships may be established for this region.

The Southern Ocean Carbon and Climate Observatory (SOCCO) and the Southern Ocean Bio-optics Research Facility have recently purchased a fleet of gliders and bio-optics floats, which are currently collecting a range of bio-optical and hydrographic measurements across the Atlantic sector of the Southern Ocean, as part of the Southern Ocean Seasonal Cycle Experiment (SOSCEx). The application of robust empirical relationships to these growing bio-optical float and glider datasets will enable the research community to observe temporal changes in phytoplankton size dominance and functional types, which will improve our understanding of species succession over the seasonal cycle. These *in situ* empirical relationships will also be used to improve regional remote sensing algorithms, thus enhancing our observational capacity and improving our understanding of the factors driving the observed patterns of variability in this globally important and under-sampled region. Developing region-specific IOP-biogeochemical relationships for the Southern Ocean may improve our ability to isolate and understand the intricacies of phytoplankton dynamics and their

response to environmental changes. However, as this study suggests, these developments are still in their infancy and much work is still required, highlighting the extensive opportunities available for future studies in the bio-optical field, particularly in this under-studied region of the Southern Ocean.

Appendices

Appendix 1

Lugols Reagents List

Reagent quantities required to make alkaline Lugols to preserve microscopy samples (after Kemp et al.,1993):

200 g	potassium iodide
100 g	iodine
100 g	sodium acetate
1400 ml	distilled or deionized water

Appendix 2

^{15}N Primary Production

Table. Uptake rates for ^{15}N primary production stations along the CTD Transect across the Weddell Gyre. Values for total nitrogen (N) uptake (NO_3+NH_4+urea) and Chl-specific uptake are reported for each light depth and for the entire euphotic zone (integrated over the depths shown) for each station.

Station No.	Latitude (°S)	% Light	Depth (m)	Total N Uptake (mmol m^{-3} d^{-1})	Total Chl-specific Uptake (mmol N mg Chl^{-1} d^{-1})	Euphotic N Uptake (mmol m^{-2} d^{-1})	Euphotic Chl-specific Uptake (mmol N mg Chl^{-1} d^{-1})
BR143	62.28	54	10	0.127	0.323	**7.02**	**15.25**
		32	15	0.138	0.375		
		18	20	0.157	0.407		
		13	30	0.110	0.180		
		3.2	40	0.105	0.182		
		1.1	50	0.033	0.059		
BR155	65.58	54	10	0.449	0.356	**19.20**	**13.65**
		32	15	0.420	0.336		
		18	20	0.476	0.338		
		13	25	0.394	0.286		
		3.2	35	0.306	0.179		
		1.1	44	0.229	0.164		
BR167	68.91	54	6	0.380	0.382	**20.27**	**19.65**
		32	12	0.348	0.286		
		18	18	0.440	0.406		
		13	21	0.437	0.453		
		3.2	36	0.188	0.176		
		1.1	47	0.277	0.298		
IS11	70.54	54	3	0.797	0.433	**29.97**	**10.72**
		32	6	0.654	0.321		
		18	9	0.734	0.342		
		13	10	1.011	0.472		
		3.2	17	1.324	0.321		
		1.1	23	0.879	0.174		

Appendix 3

POC – Backscattering Regression

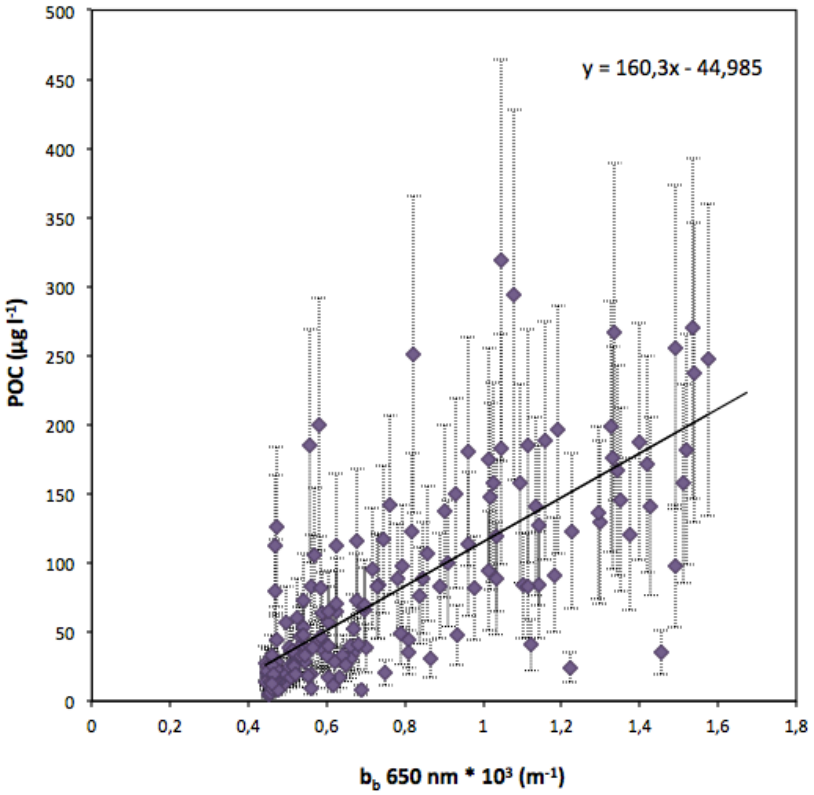

Figure. Regression of POC and b_b at 650 nm (m^{-1} *10^3) (r^2 = 0.559, n = 170). Error bars represent a standard error of 45.7%.

Appendix 4

POC – Beam Attenuation Global Comparison

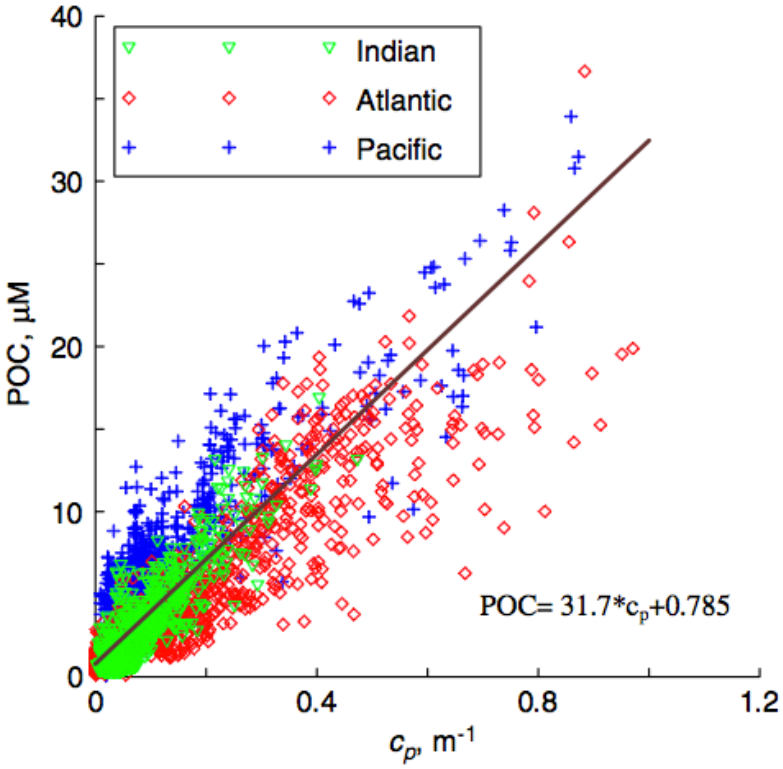

Figure. Global POC-c_p regression for all data collected in the Indian (green triangles), Atlantic (red diamonds) and Pacific (blue cross) oceans. Figure reproduced from Gardner et al. (2006).

Table. c_p – POC regression fit for this study (Weddell Sea) and two regions from a global dataset (Gardner et al., 2006): North Atlantic Bloom Experiment (NABE) and Antarctic Polar Frontal Zone (APFZ). Units are in µmol C l^{-1}.

	NABE	APFZ	Weddell Sea
Slope	25.3	33.5	21.1
Intercept	0.276	3.064	1.503
SD slope	0.610	0.609	?
SD intercept	0.178	0.125	?
n	165	659	167
R^2	0.904	0.781	0.650

Appendix 5

Size versus Backscattering spectral slope

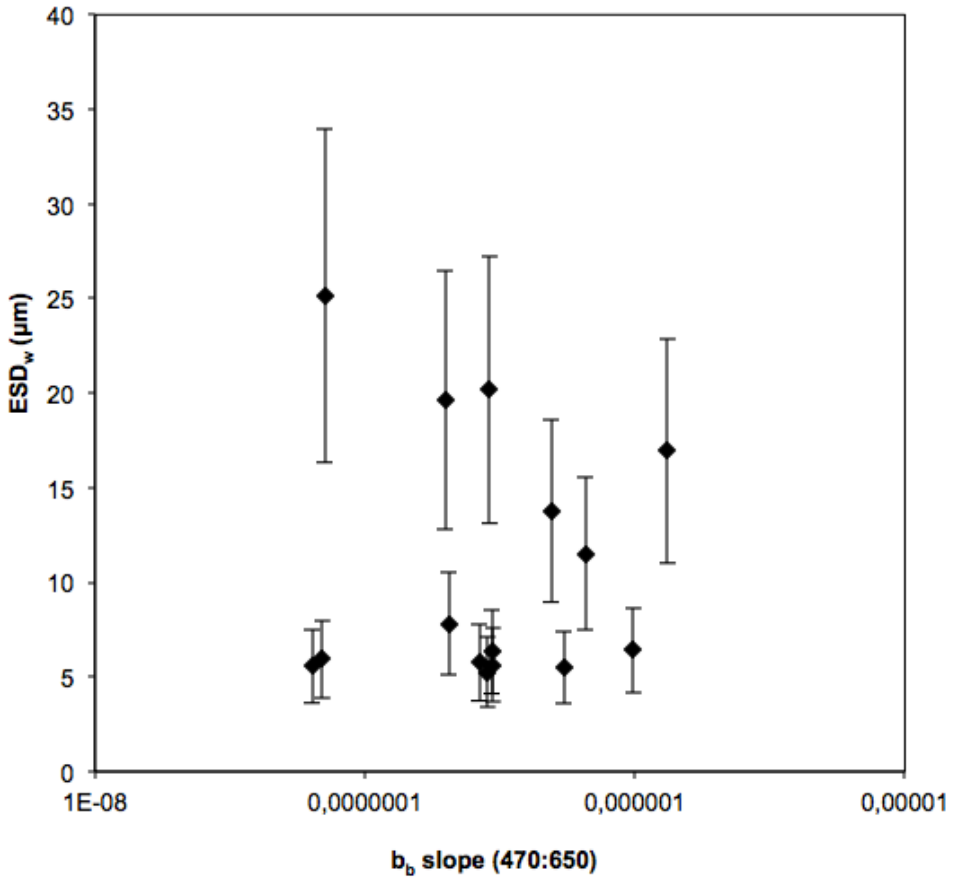

Figure. Estimated Spherical Diameter (ESD_w) versus b_b (470/650) spectral slope. Error bars show accumulated estimated error of 35% for size calculations and 10% for b_b slope calculations.

Appendix 6

Chlorophyll – Backscattering Regression

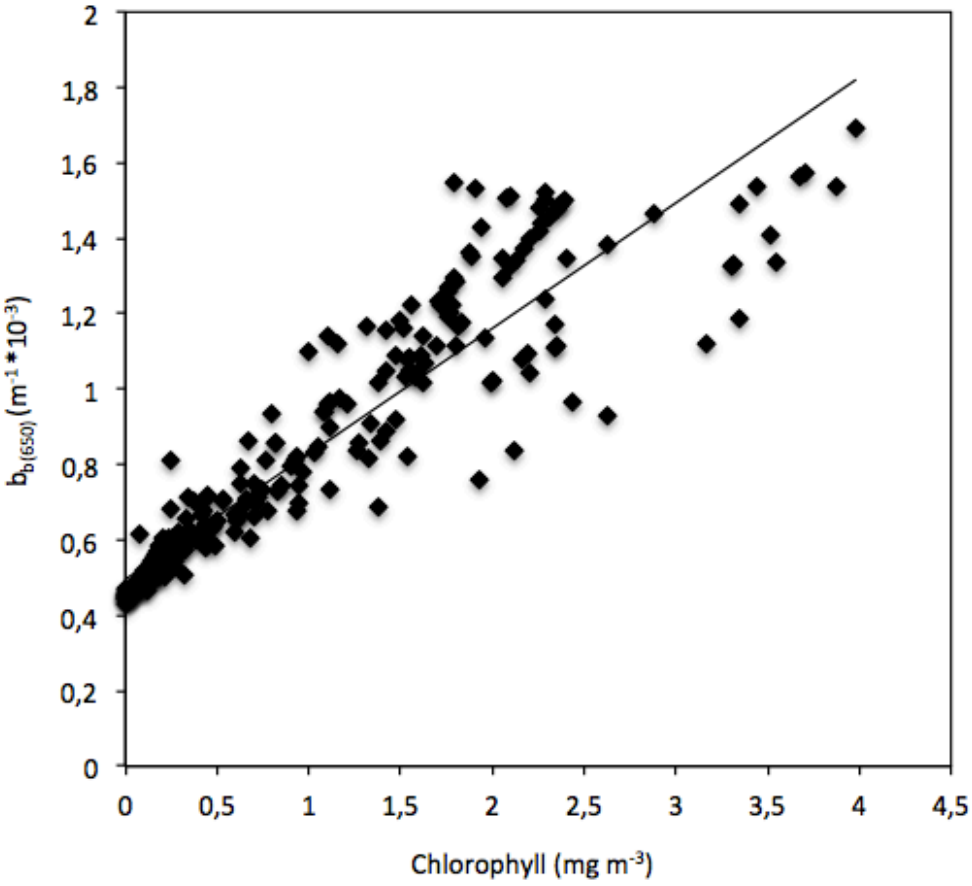

Figure. Chl:C ratios: regression plot of chl-a concentration (mg m^{-3}) against b_b (650 nm) ($m^{-1}*10^{-3}$) fitted to a linear trend line ($y = 0.333x + 0.496$, $r^2 = 0.868$, $n = 270$).

Appendix 7

Southern Boundary Retroflection

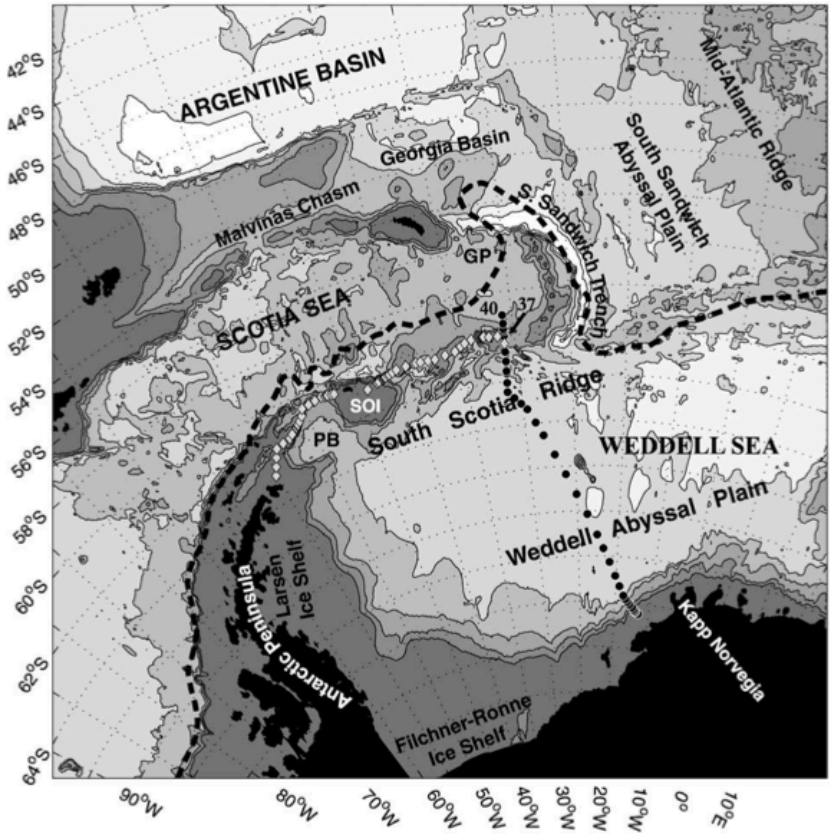

Figure. Bathymetry of the southwestern sector of the Weddell Sea (1000 m delineations). Dashed line indicates position of Southern Boundary of the ACC, highlighting the retroflection around the South Sandwich Islands. (reproduced from Garabato et al., 2002).

Appendix 8

Sea Ice Concentration

a)

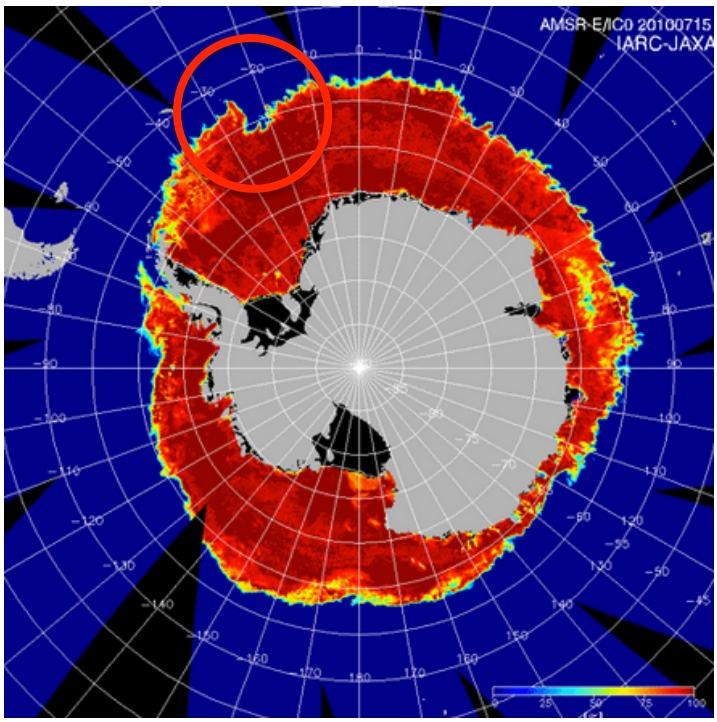

b)

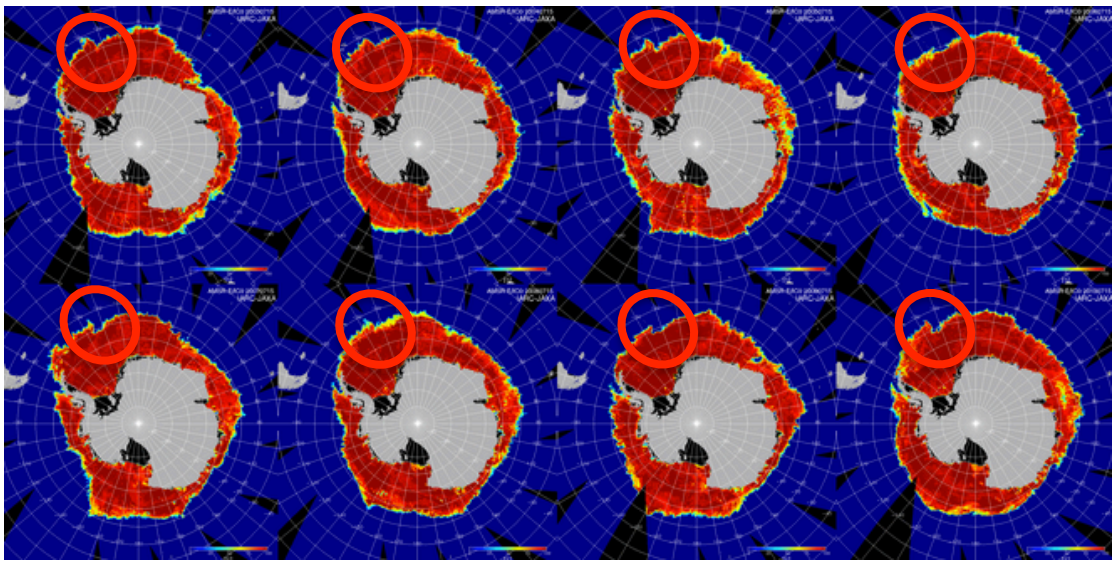

Figure. Sea ice concentration for Antarctica in a) July 2010 and b) annual July concentrations from 2003 to 2010, showing the persistent effect of the retroflection of the SBdy around 60 °S and 25 °W (circled in red)(source: Japan Aerospace Exploration Agency http://www.eorc.jaxa.jp/en/imgdata/topics/2012/tp120613.html).

References

Agrawal, Y.C. and Pottsmith, H.C., 2000. Instruments for particle size and settling velocity observations in sediment transport. Mar. Geo. 168: 89-114.

Allanson, B.R., Hart, R.C., and Lutjerharms, J.R.E., 1981. Observations on the nutrients, chlorophyll and primary production of the Southern Ocean south of Africa, S. Afr. J. Ant. Res., 10(11): 3–14.

Alvain, S., Moulin, C., Dandonneau, Y. and Loisel, H., 2008. Seasonal distribution and succession of dominant phytoplankton groups in the global ocean: A satellite view, Global Biogeochem. Cycles, 22: GB3001, doi:10.1029/2007GB003154.

Armstrong, F.A.J., Stearns, C.R. and Strickland, J.D.H., 1967. The measurement of upwelling and subsequent biological process by means of the Technicon Autoanalyzer® and associated equipment, Deep-Sea Res. and Oceanogr. Abs., 14(3): 381-389, ISSN 0011-7471, http://dx.doi.org/10.1016/0011-7471(67)90082-4.

Armstrong, R.A., 1999. Stable model structures for representing biogeochemical diversity and size spectra in plankton communities. Journal of Plankton Research, 21, 445–464.

Armstrong, R.A., Lee, C., Hedges, J.I., Honjo, S. and Wakeham, S.G., 2002. A new, mechanistic model for organic carbon fluxes in the ocean based on the quantitative association of POC with ballast minerals. Deep-Sea Res. II 49: 219–236, doi:10.1016/S0967-0645(01)00101-1.

Armstrong, R.A., 2006. Optimality-based modeling of nitrogen allocation and photo-acclimation in photosynthesis, Deep-Sea Res. II 53: 513-531, ISSN 0967-0645, http://dx.doi.org/10.1016/j.dsr2.2006.01.020.

Arrigo, K.R., Robinson, D.H., Worthen, D.L., Dunbar, R.B., DiTullio, G.R., VanWoert, M., Lizotte, M.P., 1999. Phytoplankton community structure and the drawdown of nutrients and CO2 in the Southern Ocean. Science 283(5400): 365-367.

Arrigo, K.R., Dunbar, R.B., Lizotte, M.P., Robinson, D.H., 2002. Taxon-specific differences in C/P and N/P drawdown for phytoplankton in the Ross Sea, Antarctica. Geophys. Res. Lett., 29(19): 44.1-44.4.

Arrigo, K.R., and van Dijken, G.L., 2003. Phytoplankton dynamics within 37 Antarctic coastal polynya systems, J. Geophys. Res., 108(C8): 3271, doi:10.1029/2002JC001739.

Arrigo, K. R., 2005. Marine microorganisms and global nutrient cycles, Nature, 437, 349–355, doi:10.1038/nature04158.

Arrigo, K. R., Van Dijken, G. L., and Bushinsky, S., 2008. Primary production in the Southern Ocean, 1997–2006, J. Geophys. Res., 113: C08004. doi:10.1029/2007JC004551.

Arrigo, K.R., Mills, M.M, Kropuenske, L.R. van Dijken, G.L, Alderkamp, A. and Robinson, D.H., 2010. Photophysiology in Two Major Southern Ocean Phytoplankton Taxa: Photosynthesis and Growth of *Phaeocystis antarctica* and *Fragilariopsis cylindrus* under Different Irradiance Levels. Integrative and Comparative Biology, 50(6): 950–966. doi:10.1093/icb/icq021.

Asper, V.L. and Smith, W.O. 2003. Abundance, distribution and sinking rates of aggregates in the Ross Sea, Antarctica, Deep Sea Res. I, 50: 131–150.

Azam, F.T., Fenchel, T., Field, J.G., Gray, J.S., Meyer-Reil, L.A. & Thingstad, F. 1983. The ecological role of water-column microbes in the sea. Marine Ecology Progress Series, 10: 257–263.

Babin, M., Morel, A., Fournier-Sicre, V., Fell, F. and Stramski, D. 2003. Light scattering properties of marine particles in coastal and open ocean waters as related to the particle mass concentration, Limnol. Oceanogr. 48: 843–859.

Baker, E.T. and Lavelle, J.W., 1984. The effect of particle size on the light attenuation coefficient of natural suspensions. J. Geophys. Res., 89: 8197-8203.

Bakker, D.C.E., Bozec, Y., Nightingale, P.D., Goldson, L.E., Messias, M.J., Baar, H.J.W., de, L., M.I., Skjelvan, I., Strass, V., Watson, A.J., 2005. Iron and mixing affect biological carbon uptake in SOIREE and EisenEx, two Southern Ocean iron fertilisation experiments. Deep-Sea Res. I, 51: 1001-1019.

Bakker, D.C.E., Hoppema, M., Schröder, M., Geibert, W., De Baar, H.J.W., 2008. A rapid transition from ice covered CO2-rich waters to a biologically mediated CO2 sink in the eastern Weddell Gyre. Biogeosciences 5: 1373-1386

Balch, W.M., Drapeau, D.T., Fritz, J.J., Bowler, B.C., Nolan, J., 2001. Optical backscattering in the Arabian Sea — continuous underway measurements of particulate inorganic and organic carbon. Deep-Sea Res. I, 48: 2423–2452.

Barlow, R., Mantoura, R. Gough, M. and Fileman, T., 1993. Pigment signatures of the phytoplankton composition in the northeastern Atlantic during the 1990 spring bloom, Deep Sea Res. II, 40: 459-477.

Barlow, R.G., Aiken, J., Holligan, P.M., Cummings, D.G., Mariotena, S., and Hooker, S., 2002. Phytoplankton pigment and absorption characteristics along meridional transects in the Atlantic Ocean. Deep-Sea Res. I, 49: 637–660.

Bathmann, U.V., Scharek, R., Klaas, C., Dubischar, C.D., and Smetacek, V., 1997. Spring development of phytoplankton biomass and composition in major water masses of the Atlantic sector of the Southern Ocean, Deep-Sea Res. II, 44: 51–67.

Behrenfeld, M.J. and Boss, E., 2003. The beam attenuation to chlorophyll ratio: an optical index of phytoplankton physiology in the surface ocean?" Deep Sea Res. Part I Oceanogr. Res. Pap. 50(12), 1537–1549.

Behrenfeld M.J. and Boss, E., 2006. Beam attenuation and chlorophyll concentration as alternative optical indices of phytoplankton biomass, J. Mar. Res. 64: 431–451.

Behrenfeld M.J., Halsey K.H., Milligan A.J., 2008. Evolved physiological responses of phytoplankton to their integrated growth environment. Philos. Trans. R. Soc. Lond. B., 363: 2687–703.

Behrenfeld M.J., Westberry T.K., Boss E.S., O'Malley R.T., Siegel D.A., Wiggert J.D., Franz B.A., McClain C.R., Feldman G.C., Doney S.C., Moore J.K., Dall'Olmo G, Milligan A.J., Lima I, and Mahowald N, 2009. Satellite-detected fluorescence reveals global physiology of ocean phytoplankton. Biogeosciences, 6: 779-794.

Behrenfeld, M.J., 2010. Abandoning Sverdrup's critical depth hypothesis on phytoplankton blooms. Ecology, 91(4): 977-989.

Behrenfeld, M.J. and Milligan, A.J., 2013. Photophysiological Expressions of Iron Stress in Phytoplankton. Annual Review of Marine Science, 5: 217-246.

Bernard, S., 2009. Inversion course slides. IOCCG meeting.

Bernard, S., Shillington, F. and Probyn, T., 2007. The use of equivalent size distributions of natural phytoplankton assemblages for optical modeling. Optics Express, 15(5):1995-2007

Bidigare, R.R., Frank, T.J., Zastrow, C., Brooks, J.M., 1986. The distribution of algal chlorophylls and their degradation products in the Southern Ocean. Deep-Sea Res. I, 33: 923-937.

Bishop, JK, 1986. The correction and suspended particulate matter calibration of Sea Tech transmissometer data. Deep-Sea Res. I, 33: 121-134.

Bishop, J.K.B., 1999. Transmissometer measurement of POC. Deep-Sea Res. II, 46: 353-369.

Bishop, J.K.B and Wood, T.J., 2009. Year-Round Observations of Carbon Biomass and Flux Variability in the Southern Ocean. Glob. Biogeochem. Cycles. doi:10.1029/2008GB003206.

Blinken, R., and Koch, K.R., 2001. Geoid and sea surface topography derived from ERS-1 altimeter data by the adjoint method. Studia Geophysica et Geodaetica, 45(3): 235-250.

Bopp, L., Aumont, O., Cadule, P., Alvain, S., and Gehlen, M., 2005. Response of diatoms distribution to global warming and potential implications: A global model study. Geophys. Res. Lett., 32: L19606.

Boss, E., Twardowski, M.S. and Herring, S., 2001. Shape of the particulate beam attenuation spectrum and its inversion to obtain the shape of the particulate size distribution, Appl. Opt. 40: 4885-4893.

Boss, E., Slade, W.H., Behrenfeld, M. and Dall'Olmo, G., 2009. Acceptance angle effects on the beam attenuation in the ocean. Opt. Express 17: 1535–1550.

Boyd, P.W., 2002. Environmental factors controlling phytoplankton processes in the Southern Ocean. J. Phycol., 38: 844-861.

Boyd, P.W., La Roche, J., Gall, M., Frew, R., McKay, R.M.L., 1999. The role of iron, light and silicate in controlling algal biomass in sub-Antarctic waters of SE New Zealand. J. Geophys. Res. 104: 13395-13408.

Boyd, P.W., Watson, A.J., Law, C.S., Abraham, E.R., Trull, T., Murdoch, R., Bakker, D.C.E., Bowle, A.R., Buesseler, K.O., Chang, H., Charette, M., Croot, P., Downing, K., Frew, R., Gall, M., Hadfield, M., Hall, J., Harvey, M., Jameson, G., LaRoche, J., Liddicoat, M., Ling, R., Maldonado, M.T., McKay, R.M., Nodder, S., Pickmere, S., Pridmore, R., Rintoul, S., Safi, K., Sutton, P., Strzepek, R., Tanneberger, K., Turner, S., Walte, A., Zeldis, J., 2000. A meso-scale phytoplankton bloom in the polar Southern Ocean stimulated by iron fertilization. Nature, 407: 695-702.

Boyd P.W., Jickells T, Law C.S., Blain S, Boyle E.A., et al. 2007. Mesoscale iron enrichment experiments 1993–2005: synthesis and future directions. Science, 315: 612–17.

Boyd, P.W., Strzepek, R., Fu, F. and Hutchins, D.A., 2010. Environmental control of open-ocean phytoplankton groups: Now and in the future. Limnol. Oceanogr. 55(3): 1353–1376 doi:10.4319/lo.2010.55.3.1353.

Boyd, P.W., et al., 2012. Microbial control of diatom bloom dynamics in the open ocean, Geophys. Res. Lett., 39, L18601, doi:10.1029/2012GL053448.

Brainerd, K.E. and Gregg, M.C., 1995. Surface mixed and mixing layer depths. Deep-Sea Res. I, 9: 1521–1543.

Bricaud, A. and Morel, A., 1986. Light attenuation and scattering by phytoplanktonic cells: a theoretical modeling. Appl. Opt. 25: 571–580.

Bricaud, A. and Stramski, D., 1990. Spectral absorption coefficients of living phytoplankton and non-algal biogenous matter: A comparison between the Peru upwelling area and the Sargasso Sea. Limnol. Oceanogr., 35(3):562-582.

Bricaud, A., M. Babin, A. Morel, and H. Claustre, 1995. Variability in the chlorophyll-specific absorption coefficients of natural phytoplankton: Analysis and parameterization, *J. Geophys. Res., 100,* 13,321-13,332.

Bricaud, A., Morel, A., Babin, M., Allali, K. and Claustre, H., 1998. Variations of light absorption by suspended particles with chlorophyll a concentration in oceanic (case 1) waters: Analysis and implications for bio-optical models, J. Geophys. Res., 103(C13), 31033-31044, doi:10.1029/98jc02712.

Bricaud, A., Claustre, H., Ras, J. and Oubelkheir, K., 2004. Natural variability of phytoplanktonic absorption in oceanic waters: Influence of the size structure of algal populations, *J. Geophys. Res, 109(C11),* C11010.

Briggs, N., M. J. Perry, I. Cetinić, C. Lee, E. A. D'Asaro, A. M. Gray, and E. Rehm (2011), High-resolution observations of aggregate flux during a sub-polar North Atlantic spring bloom, *Deep Sea Res., Part I, 58(10),* 1031-1039, doi:10.1016/j.dsr.2011.07.007.

Brzezinski, M.A., Dickson, M.L., Nelson, D.M., and Sambrotto, R., 2003. Ratios of Si, C and N uptake by microplankton in the Southern Ocean. Deep-Sea Res. Pt. II 50: 619–633.

Burd, A.B., et al., 2010. Assessing the apparent imbalance between geochemical and biochemical indicators of meso- and bathypelagic biological activity: What the @$#! is wrong with present calculations of carbon budgets? Deep-Sea Res. II, 57: 1557-1571. (doi:10.1016/j.dsr2.2010.02.022).

Caldeira, K. and Duffy, P.B., 2000. The role of the Southern Ocean in up- take and storage of anthropogenic carbon dioxide, Science, 297: 620–622.

Canadell, J.G., Le Quéré, C., Raupach, M.R., Field, C.B., Buitenhuis, E.T., Ciais, P., Conway, T.J., Gillett, N.P., Houghton, R.A. and Marland, G., 2007. Contributions to accelerating atmospheric CO_2 growth from economic activity, carbon intensity, and efficiency of natural sinks. PNAS 104 (47) 18866-18870, doi:10.1073/pnas.0702737104.

Capone, D.G., Burns, J.A., Montoya, J.P., Subramaniam, A., Mahaffy, C., Gunderson, T., Michaels, A.F., Carpenter, E.J., 2005. Nitrogen fixation by *Trichodesmium* spp.: An important source of new nitrogen to the tropical and subtropical North Atlantic Ocean. Global Biogeochemical Cycles 19, doi:10.1029/2004GB002331.

Cassar, N., Bender, M.L., Barnett, B.A., Songmiao, F., Moxim, W.J., Levy II, H. and Tilbrook, B., 2007. The Southern Ocean biological response to Aeolian iron deposition. Science 317: 1067–1070.

Cetinić, I., Perry, M.J., Briggs, N.T., Kallin, E., D'Asaro, E.A. and Lee, C.M., 2012. Particulate organic carbon and inherent optical properties during 2008 North Atlantic Bloom Experiment, J. Geophys. Res. (C Oceans), 117(C6):C06028, doi:10.1029/2011JC007771.

Chisholm, S.W. and Morel, F.M.M., 1991. What controls phytoplankton production in nutrient-rich areas of the open sea?, Limnol. Oceanogr., 36, U1507–U1511.

Ciotti, Á.M., Cullen, J.J and Lewis, M.R., 1999. A semi-analytical model of the influence of phytoplankton community structure on the relationship between light attenuation and ocean color. J. Geophys. Res., 104: 1559–1578, doi:10.1029/1998JC900021

Ciotti, Á.M., Lewis, M.R, and Cullen, J.J., 2002. Assessment of the relationships between dominant cell size in natural phytoplankton communities and the spectral shape of the absorption coefficient, Limnol. Oceanogr. 47: 404-417.

Ciotti, Á.M. and Bricaud, A. 2006. Retrievals of a size parameter for phytoplankton and spectral light absorption by Colored Detrital Matter from water-leaving radiances at SeaWiFS channels in a continental shelf region off Brazil. Limno. Oceanogr. Methods, 4: 237–253.

Claustre, H., Morel, A., Babin, M., Cailliau, C., Marie, D., Marty, J.-C., Tailliez, D., Vaulot, D., 1999. Variability in particle attenuation and chlorophyll fluorescence in the tropical Pacific: scales, patterns and biogeochemical implications. J. Geophys. Res. 104: 3401-3422.

Claustre, H. and Maritorena, S., 2003. The Many Shades of Ocean Blue. Science, 302: 1514-1515.

Clavano, W., Boss, E. and Karp-Boss, L., 2007. Inherent optical properties of non-spherical marine-like particles—from theory to observation, Oceanogr. Mar. Biol. 45: 1–38.

Coale, K.H., Johnson, K.S., Chavez, F.P., Buesseler, K.O., Barber, R.T., Brzezinski, M.A., Cochlan, W.P., Millero, F.J., Falkowski, P.G., Bauer, J.E., Wanninkhof, R.H., Kudela, R.M., Altabet, M.A., Hales, B.E., Takahashi, T., Landry, M.R., Bidigare, R.R., Wang, X., Chase, Z., Strutton, P.G., Friederich, G.E., Gorbunov, M.Y., Lance, V.P., Hilting, A.K., Hiscock, M.R., Demarest, M., Hiscock, W.T., Sullivan, K.F., Tanner, S.J., Gordon, R.M., Hunter, C.N., Elrod, V.A., Fitzwater, S.E., Jones, J.L., Tozzi, S., Koblizek, M., Roberts, A.E., Herndon, J., et al. 2004. Southern ocean iron enrichment experiment: Carbon cycling in high- and low-Si waters. Science 304(5669): 408-414.

Cochlan, W.P., 2008. Nitrogen uptake in the Southern Ocean, in: Nitrogen in the Marine Environment, 2nd Edn., edited by: Capone, D. G., Bronk, D. A., Mulholland, M. R., and Carpenter, E. J., Academic Press, Elsevier, 569–596.

Cullen, J.J and Boyd, P.W., 2008. Predicting and verifying the intended and unintended consequences of large-scale ocean fertilization. Mar. Ecol. Prog. Ser. 364: 295–301, doi:10.3354/meps07551.

Dall'Olmo, G., Westberry, T. K., Behrenfeld, M.J., Boss, E. and Slade, W.H., 2009. Significant contribution of large particles to optical backscattering in the open ocean," Biogeosciences 6: 947-967.

Davidson, I.R., 1991. Environmental effects on algal photosynthesis: temperature. Journal of Phycology 27: 2-8.

De Baar, H.J.W., 1994. von Liebig's law of the minimum and plankton ecology (1899- 1991). Progress in Oceanography 33, 347-386.

De Baar, H.J.W., Buma, A.G.J., Nolting, R.F., Cadee, G.C., Jacques, G., Treguer, P.J., 1990. On iron limitation in the Southern Ocean: Experimental observations in the Weddel and Scotia Seas. Marine Ecology Progress Series 65: 105-122.

De Baar, H.J.W., De Jong, J.T.M., Bakker, D.C.E., Loscher, B.M., Veth, C., Bathmann, U., Smetacek, V., 1995. Importance of iron for plankton blooms and carbon dioxide draw-down in the Southern Ocean. Nature 373: 412-415.

De Baar, H.J.W., Boyd, P.W., 2000. The role of iron in plankton ecology and carbon dioxide transfer of the global oceans. In: Hanson, R. B., Ducklow, H. W., Field, J. G. (Eds.), The dynamic ocean carbon cycle: A midterm synthesis of the Joint Global Ocean Flux Study, International Geosphere Biosphere Programme Book Series Vol. 5, Cambridge University Press, Cambridge, pp. 61-140.

De Baar, H.J.W., Boyd, P.W., Coale, K.H., Landry, M.R., Tsuda, A., Assmy, P., Bakker, D.C.E., Bozec, Y., Barber, R.T., Brzezinski, M.A., Buesseler, K.O., Boye, M., Croot, P.L., Gervais, F., Gorbunov, M.Y., Harrison, P.J., Hiscock, W.T., Laan, P., Lancelot, C., Law, C.S., Levasseur, M., Marchetti, A., Millero, F.J., Nishioka, J., Nojiri, Y., Van Oijen, T., Riebesell, U., Rijkenberg, M.J.A., Saito, H., Takeda, S., Timmermans, K.R., Veldhuis, M.J.W., Waite, A.M., Wong, C.-S., M., Bugg, W., Efremenko, Y., Kamyshkov, Y., Kozlov, A., Nakamura, Y., Karwowski, H.J., Markoff, D.M., Nakamura, K., Rohm, R.M., Tornow, W., Wendell, R., Chen, M.-J., Wang, Y.-F., Piquemal, F., Wong, C.S.D.M., 2005. Synthesis of iron fertilization experiments: From the Iron Age in the Age of Enlightenment. Journal of Geophysical Research 110, C09S16, doi:10.1029/2004JC002601.

De Boyer Monte'gut, C., Madec, G., Fischer, A. S., Lazar, A., and Iudicone, D., 2004. Mixed layer depth over the global ocean: An examination of profile data and a profile-based climatology, J. Geo- phys. Res., 109, C12003, doi:10.1029/2004JC002378.

De La Rocha, C. L. and Passow, U., 2007. Factors influencing the sinking of POC and the efficiency of the biological carbon pump, Deep Sea Res. Part II, 54, 639–658, doi:10.1016/j.dsr2.2007.01.004.

Denman, K.L., 2003. Modelling planktonic ecosystems: parameterizing complexity. Progress In Oceanography 57(34): p 429-452.

Dierssen, H.M., Kudela, R.M., Ryan, J.P. and Zimmerman, R.C., 2006. Red and black tides: Quantitative analysis of water-leaving radiance and perceived color for phytoplankton, colored dissolved organic matter, and suspended sediments, Limnol. Oceanogr., 51(6), 2646–2659.

Doney, S.C., 1999. Major challenges confronting marine biogeochemical modeling. Global Biogeochemical Cycles, 13, 705–714.

Doney, S.C., 2006. Plankton in a warmer world. Nature 444: 695-696.

Doney, S.C., Lima, I. , Lindsay, K., Moore, J.K., Dutkiewicz, S., Friedrichs, M.A.M. and Matear, R.J., 2001. Marine biogeochemical modeling: Recent advances and future challenges. Oceanography 14(4):93–107. http://dx.doi.org/10.5670/oceanog.2001.10

Dong, S., Gille, S.T., Sprintall, J. and Gentemann, C., 2006. Validation of the Advanced Microwave Scanning Radiometer for the Earth Observing System (AMSR-E) sea surface temperature in the Southern Ocean, J. Geophys. Res., 111, C04002, doi:10.1029/2005JC002934

Dower, K.M. and Lucas, M.I., 1993. Photosynthesis-irradiance relation- ships and production associated with a warm-core ring shed from the Subtropical Retroflection south of Africa, Mar. Ecol. Prog.- Ser., 95: 141–154.

Dugdale, R.C., and Goering, J.J., 1967. Uptake of new and regenerated forms of nitrogen in primary production. Limnol. Oceangr. 12: 199-206.

Dugdale, R.C. and Wilkerson, F.P., 1986. The use of ^{15}N to measure nitrogen uptake in eutrophic oceans; experimental considerations. Limnol. Oceanogr. 31(4): 673-689.

DuRand, M.D., Olson, R.J., 1996. Contributions of phytoplankton light scattering and cell concentration changes to diel variations in beam attenuation in the equatorial Pacific from flow cytometric measurements of pico-, ultra-, and nanoplankton. Deep-Sea Res. II 43: 891–906.

Eppley, R.W. and Peterson, B.J., 1979. Particulate organic matter flux and planktonic new production in the deep ocean. Nature 282: 677-680.

Eppley, R.W., Chavez, F.P., Barber, R.T., 1992. Standing stocks of particulate carbon and nitrogen in the equatorial Pacific at 1501W. J. Geophys. Res. 97: 655–661.

Falkowski, P.G., 1992. Molecular ecology of phytoplankton photosynthesis. *In* Falkowski PG, Woodhead AD [Eds] Primary productivity and biogeochemical cycles in the sea. Plenum Press, New York, 47-68.

Falkowski, P.G., and Kolber, Z., 1995. Variations in chlorophyll fluorescence yields in phytoplankton in the world oceans, Funct. Plant Biol., 22(2): 341-355.

Falkowski, P.G. and Raven, J. A., 1997. Aquatic photosynthesis, Blackwell Science, Oxford.

Falkowski, P.G., Barber, R.T. and Smetacek, V., 1998. Review: Biogeochemical Controls and Feedbacks on Ocean Primary Production Science 281:200-206

Falkowski, P.G., Scholes, R.J., Boyle, E., Canadell, J., Canfield, D., Elser, J., Gruber, N., Hibbard, K., Högberg, P., Linder, S., Mackenzie, F.T., Moore III, B., Pedersen, T., Rosenthal, Y., Seitzinger, S., Smetacek, V., Steffen, W., 2000. The global carbon cycle: a test of our knowledge of earth as a system. Science 290: 291-296.

Falkowski, P.G., Laws, E.A., Barber, R.T., Murray, J.W., 2003. Phytoplankton and their role in primary, new and export production. In: Fasham, M. J. R. (Ed.), Ocean Biogeochemistry: The role of the ocean carbon cycle in global change, Springer-Verlag, Berlin, pp. 99-121.

Falkowski, P.G., et al., 2008. Biogeochemical cycles: The microbial engines that drive earth's biogeochemical cycles. Science 320:1034 doi: 10.1126/science.1153213.

Feely, A., Sabine, C.L., Lee, K., Berelson, W., Kleypas, J., Fabry,V.J., and Millero, F.J., 2004. Impact of Antropogenic CO_2 on the $CaCO_3$ System in the Oceans, Science, 305: 362–366.

Fennel, K., Boss, E., 2003. Subsurface maxima of phytoplankton and chlorophyll steady state solutions from a simple model. Limno. Oceanogr. 48: 1521–1534.

Fernandez, C. and Raimbault, P., 2007. Nitrogen regeneration in the Northeast Atlantic Ocean and its impact on seasonal new, regenerated and export production, Mar. Ecol. Prog.-Ser., 337, 79–92.

Ferreira, A., Stramski, D., Garcia, C.A.E., Garcia, V.M.T., Ciotti, Á.M. and Mendes, C.R.B., 2013. Variability in light absorption and scattering of phytoplankton in Patagonian waters: Role of community size structure and pigment composition, J. Geophys. Res. Oceans, 118, 698–714, doi:10.1002/jgrc.20082

Field, C.B., Behrenfeld, M.J., Randerson, J.T., Falkowski, P.G., 1998. Primary production of the biosphere: integrating terrestrialandoceaniccomponents.Science281,237–240.

Finkel, Z.V., Beardall, J., Flynn, K.J., Quigg, A., Alwyn, T., Rees, V., Raven, J.A., 2010. Phytoplankton in a changing world: cell size and elemental stoichiometry. Journal of Plankton Research 32:119-137.

Fischer, G. and Karakas, G., 2009. Sinking rates and ballast composition of particles in the Atlantic Ocean: implications for the organic carbon fluxes to the deep ocean, Biogeosciences 6: 85–102.

Fitch, D. and Moore, J.K., 2007. Wind speed influence on phytoplankton bloom dynamics in the Southern Ocean marginal ice zone. JGR-Oceans, 112: C08006, doi:10.1029/2006JC004061.

Froneman, P.W. and Perissinotto, R., 1996. Microzooplankton grazing and protozooplankton community structure in the South Atlantic and in the Atlantic sector of the Southern Ocean, Deep-Sea Res. I, 43, 703–721.

Gall, M.P., Boyd, P.W., Hall, J., Sa, K.A and Chang, H., 2001. Phytoplankton processes. Part 1: Community structure during the Southern Ocean Iron RElease Experiment (SOIREE). Deep-Sea Res. II, 48: 2551-2570.

Gardner, W.D., Blakey, J.C., Walsh, I.D., Richardson, M.J., Pegau, S., Zaneveld, J.R.V., Roesler, C., Gregg, M.C., MacKinnon, J.A., Sosik, H.M., Williams, A.J., 2001. Optics, particles, stratification, and storms on the New England continental shelf. Journal of Geophysical Research—Oceans 106 (C5), 9473–9497.

Gardner, W.D., Mishonov, A.V. and Richardson, M.J., 2006. Global POC concentrations from in-situ and satellite data, Deep Sea Res. Part II, 53, 718–740, doi:10.1016/j.dsr2.2006.01.029.

Gehlen, M., Bopp, L., Emprin, N., Aumont, O., Heinze, C., and Ragueneau, O., 2006. Reconciling surface ocean productivity, export fluxes and sediment composition in a global biogeochemical ocean model, Biogeosciences, 3: 521–537, http://www.biogeosciences.net/3/521/2006/

Geider, R.J., MacIntyre, H.L., Kana, T.M., 1998. A dynamic regulatory model of phytoplanktonic acclimation to light, nutrients, and temperature. Limnology and Oceanography 43 (4), 679–694.

Gitelson, A., Karnieli, A., Goldman, N., Yacobi, Y. Z., and Mayo, M., 1996. Chlorophyll estimation in the Southeastern Mediterranean using CZCS images: adaptation of an algorithm and its valida- tion, J. Mar. Syst., 9: 283–290.

Glibert, P.M., Biggs, D.C and McCarthy, J.J., 1982a. Utilization of ammonium and nitrate during austral summer in the Scotia Sea. Deep-Sea Res. 29: 837-850.

Glibert, P. M., Lipschultz, F., McCarthy, J. J., and Altabet, M. A., 1982b. Isotope dilution models of uptake and re-mineralization of ammonium by marine plankton, Limnol. Oceanogr., 27, 639–650.

Grasshoff, K. M., Ehrhardt, M., and Kremling, K., 1983. Methods of seawater analysis, 2nd Edn., Verlag Chemie, Wienheim, Germany, 158–162.

Green, R.E., Sosik, H.M., 2004. Analysis of apparent optical properties and ocean color models using measurements of seawater constituents in New England continental shelf surface waters. Journal of Geophysical Research, 109, doi:10.1029/2003JC001977.

Grotti, M., Francesco, S., Carmela, I., and Roberto, F., 2005 Trace metals distributions in coastal sea ice of Terra Nova Bay, Ross Sea, Antarctica, Antarct, Science, 17, 290–300.

Hasle, G. 1978. The inverted microscope method. In: Sournia, A. (Ed.), Phytoplankton Manual. UNESCO, Paris.

Hirata, T., Aiken, J., Hardman-Mountford, N., Smyth, T.J., Barlow, R.G., 2008. An absorption model to determine phytoplankton size classes from satellite ocean colour. Remote Sensing of Environment 112, 3153–3159. doi:10.1016/j.rse.2008.03.011

Hiscock, M.R., Lance, V.P., Apprill, A.M., Bidigare, R.R., Johnson, Z.I., Mitchell, B.G., Smith Jr, W.O., and Barber, R.T., 2007. Photosynthetic maximum quantum yield increases are an essential component of the Southern Ocean phytoplankton response to iron. PNAS 105:12 4775-4780

Hoffert, M.I., Caldeira, K., Jain, A.K., Haites, E.F., Harvey, L.D.D., Potter, S.D., Schlesinger, M.E., Schneider, S.H., Watts, R.G., Wigley, T.M.L., Wuebbles, D.J., 1998. Energy implications of future stabilization of atmospheric CO2 content. Nature 395, 881-884.

Holmes, R.M., Aminot, A., Kerouel, R., Hooker, B.A. and Peterson, B.J. 1999. A simple and precise method for measuring ammonium in marine and freshwater ecosystems. Can. J. Fish. Aquat. Sci. 56: 1801-1808.

Hoppema, M., Fahrbach, E., Schröder, M., 1997. On the total carbon dioxide and oxygen signature of the Circumpolar Deep Water in the Weddell Gyre. Oceanologica Acta 20: 783–798.

Honjo, S., Francois, R., Manganini, S., Dymond, J., and Collier, R., 2000. Particle fluxes to the interior of the Southern Ocean in the Western Pacific sector along 170◦ W, Deep-Sea Res. II, 47(15– 16), 3521–3548.

Huot, Y., Brown, C.A. and Cullen, J.J., 2007 Retrieval of phytoplankton biomass from simultaneous inversion of reflectance, the diffuse attenuation coefficient, and sun-induced fluorescence in coastal waters, J. Geophys. Res., 112, C06013, doi:10.1029/2006JC003794.

Hutchins, D.A., et al., 2002. Phytoplankton iron limitation in the Humbolt Current and Peru Upwelling. Limnol. Oceangr. 47: 997-1011.

Hutchins, D.A. and Fu, F.-X., 2008. Linking the oceanic biogeochemistry of iron and phosphorus with the marine nitrogen cycle, p. 1627–1653. In D. G. Capone, D. A. Bronk, M. R. Mulholland and E. J. Carpenter [eds.], Nitrogen in the marine environment, 2nd ed. Elsevier Press.

Imbrie, J., Mix, A.C. and Martinson D.G., 1993. "Milankovitch theory viewed from Devils Hole." Nature 363, 6429: 531-533.

IOCCG, 2006. Remote sensing of inherent optical properties: fundamentals, tests of algorithms, and applications, Reports of the International Ocean-Colour Coordinating Group, No. 5, IOCCG, Dartmouth, Canada. http: //www.ioccg.org

IOCCG, 2011. Bio-Optical Sensors on Argo Floats. Claustre, H. (ed.), Reports of the International Ocean-Colour Coordinating Group, No. 11, IOCCG, Dartmouth, Canada. http: //www.ioccg.org

IPCC, 2007. 4th Assessment Report, Climate Change 2007: The Physical Science Basis. Contribution of Working Group I to the Fourth Assessment Report of the Intergovernmental Panel on Climate Change [Solomon, S., D. Qin, M. Manning, Z. Chen, M. Marquis, K.B. Averyt, M. Tignor and H.L. Miller (eds.)]. Cambridge University Press, Cambridge, United Kingdom and New York, NY, USA.

Irigoien, X., Huisman, J., and Harris, R.P., 2004. Global biodiversity patterns of marine phytoplankton and zooplankton, *Nature, 429(6994),* 863-867.

Jennings, S. and Warr, K.J., 2003. Smaller predator-prey body size ratios in longer food chains, Proc. R. Soc. B 270, 1413–1417.

Jonasz, M. and Fournier, G., 2007. Light Scattering by Particles in Water: Theoretical and Experimental Foundations. Academic Press.

Johnson, K.S., Chavez, F.P., and Friederich, G.E., 1999. Continental shelf sediment as a primary source of iron for coastal phytoplankton. Nature 398: 697–700.

Karsh, K.L., Trull, T.W., Lourey, M.J. and Sigman, D.M., 2003. Relationship of nitrogen isotope fractionation to phytoplankton size and iron availability during the Southern Ocean Iron Release Experiment (SOIREE). *Limnology and Oceanography*. Vol. 48, No. 3, pp. 1058-1068 URL: http://www.jstor.org/stable/3096632

Kemp, P. F., Cole, J.J., Sherr, B.F. and Sherr, E.B., 1993. Handbook of Methods in Aquatic Microbial Ecology. Round, Crawford & Mann, 800 pp.

Klunder, M., Laan, P., Middag, R., de Baar, H.J.W., and Van Ooijen, J., 2011. Dissolved iron in the Southern Ocean (Atlantic Sector), Deep-Sea Res. Pt. II, 58, 2678–2694, 2011.

Knap, A.H., Michaels, A.F., Close, A., 1994. The JGOFS Protocols. Intergovernmental Oceanographic Commission, 198pp.

Knox, G.A., 1994. Phytoplankton and primary production. In: studies in Polar Research; the biology of the Ocean. Cambridge University Press, London. Pp. 13-39.

Koeve, W., 2001. Wintertime nutrients in the North Atlantic - new approaches and implications for new production estimates. Marine Chemistry 74(4), 245-260.

Kohfeld, K.E., Le Quéré, C., Harrison, S.P. and Anderson, R.F, 2005. Role of marine biology in glacial-interglacial CO2 cycles. Science 308:74–78.

Kostadinov, T.S., Siegel, D.A. and Maritorena, S., 2009. Retrieval of the particle size distribution from satellite ocean color observations, J. Geophys. Res. 114, C09015.

Kowalczuk, P., Darecki, M., Zabłocka, M., Górecka, I., 2010. Validation of empirical and semi-analytical remote sensing algorithms for estimating absorption by Coloured Dissolved Organic Matter in the Baltic Sea from SeaWiFS and MODIS imagery. Oceanologia, 52 (2): 171–196.

Lal, R., 2008. Sequestration of atmospheric CO_2 in global carbon pools. Energy Environ. Sci.,1: 86-100. DOI: 10.1039/B809492F.

Lannuzel, D., Schoemann, V., de Jong, J., Chou, L., Delille, B., Becquevort, J.L., and Tison, S., 2008. Iron study during a time series in the Western Weddell pack ice, Mar. Chem., 108, 85–95.

Laws, E.A., Falkowski, P.G., Smith, W.O., Ducklow, H., McCarthy, J.J., 2000. Temperature effects on export production in the open ocean. Global Biogeochemical Cycles 14(4), 1231-1246.

LeQuére C, et al., 2009. "Global Carbon Project" Trends in the sources and sinks of carbon dioxide. Nature Geoscience 2:831-836 [www.globalcarbonproject.org, 26 September 2008]

Li, X.S., Berger, A., Loutre, M.F., 1998. CO_2 and northern hemisphere ice volume variations over the middle and late quaternary. Climate Dynamics 14, 537- 544.

Lipschultz, F., 2001. A time-series assessment of the nitrogen cycle at BATS. Deep- Sea Research II 48, 1897-1924.

Loisel, H., Nicolas, J.M., Sciandra, A., Stramski, D. and Poteau, A., 2006. Spectral dependency of optical backscattering by marine particles from satellite remote sensing of the global ocean, J. Geophys. Res. 111, C09024.

Longhurst, A. R., 1991. Role of the marine biosphere in the global carbon cycle, Limnol. Oceanogr., 36, 1507–1526.

Lucas, M. I., Seeyave, S., Sanders, S., Moore, M. C., Williamson, R., and Stinchcombe, M.: Nitrogen uptake response to a naturally Fe fertilised phytoplankton bloom during the 2004/2005 CROZEX study, Deep-Sea Res. Pt. II, 54, 2138–2173, 2007.

Lucas, M.I., 2011. What happens to man-made CO_2 emissions? Quest 7 (4), 10-12.

Luo, Y., Su, B., Currie, W.S., Dukes, J.S., Finzi, A., Hartwig, U., Hungate, B., Mcmurtrie, R.E., Oren, R., Parton, W.J., Pataki, D.E., Shaw, M.R., Zak, D.R. and Field, C.B., 2003. Progressive nitrogen limitation of ecosystem responses to rising atmospheric carbon dioxide. BioScience, 54 (8): 731-739.

Lutjeharms, J. R. E., Walters, N. M., and Allanson, B. R.: Oceanic frontal systems and biological enhancement, in: Antarctic nutri- ent cycles and food webs, edited by: Siegfried, W. R., Condy, P. R., and Laws, R. M., Springer-Verlag, Berlin, 11–21, 1985.

Maldonado, M., Boyd, P. W., Price, N. M., and Harrison, P.J., 1999. Co-limitation of phytoplankton by light and Fe during winter in the NE subarctic Pacific Ocean. Deep-Sea Res. II 46: 2475–2486.

Marinov, I., Gnanadesikan, A., Toggweiler, J.R. and Sarmiento, J.L., 2006. The Southern Ocean biogeochemical divide. 441 doi:10.1038/nature04883

Marinov, I., Doney, S. and Lima, I., 2010. Response of ocean phytoplankton community structure to climate change over the 21st century: partitioning the effects of nutrients, temperature and light, Biogeosciences 7: 3941–3959, doi:10.5149/bg-7-3941-2010.

Martin, J., 1990. Glacial-interglacial CO_2 change: the iron hypothesis, Paleoceanography, 5: 1-3.

Martinez-Vincente, V., Simis, S.G.H., Alegre, R., Land, P.E. and Groom, S.B., 2013. Above-water reflectance for the evaluation of adjacency effects in Earth observation data: initial results and methods comparison for near-coastal waters in the Western Channel, UK. J. Europ. Opt. Soc. Rap. Public. 8, 13060. [DOI:http://dx.doi.org/10.2971/jeos.2013.13060]

Martinson, D.G. and Iannuzzi, R.A., 2003. Spatial/temporal patterns in Weddell gyre characteristics and their relationship to global climate. JGR, Vol:108 No: C4, 8083 doi:10.1029/2000JC000538

Metzl, N., Tilbrook, B., and Poison, A., 1999. The annual fCO_2 cycle and the air-sea CO_2 flux in the sub-Antarctic Ocean, Tellus, 51B, 849–861.

Mikaloff-Fletcher, S.E., Gruber, N., Jacobson, A.R., Doney, S.C., Dutkiewicz, S., Gerber, M., Follows, M., Joos, F., Lindsay, K., Menemenlis, D., Mouchet, A., Mueller, S.A., Sarmiento, J.L., 2006. Inverse estimates of anthropogenic CO2 uptake, transport, and storage by the ocean. Global Biogeochemical Cycles 20, GB2002, doi:2010.1029/2005GB002530.

Milankovitch, M., 1930. Mathernatische Klirnalehre und Astronornische Theorie der Klirnaschwankungen, Gebruder Borntreger, Berlin, 176 pp.

Mills, M.M., Ridame, C., Davey, M., La Roche, J. and Geider, R.J., 2004. Iron and phosphorus co-limit nitrogen fixation in the eastern tropical North Atlantic. Nature 429: 292–294, doi:10.1038/nature02550

Mitchell, B.G., 1992. Predictive bio-optical relationships for polar oceans and marginal ice zones, *J. Mar. Syst., 3,* 1-2.

Mitchell, J.F.B., Johns, T.C., Gregory, J.M., Tett, S.F.B., 1995. Climate response to increasing levels of greenhouse gases and sulphate aerosols. Science 376, 501- 504.

Mitchell, B.G., Holm-Hansen, O., 1991. Bio-optical properties of Antarctic Peninsula waters differentiation from temperate ocean models. Deep-Sea Research 38, 1009–1028.

Moore, J.K., and M.R. Abbott, 2000. Phytoplankton chlorophyll distributions and primary production in the Southern Ocean, J. Geophys. Res., 105(C12), 28,709– 28,722, doi:10.1029/1999JC000043

Moore, J.K., and Abbott, M.R., 2002. Surface chlorophyll concentrations in relation to the Antarctic Polar Front: seasonal and spatial patterns from satellite observations. Journal of Marine Systems 37, 69-86.

Moore, M.C., Seeyave, S., Hickman, A.E., Allen, J.T., Lucas, M.I., Planquette, H., Pollard, R., Poulton, A.J., 2007a. Iron-light interactions during the CROZet natural iron bloom and EXport experiment (CROZEX) I: phytoplankton growth and photophysiology. Deep-Sea Research II.

Moore, M.C., Hickman, A.E., Poulton, A.J., Seeyave, S., and Lucas, M.I., 2007b Iron-light interactions during the CROZet natural iron bloom and Export experiment (CROZEX) II: taxonomic responses and elemental stoichiometry, Deep-Sea Res. II, 54, 2066–2084.

Moore, C.M., et al., 2009. Large-scale distribution of Atlantic nitrogen fixation controlled by iron availability. Nat. Geosci. 2: 867–871.

Morel, A., 1974. Chapter I. Optical Properties of Pure Water and Pure Sea Water. U'niversité de Paris, Laboratoire d'Océanogmphie Physique. www.obs-vlfr.fr/LOV/OMT/fichiers_PDF/Morel_OAO_74.pdf

Morel, A., and L. Prieur, 1977: Analysis of variations in ocean color. Limnol. Oceanogr., 22(4), 709-722.

Morel, A., and Bricaud, A., 1981, Theoretical results concerning light absorption in a discrete medium, and application to specific absorption of phytoplankton, Deep Sea Research Part A. Oceanographic Research Papers, 28(11): 1375-1393.

Morel, A. and Ahn. Y.H., 1990. Optical efficiency factors of free living marine bacteria: Influence of bacterioplankton upon the optical properties and particulate organic carbon in oceanic water. J. Mar. Res., 48, 145-175.

Morel, A., and Antoine, D., 1994, Heating rate within the upper ocean in relation to its bio-optical state, J. Phys. Oceanogr., 24(7), 1652-1665.

Morrow, J.H., Chamberlin, W.S., and Kiefer, D.A, 1989. A two-component description of spectral absorption by marine particles. Limnol. Oceanogr., 34(8):1500-1509.

Murphy, J.A.M.E.S. and Riley, J.P., 1962. A modified single solution method for the determination of phosphate in natural waters. Analytica chimica acta 27: 31-36.

Nalli, N.R., and Smith, W.L., 1998. Improved remote sensing of sea surface skin temperature using a physical retrieval method, J. Geophys. Res., 103(C5), 10527–10542, doi:10.1029/98JC00196.

Nelson, D.M. and Smith Jr., W.O., 1991. Sverdrup re-visited: critical depths, maximum chlorophyll levels, and the control of Southern Ocean productivity by the irradiance-mixing regime. Limnology and Oceanography 36, 1650-1661.

Nelson, D.M., Brzezinski, M.A., Sigmon, D.E. and Franck, V.M., 2001. A seasonal progression of Si limitation in the Pacific sector of the Southern Ocean. Deep-Sea Res. II 48: 3973–3995.

Niewiadomska K., Claustre, H., Prieur, L. and d'Ortenzio, F., 2008. Sub-mesoscale physical-biogeochemical coupling across the Ligurian Current (northwestern Mediterranean) using a bio-optical glider. Limnol. Oceanogr., 53(5/2): 2210–2225.

Orsi, A.H., Whitworth, T., and Nowlin, W.D., 1995. On the meridional extent and fronts of the Antarctic Circumpolar Current, Deep- Sea Res., 42, 641–673.

Oubelkheir, K., Claustre, H., Babin, M., and Sciandra, A., 2005. The comparative bio-optical and biogeochemical properties of contrasted trophic regimes, Limnol. Oceanogr., 50: 1795–1809.

Pak, H., Beardsley, G.F., Heath, G.R. and Curl, H., 1970. Light-scattering vectors of some marine particles. Limnol. Oceanogr. 15: 683–687, doi:10.4319/lo.1970.15.5.0683

Parsons, T.R., Maita, Y., and Lalli, C.M., 1984. A manual of chemical and biological methods for seawater analysis, Pergamon Press, Oxford, 173 pp.

Particle Dynamics Group: Global POC-IOP data downloaded from http://oceanography.tamu.edu/~pdgroup/SMP_prj/Downloads/Downloads.htm

Pollard, R.T., Lucas, M.I. and Read, J.F., 2002. Physical controls on biogeochemical zonation in the Southern Ocean. Deep-Sea Research II 49: 3289-3305.

Pollard, R.T., Venables, H.J., Read, J.F. and Allen, J.T., 2007. Large-scale circulation around the Crozet Plateau controls an annual phytoplankton bloom in the Crozet Basin. Deep Sea Research Part II 54: 1915–1929.

Pollard, R.T., Salter, I., Sanders, R.J., Lucas, M.I., Moore, C.M., Mills, R.A., Statham, P.J., Allen, J.T., Baker, A.R., Bakker, D.C.E., Charette, M.A., Fielding, S., Fones, G.R., French, M., Hickman, A.E., Holland, R.J., Hughes, J.A., Jickells, T.D., Lampitt, R.S., Morris, P.J., Nedelec, F.H., Nielsdottir, M., Planquette, H., Popova, E.E., Poulton, A.J., Read, J. F., Seeyave, S., Smith, T., Stinchcombe, M., Taylor, S., Thomalla, S.J., Venables, H.J., Williamson, R., and Zubkov, M.V., 2009. Southern Ocean deep-water carbon export enhanced by natural iron fertilization, Nature, 457, 577–580.

Poulton, A.J, Moore, C.M., Seeyave, S., Lucas, M.I., Fielding, S. and Ward, P., 2007. Phytoplankton community composition around the Crozet Plateau, with emphasis on diatoms and *Phaeocystis.* Deep-Sea Research II 2085-2105.

Preisendorfer, R.W., 1961. Application of radiative transfer theory to light measurements in the sea, *Monogr. 10,* pp. 11-30, *Int. Union of Geod. and Geophys. Paris*.

Price, N.M., Ahner, B.A., and Morel, F.M.M., 1994. The equatorial Pacific Ocean: Grazer-controlled phytoplankton in an iron-limited ecosystem, Limnol. Oceanogr., 39, 520–534.

Priddle, J. and Fryxell, G., 1985. Handbook of the common planktonic diatoms of the Southern Ocean. Cambridge: British Antarctic Survey, 159pp.

Prieur, L. and Sathyendranath, S., 1981. An optical classification of coastal and oceanic waters based on the specific spectral absorption of phytoplankton pigments, dissolved organic matter, and other particulate materials. *Limnol. Oceanogr.* 26(4):671-689.

Probyn, T.A. and Painting, S.J., 1985. Nitrogen uptake by size-fractionated phytoplankton populations in Antarctic surface waters. Limnol. Oceangr. 30(6): 1327-1332.

Raven, J. and Geider, R.J., 1988. Temperature and algal growth. New Phytol. 110: 441–461, doi:10.1111/j.1469-8137.1988.tb00282.x

Raven, J., et al. [Eds.]. 2005. Ocean acidification due to increasing atmospheric carbon dioxide. The Royal Society.

Raven, J.A., Caldeira, K., Elderfield, H. et al., 2005. Ocean acidification due to increasing atmospheric carbon dioxide. The Royal Society of London, Policy document. 12/05, 60pp. royalsociety.org/uploadedFiles/Royal_Society.../policy/.../2005/9634.pdf

Redfield, A.C., Ketchum, B.H., Richards, F.A., 1963. The influence of organisms on the composition of sea-water. In Hill, M. N. (Ed.), The Sea: Vol 2: Composition of Seawater Comparative and Descriptive Oceanography. Interscience, London, pp. 26-77.

Richardson, T.L. and Jackson, G.A., 2007. Small phytoplankton and carbon export from the surface ocean. Science 315, 838-840.

Riley, J.P. and Chester, R., 1971. Introduction to Marine Chemistry. Academic Press, London. 465pp.

Rintoul, S.R. 1991, South Atlantic inter-basin exchange, J. Geophys. Res., 96(C2), 2675-2692.

Roesler, C.S., Perry, M.J. and Carder, K.L., 1989. Modeling *in situ* phytoplankton absorption from total absorption spectra in productive inland waters, *Limnol. Oceanogr., 34,* 1510-1523.

Roesler, C. and Boss, E., 2003. A novel ocean color inversion model: retrieval of beam attenuation and particle size distribution, Geophys. Res. Let. 30

Roesler, C. 2013, Absorption by oceanic constituents. In: Ocean Optics Web Book, http://www.oceanopticsbook.info/view/absorption/absorption_by_oceanic_constituents

Sabine, C.L., Feely, R.A., Johnson, G.C., Strutton, P.G., Lamb, M.F. and McTaggart, K.E., 2004. A

mixed layer carbon budget for the GasEx-2001 experiment, J. Geophys. Res., 109, C08S05, doi:10.1029/ 2002JC001747.

Sabine, C.L. and Feely, R.A. 2007. The oceanic sink for carbon dioxide. pp. 31–49. In D. Reay, N. Hewitt, J. Grace and K. Smith (Eds.), Greenhouse Gas Sinks, CABI Publishing, Oxfordshire, UK.

Saito, M.A., Goepfert, T.J. and Ritt., J.T., 2008. Some thoughts on the concept of co-limitation: Three definitions and the importance of bioavailability. Limnol. Oceanogr. 53: 276–290.

Sarmiento, J.L. et al., 2004a. Response of ocean ecosystems to climate warming. Glob. Biogeochem Cycles 18: GB3003

Sarmiento, J.L., Dunne, J., Armstrong, R.A., 2004b. Do we now understand the ocean's biological pump? U.S. JGOFS News 12, 1-5.

Sarmiento, J.L., 2006. Inverse estimates of anthropogenic CO_2 uptake, transport, and storage by the ocean. Global Biogeochemical Cycles 20, GB2002, doi:2010.1029/2005GB002530.

Sarthou, G., Timmermans, K.R., Blain, S. and Treguer, P., 2005. Growth physiology and fate of diatoms in the ocean: A review. J. Sea Res. 53: 25-42.

Sathyendranath, S., Lazzara, L. and Prieur, L., 1987. Variations in the spectral values of specific absorption of phytoplankton, *Limmol. Oceanogr., 32(2),* 403-415.

Sathyendranath, S., Cota, G., Stuart, V., Maass, H., Platt, T., 2001. Remote sensing of phytoplankton pigments: a compar- ison of empirical and theoretical approaches. International Journal of Remote Sensing 22 (2–3), 249–273.

Sathyendranath, S., Watts, L., Devred, E., Platt, T., Caverhill, C., & Maass, H., 2004. Discrimination of diatoms from other phytoplankton using ocean-colour data. Marine Ecology. Progress Series, 272, 59–68.

Sathyendranath, S. and Platt, T., 2007. Spectral effects in bio-optical control on the ocean system. Oceanologia 49.1.

Sathyendranath S, Stuart V, Nair A, Oka K, Nakane T, et al., 2009. Carbon-to-chlorophyll ratio and growth rate of phytoplankton in the sea. Mar Ecol-Prog Ser 383: 73–84.

Savoye, N., Dehairs, F., Elskens, M., Cardinal, D., Kopczynska, E.E., Trull, T.W., Wright, S., Baeyens, W., and Griffiths, F.B., 2004. Regional variation of spring N-uptake and new production in the Southern Ocean, Geophys. Res. Lett., 31, L03301, doi:10.1029/2003GL018946.

Schlitzer, R., 2002. Carbon export fluxes in the Southern Ocean: Results from inverse modeling and comparisons with satellite based estimates, Deep Sea Res. Part II, 49, 1623–1644, doi:10.1016/S0967-0645(02) 00004-8.

Schoemann, S., Becquevort, S., Stefels, J., Rousseau, V. and Lancelot, C., 2005. *Phaeocystis* blooms in the global ocean and their controlling mechanisms: A review. J. Sea Res. 53: 43–66, doi:10.1016/j.seares.2004.01.008

Sedwick, P.N. and DiTullio, G.R., 1997. Regulation of algal blooms in Antarctic shelfwater by the release of iron from melting sea ice, Geophys. Res. Lett., 24, 2515–2518.

Seeyave, S., Lucas, M., Moore, C.M., and Poulton, A.J., 2007. Phytoplankton productivity and community structure in the vicinity of Crozet Plateau during austral summer 2004/2005, Deep-Sea Res. Pt. II, 54, 2020–2044.

Shum, C.K., Ries, J.C. and Tapley, B.D., 1995. The accuracy and applications of satellite altimetry. Geophysical Journal International, 121: 321–336. doi: 10.1111/j.1365-246X.1995.tb05714.x

Siegel H., Gerth M., Ohde T., Heene T., 2005, Ocean colour remote sensing relevant water constituents and optical properties of the Baltic Sea, Int. J. Remote Sens., 26 (2): 315–334.

Sigman, D.M. and Boyle, E.A., 2000. Glacial/Interglacial variations in atmospheric carbon dioxide, Nature, 407: 859–869.

Smetacek, V.S., 1985. Role of sinking in diatom life-history cycles: Ecological, evolutionary and geological significance, Mar. Biol. Berlin, 84: 239–251, doi:10.1007/BF00392493.

Smetacek, V., Assmy, P., Henjes, J., 2004. The role of grazing in structuring Southern Ocean pelagic ecosystems and biogeochemical cycles. Antarctic Science 16(4): 541-558.

Smetacek V, Klaas C, Strass VH, Assmy P, Montresor M, Cisewski B, Savoye N, Webb A, d'Ovidio F, Arrieta JM, Bathmann U, Bellerby R, Berg GM, Croot P,Gonzalez S, Henjes J, Herndl GJ, Hoffmann LJ, Leach H, Losch M, Mills MM, Neill C, Peeken I, Röttgers R, Sachs O, Sauter E, Schmidt MM, Schwarz J,Terbrüggen A, Wolf-Gladrow D. 2012. Deep carbon export from a Southern Ocean iron-fertilized diatom bloom. Nature. 18;487(7407):313-9. doi: 10.1038/nature11229.

Smith, R.C., and Baker, K.S., 1981. Optical properties of the clearest natural waters (200–800 nm). Appl. Opt. 20: 177–184.

Smith Jr., W.O. and Nelson, D.M., 1986. Importance of ice edge phytoplankton production in the Southern Ocean, BioScience, 36, 251–257.

Smith, W.O., Marra, J., Hiscock, M.R. and Barber, R.T., 2000. The seasonal cycle of phytoplankton biomass and primary productivity in the Ross Sea, Antarctica. Deep-Sea Res. II 47: 3119–3140.

Sokolov, S. and Rintoul, S.R., 2007. On the relationship between fronts of the Antarctic Circumpolar Current and surface chlorophyll concentrations in the Southern Ocean, J. Geophys. Res., 112, C07030, doi:10.1029/2006JC004072.

Sokolov, S. and Rintoul, S.R., 2009. Circumpolar structure and distribution of the Antarctic Circumpolar Current fronts: Mean circumpolar paths. Journal of Geophysical Research 114: C11018

Sosik, H.M., and Mitchell, B.G., 1994. Effects of temperature on growth, light absorption, and quantum yield in *Dunaliella tertiolecta* (Chlorophyceae), *J. Phycol., 30(5),* 833-840.

Sosik, H.M. and Olson, R.J., 2002. Phytoplankton and iron limitation of photosynthetic efficiency in the Southern Ocean during late summer. Deep-Sea Res. I 49:1195–216.

Stemman, L. and Boss, E., 2012. Plankton and particle size and packaging: from determining optical properties to driving the biological pump. Annu. Rev. Mar. Sci., 4: 263–90.

Stramski, D., and Kiefer, D.A., 1991. Light scattering by micro-organisms in the open ocean, *Prog. Oceanogr., 28,* 343-383.

Stramski, D., Reynolds, R.A., Kahru, M., Mitchell, G., 1999. Estimation of Particulate Organic Carbon in the Ocean from Satellite Remote Sensing. *Science* 285, 239; DOI: 10.1126/science.285.5425.239.

Strzepek, R.F., Maldonado, M.T., Higgins, J.L., Hall, J., Safi, K., Wilhelm, S.W., and Boyd, P.W., 2005. Spinning the "Ferrous Wheel": The importance of the microbial community in an iron budget during the FeCycle experiment, Global Biogeochem. Cy., 19, GB4S26, doi:10.1029/2005/gb002490.

Stramski, D., et al., 2008. Relationships between the surface concentration of particulate organic carbon and optical properties in the eastern South Pacific and eastern Atlantic Oceans, Biogeosciences, 5, 171–201.

Strzepek, R.F., Hunter, K.A., Frew, R.D., Harrison, P.J. and Boyd, P.W., 2012. Iron–light interactions differ in Southern Ocean phytoplankton *Limnol. Oceanogr.* 57(4), 1182–1200 doi:10.4319/lo.2012.57.4.1182.

Sunda, W.G. and Huntsman, S.A., 1997. Interrelated influence of iron, light and cell size on marine phytoplankton growth. Nature 390, 389-392.

Sverdrup, H.U., 1953. On conditions for the vernal blooming of phytoplankton. Journal du Conseil International pour l'Exploration de la Mer 18:287–295.

Tagliabue, A., Mtshali, T., Aumont, O., Bowie, A.R., Klunder, M. B., Roychoudhury, A.N., and Swart, S., 2012. A global compilation of dissolved iron measurements: focus on distributions and processes in the Southern Ocean, Biogeosciences, 9, 2333-2349, doi:10.5194/bg-9-2333-2012.

Takahashi, T., Feely, R.A., Weiss, R.F., Wanninkhof, R.H., Chipman, D.W., Sutherland, S.C., 1997. Global air-sea flux of CO_2: an estimate based on measurements of sea-air pCO2 difference. Proceedings of the National Academy of Science 94, 8292-8299.

Takahashi, T., Sutherland, S.C., Sweeny, C., Poisson, A., Metzl, N., Tilbrook, B., Bates, N., Wanninkof, R., Feely, R.A., Sabine, C., Olafsson, J., and Yukihiro, N., 2002. Global sea-air CO_2 flux based on climatological surface ocean pCO_2, and seasonal biological temperature effects. Deep-Sea Res. Pt. II, 49, 1601–1622.

Talley, L., Chereskin, T., Dickson, A., Fine, R., Farias, L., Ulloa, O. and Sloyan, B., 2008. AIW formation in the southeast Pacific. http://www-pord.ucsd.edu/~ltalley/aaiw/ Updated October 23 2008.

Taucher, J. and Oschlies, A., 2011. Can we predict the direction of marine primary production change under global warming? Geophysical Research Letters 38: L02603 doi:10.1029/2010GL045934

Thomalla, S.J., Waldron, H.N., Lucas, M.I., Read, J.F., Ansorge, I.J. and Pakhomov, E., 2011. Phytoplankton distribution and nitrogen dynamics in the southwest Indian subtropical gyre and Southern Ocean waters. Ocean Sci., 7, 113–127.

Tilzer M.M, Elbrachter M, Gieskes W.W, Besse B., 1986. Light–temperature interactions in the control of photosynthesis in Antarctic phytoplankton. Polar Biol. 5:105–111

Timmermans, K.R., al., e., 2001. Co-limitation by iron and light of *Chaetoceros brevis*, *C. dichaeta* and *C. calcitrans* (Bacillariophyceae). Marine Ecology Progress Series 217, 287-297.

Tomas, C.R., 1997. Identifying Marine Phytoplankton. Academic Press, New York, pp. 858.

TréGuer, P. and Jacques, G., 1992. Dynamics of nutrients and phytoplankton, and fluxes of carbon, nitrogen and silicon in the Antarctic Ocean, Polar Biol. 12, 149–162.

Trull, T.W., Bray, S.G., Manganini, S.J., Honjo, S. and Francois, R., 2001. Moored sediment trap measurements of carbon export in the Sub-antarctic and Polar Frontal Zones of the Southern Ocean, south of Australia, J. Geophys. Res., 106, 31,489–31,509, doi:10.1029/2000JC000308.

Uitz, J., Claustre, H., Morel, A. and Hooker, S.B., 2006. Vertical distribution of phytoplankton communities in open ocean: An assessment based on surface chlorophyll, *J. Geophys. Res., 111(C8),* C08005.

Vaillancourt, R.D., Brown, C.W., Guillard, R.L. and Balch, W., 2002. Light backscattering properties of marine phytoplankton: relationships to cell size, chemical composition and taxonomy. Journal of Plankton Research, 26(2): 191-212.

Van de Hulst, H.C., 1981. Light Scattering by Small Particles (Dover).

Van Leeuwe, M.A. and De Baar, H.J.W., 2000. Photo-acclimation by the Antarctic flagellate *Pyramimonas* sp. (Prasinophyceae) in response to iron limitation. Eur. J. Phycol. 35: 295–303, doi:10.1080/09670260010001735891

Van Leeuwe, M.A., Stefels, J., Belviso, S., Lancelot, C., Verity, P.G. and Gieskes, W.W.C. [Eds.], 2007. *Phaeocystis*, major link in the biogeochemical cycling of climate-relevant elements. Springer.

Volk, T., and Hoffert, M.I., 1985. Ocean carbon pumps: Analysis of relative strengths and efficiencies in ocean-driven atmospheric CO_2 changes, in The Carbon Cycle and Atmospheric CO2: Natural Variations Archean to Present, Geophys. Monogr. Ser., vol. 32, edited by E. T. Sundquist and W. S. Broecker, pp. 99–110, AGU, Washington, D. C.

Waldron, H.N., Attwood, C.G., Probyn, T.A. and Lucas, M.I., 1995. Nitrogen dynamics in the Bellingshausen Sea during the Austral spring of 1992. Deep-Sea Research II 42(4-5): 1253-1276.

Wang, J., Tang, D. and Sui, Y., 2010. Winter phytoplankton bloom induced by subsurface upwelling and mixed layer entrainment southwest of Luzon Strait. Journal of Marine Systems, 83(3), pp.141-149.

Watson, A.J., Bakker D.C.E., Ridgwell, A.J., Boyd, P.W. and Law, C.S., 2000. Effect of iron supply on Southern Ocean CO_2 uptake and implications for glacial atmospheric CO_2. *Nature* 407, 730-733. doi:10.1038/35037561.

Watson, A.J. and Orr, J.C., 2003. Carbon dioxide fluxes in the global ocean. In: Fasham, M.J.R. (Ed.), Ocean Biogeochemistry: The role of the ocean carbon cycle in global change. Springer-Verlag, Berlin, pp. 123-143.

WetLabs, 2011. ECO BB User's Guide (BB): Scattering Meter, http://www.wetlabs.com/manuals

WetLabs, 2011. C-Star User's Guide (cstar): Transmissometer, http://www.wetlabs.com/manuals

Williams, R.G. and Follows, M.J., 2003. Physical transport of nutrients and the maintenance of biological production. In: Fasham, M. J. R. (Ed.), Ocean Biogeochemistry: The role of the ocean carbon cycle in global change. Springer-Verlag, Berlin, pp. 18-51.

Yentsch, C.S., and D.A. Phinney, 1989. A bridge between ocean optics and microbial ecology, *Limnol. Oceanogr., 34(8),* 1694-1705.

Yool, A., Martin, A.P., Fernandez, C., and Clark, R.J., 2007. Not so new: the significance of nitrification for oceanic "new" production, Nature 447, 999–1002.

Zender, C., Bian, H., and Newman, D., 2003. Mineral dust entrainment and deposition (DEAD) model: Description and 1990s dust climatology, J. Geophys. Res., 108, 4416, doi:10.1029/2002JD002775.